5-2011

Stratigraphic, Microfossil, and Geochemical Analysis of the Neoproterozoic Uinta Mountain Group, Utah: Evidence fo a Eutrophication Event?

Dawn Schmidli Hayes
Utah State University

STRATIGRAPHIC, MICROFOSSIL, AND GEOCHEMICAL ANALYSIS OF THE NEOPROTEROZOIC UINTA MOUNTAIN GROUP, UTAH: EVIDENCE FOR A EUTROPHICATION EVENT?

by

Dawn Schmidli Hayes

A thesis submitted in partial fulfillment of the requirements for the degree

of

MASTER OF SCIENCE

in

Geology

Approved:

_____	_____
Dr. Carol M. Dehler	**Dr. John Shervais**
Major Advisor	**Committee Member**
_____	_____
Dr. W. David Liddell	**Dr. Byron R. Burnham**
Committee Member	**Dean of Graduate Studies**

UTAH STATE UNIVERSITY
Logan, Utah

2010

ABSTRACT

Stratigraphic, Microfossil, and Geochemical Analysis of the Neoproterozoic Uinta Mountain Group, Utah: Evidence for a Eutrophication Event?

by

Dawn Schmidli Hayes, Master of Science

Utah State University, 2010

Major Professor: Dr. Carol M. Dehler
Department: Geology

Several previous Neoproterozoic microfossil diversity studies yield evidence for a relatively sudden biotic change prior to the first well-constrained Sturtian glaciations. In an event interpreted as a mass extinction of eukaryotic phytoplankton followed by bacterial dominance, diverse assemblages of complex acritarchs are replaced by more uniform assemblages consisting of simple leiosphaerid acritarchs and bacteria. Recent data from the Chuar Group of the Grand Canyon (770-742 Ma) suggest this biotic change was caused by eutrophication rather than the direct effects of Sturtian glaciation; evidence includes total organic carbon increases indicative of increasing primary productivity followed by iron speciation values that suggest sustained water column anoxia. A new data set (this study) suggests that this same eutrophication event may be recorded in shale units of the formation of Hades Pass and the Red Pine Shale of Utah's Neoproterozoic Uinta Mountain Group (770-742 Ma). Results of this study include a significant shift from a higher-diversity (H'= 0.60) fauna that includes some ornamented acritarchs to a lower-diversity (H' = 0.11) fauna dominated by smooth leiosphaerids and microfossils of a bacterial origin (*Bavlinella/ Sphaerocongregus sp.*). This biotic change co-occurs with a significant increase in total

organic carbon values that directly follows a positive carbon-isotopic excursion, suggesting increased primary productivity that may have been the result of elevated sediment influx and nutrient availability. Both the biotic change and period of increased total organic carbon values correspond with the onset of an interval of anoxia (indicated by total iron to aluminum ratios above 0.60) and a spike in sulfur concentration. Like those reported from the Chuar Group, these biotic and geochemical changes in the upper Uinta Mountain Group are independent of changes in lithofacies , and they suggest that either a eutrophication event or direct inhibition of eukaryotes by sulfide (or perhaps both) may have been the cause of the biotic turnover. These findings support current correlations between the Uinta Mountain and Chuar Groups, the idea that the biotic turnover preserved in both strata was at least a regional phenomenon, and current models of punctuated global ocean anoxia during mid- to late-Neoproterozoic time. Whether or not this hypothesized eutrophication event was more than regional in extent remains a very interesting question and will certainly be a focus of future research.

(122 pages)

ACKNOWLEDGMENTS

There are many people to thank for encouraging me to pursue a career in geology and for supporting this research. Many years ago, Scott Wilkerson at DePauw University pulled me aside after his Geology of American National Parks class and asked why I wasn't a geology major. That was a great question, and Scott's encouragement led me to a geology minor and a senior research project that involved both my biology major and geology minor; this also resulted in my meeting Jim Mills and Fred Soster, DePauw's other two amazing faculty members who, along with Scott, accompanied me on my very first geologic adventures back in the 1990s. Thanks guys! I'll never forget you and how you pointed me down the "right" path.

Then there is Paul Link, my geo-dad. I remember the first class I took with Paul (a geology course for teaching majors at Idaho State University) and how excited I was to learn about local geology from someone so enthusiastic and dedicated to education. That class led to several more of Paul's courses, a teaching minor in earth science, and a love of western United States geology that lured me back to Idaho after five years of teaching high school science in South Carolina and Florida. When I came back west, the first thing I did was look up Paul and re-join ISU's geology department. The second thing I did was become a member of the Neoproterozoic sedimentology fan club. With a mentor like Paul, it was impossible NOT to love this time period and area of study – even when almost coaxed out of the Precambrian by Leif Tapanila's amazing teaching and non-microscopic paleontology research. Hundreds of millions of thanks, Paul! Of course I can't thank you enough for all of your enthusiasm, encouragement, and assistance, but I can sure try by working my tail off and hoping I can someday be as inspiring to one of my students as you have been to me!

Carol Dehler, my geo-mom, has been and continues to be the best graduate advisor and colleague I could ever hope for, a fabulous friend, and one of the most positive and

influential people in my life. She brings out the best in me both personally and professionally, and I could never thank her enough for all of the amazing opportunities she has provided for me. Perhaps 742 million thanks might be a good start, Carol! I look forward to the continuation of our exceptional working relationship – and all of the fun we will surely have along the way.

I must thank my committee members at Utah State University, Dave Liddell and John Shervais, for taking the time to help me with my thesis research. Your comments on my thesis and your assistance in its completion were key, and I am very appreciative. It is certainly a better project because of your input.

Of course there are also several field assistants to thank! My husband, Ashley, and my dog, Muffet, provided much needed help in the field and the best of company as well. Thanks Ashley and Muff for your loyalty, persistence, enthusiasm, love, and support – this research would not have been possible (or nearly as fun!) without you. My field assistants at Leidy Peak were Carol and Sienna Dehler, Esther and Ellie Kingsbury, Emilee and Quinn Skyles, Reed Myer, and two lovely llamas (Tomas and Coal) – thanks to all of you for your help, good company, muscles, and patience on that trip! I also owe a big "thank you" to Robin Nagy for her help in the lab with microfossil identification.

Financial aid for this research was provided by the National Science Foundation (Grant EAR -0819759), Sigma Xi Scientific Society and The Society for Organic Petrology. Additional thanks go to Tim Lyons and Clint Scott at UC-Riverside and Steve Nelson at BYU for the use of and training in their laboratory facilities.

Dawn Hayes

CONTENTS

Page

LIST OF TABLES

LIST OF FIGURES

CHAPTER 1

INTRODUCTION AND GEOLOGIC BACKGROUND

1.1 – Introduction and Significance of Research

The Uinta Mountain Group (UMG) of Utah, much like the Chuar Group of Arizona, contains an assemblage of microfossils that were preserved in a dominantly clastic marine setting during mid-Neoproterozoic time. Despite moderate to good preservation of these microbiotas, species diversity in the Uinta Mountain Group is much lower than that of the Chuar Group and other coeval clastic deposits (Butterfield, 1994; Knoll et al., 1991; Vidal, 1976). Morphologically simple filaments, the colonial bacteria *Bavlinella faveolata*, and species of the unornamented acritarch *Leiosphaeridia* dominate the Uinta Mountain Group microfossil assemblages; *Chuaria circularis*, vase-shaped microfossils, and ornamented acritarchs are present but very rare (Nagy and Porter, 2005). The relative lack of diversity and complexity in Uinta Mountain Group fossil assemblages is interesting because it cannot be readily explained by age or poor preservation; a more likely cause is that paleoenvironmental conditions excluded the diverse communities of morphologically complex eukaryotes found in other coeval clastic deposits (Anbar and Knoll, 2002).

The most fossiliferous formation in the Uinta Mountain Group, and thus the most ideal for microfossil analyses, is the Red Pine Shale. In this youngest UMG formation, all of the microfossil types listed above and a few additional taxa have been described (Nagy and Porter, 2005), yet no study thus far has attempted to document temporal or spatial changes in Red Pine Shale microfossil assemblages

and their potential correlations with paleoenvironmental conditions. Several other Neoproterozoic successions worldwide, including the likely correlative Chuar Group, provide evidence of sudden biotic turnover from diverse ornamented acritarch assemblages to bacterial and/or leiosphaerid-dominated assemblages (Knoll et al., 1991; Knoll, 1994; Vidal and Knoll, 1982; Vidal and Moczydlowska, 1992). This dramatic biotic change has been hypothesized to represent a mass extinction of eukaryotic phytoplankton, possibly due to eutrophication rather than the onset of low latitude Sturtian glaciations (Nagy et al., 2009). In the Chuar Group, paleontological, total organic carbon, and iron speciation data support this interpretation (Nagy et al., 2009). The intent of this thesis is to conduct a stratigraphic, microfossil, and geochemical analysis of the Red Pine Shale to 1) document whether a similar biotic change is present, and 2) determine if biotic changes in the Red Pine correlate with geochemical indicators of paleoenvironmental eutrophication.

If the Red Pine Shale contains biotic evidence of eutrophication, the microfossil assemblage in the strata should shift upsection from a lower-density higher-diversity assemblage to a higher-density one with less-diverse, simpler organisms. Increasing total organic carbon content, indicative of increasing primary productivity, would also be an expected upsection trend, as would a shift in $\delta^{13}C_{org}$ values. Since eutrophication ultimately results in oxygen depletion due to increased organic decay rates, evidence of anoxia should be present in any Red Pine sediments deposited during eutrophication. Where the Red Pine Shale contains geochemical

evidence of eutrophication, $\delta^{34}S$ and iron speciation signatures should indicate sustained sediment pore-water and water column anoxia. To support eutrophication, the microfossil change(s) should correlate with the chemical change(s). Specifically, a shift from a higher-diversity fauna including ornamented acritarchs to a lower-diversity fauna dominated by bacteria and/or leiosphaerids should co-occur with increasing organic carbon and be followed by anoxia, as indicated by sulfur isotopic composition and iron speciation (Nagy et al., 2009). Ideally, this correlation will not co-occur with a major lithofacies change.

In addition to addressing the question of possible paleoenvironmental eutrophication, this study of the Red Pine Shale also has several secondary goals: 1) it will provide detailed descriptions of the Red Pine Shale in an area where there currently are none and mapping has been done only very generally, 2) add to the carbon isotope data set of the Red Pine Shale, possibly allowing for more robust correlations between measured sections in the Red Pine Shale and between the UMG and the Chuar Group of the Grand Canyon, 3) yield additional microfossil data for a formation that has received little paleontological attention, 4) provide the first iron speciation and total sulfur data for the Uinta Mountain Group, and 5) enhance the sequence stratigraphic framework for the Red Pine Shale and underlying Hades Pass Quartzite. This study's broader significance is that information about UMG microfossils and paleoenvironment should contribute to our understanding of eukaryotic biodiversification and pre-Sturtian oceanic and atmospheric conditions on Earth.

1.2 – Geologic Background – The Uinta Mountain Group

The Uinta Mountain Group, located in northeastern Utah near the Utah-Wyoming border (Figure 1) is one of the only mid-Neoproterozoic successions in North America that remains well-preserved. It is a thick, siliciclastic succession of mostly shale and sandstone, yet is unmetamorphosed (Wallace and Crittenden, 1969). The Uinta Mountain Group ranges from four to seven kilometers thick. Although it is not completely clear how the eastern and western parts of the Uinta Mountain Group correlate, it has been determined that strata in the northern part of the Uinta Mountain Group are dominated by sediments derived from the Wyoming craton, and strata from the southern part are dominated by sediments from Paleoproterozoic and Mesoproterozoic sources to the east (Sanderson, 1984; Ball and Farmer, 1998; Condie et al., 2001; Mueller et al., 2007; Dehler et al., 2010).

1.3 – Geologic Background – The Red Pine Shale

The youngest formation of the Uinta Mountain Group is the Red Pine Shale (Figure 2), a >1124 meter thick organic-rich sedimentary succession formally named by Williams (1953) consisting of silt, mud, and clayshale interbedded with fine-to-coarse-grained quartz and arkosic arenite (Figure 2). The Red Pine Shale has most recently been interpreted as a prograding deltaic system in an interior seaway receiving immature sediment from the north and more-mature sediment from the east (Myer, 2008; Dehler, pers. comm.).

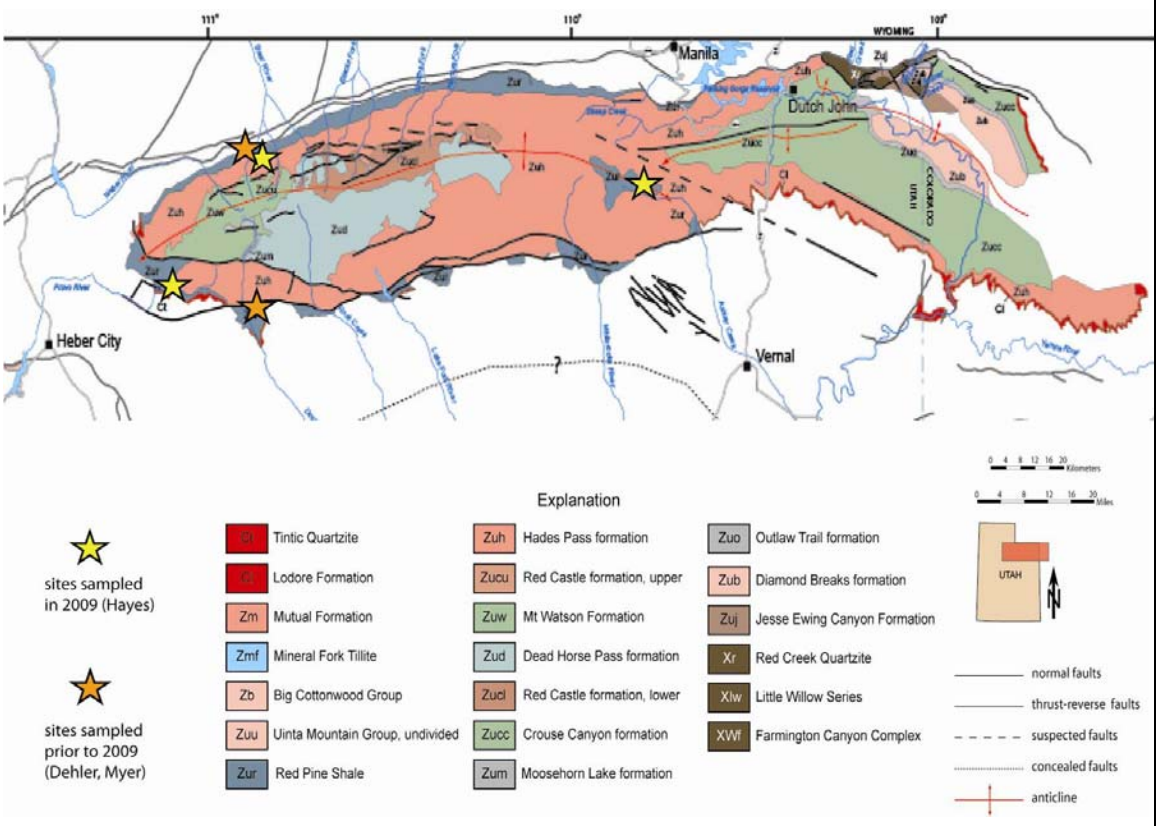

Figure 1. Geologic map of the Uinta Mountain Group showing sample sites for this study. Figure modified from Sprinkel and Rybczinski, 2009.

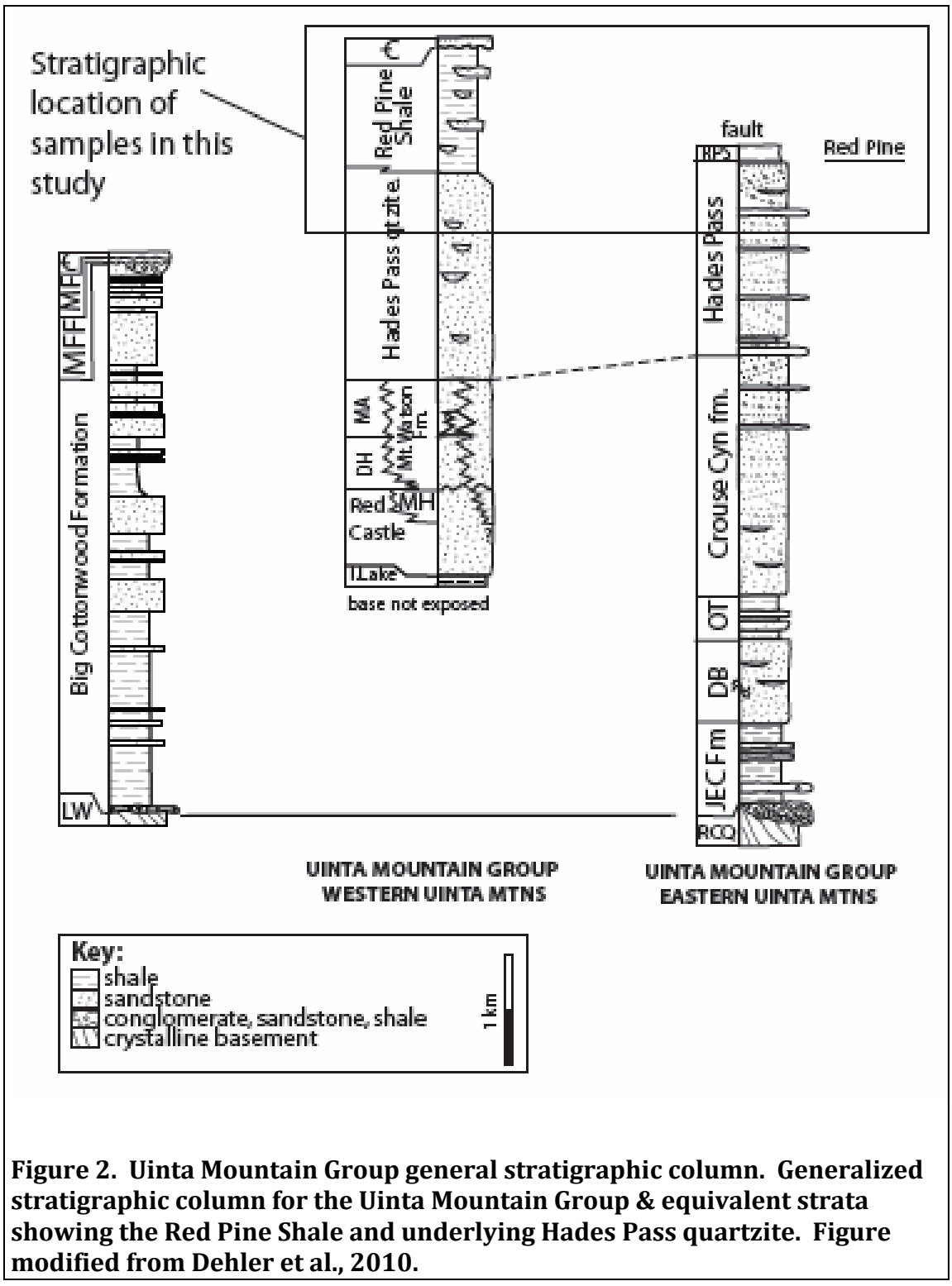

Figure 2. Uinta Mountain Group general stratigraphic column. Generalized stratigraphic column for the Uinta Mountain Group & equivalent strata showing the Red Pine Shale and underlying Hades Pass quartzite. Figure modified from Dehler et al., 2010.

PREVIOUS WORK

2.1- Mapping and Stratigraphy

The Red Pine Shale was formally named by Williams (1953) and described as consisting of silt, mud, and clayshales interbedded with fine-to-coarse-grained quartz and arkosic arenites. Williams differentiated the Red Pine Shale from the overlying Cambrian strata based upon an angular unconformity between the two, determined the Red Pine Shale to be Precambrian, and formally named the unit for the type section exposure in Red Pine Canyon. In 1954, Larsen described the stratigraphy of the unit, its relation to adjacent units, and reported a maximum thickness for the Red Pine Shale of over 900 meters. An additional stratigraphic description of the Red Pine Shale along with a description of its lower contact as being gradational was provided in 1969 by Wallace and Crittenden. In 1972, Wallace mapped the Red Pine Shale in the western Uinta Mountains and provided a new thickness of 1830 meters. In 1992, Bryant created a geologic map of the 1 x 2 Salt Lake City Quadrangle which included all locations of the Red Pine Shale in the western Uinta Mountains and was based mainly on Wallace's 1972 mapping. Most recently, the Uinta Mountain Group and Red Pine Shale have been mapped east of 110° longitude to the Goslin Mountain area (Sprinkel and Rybczinski, 2009).

2.2- Facies Analysis

In 2007, Dehler et al. studied the Red Pine Shale, measuring partial and complete sections and constructing a composite section. Dehler et al. (2007) proposed three main facies for the Red Pine Shale: 1) a shale facies consisting of organic-rich gray to black siltshale, mudshale, and clayshale that makes up about 70% of the composite section, 2) a shale-and-sandstone facies that is composed of organic-rich shale interbedded with fine-to-coarse-grained quartz arenite to arkosic arenite in thin beds and makes up about 20% of the composite section, 3) a sandstone facies composed of mostly fine-grained to granule quartz arenite to arkosic arenite with sedimentary structures. Building on the work of Dehler et al. (2007), Myer (2008) added three new facies and expanded the descriptions of the three previously identified facies, resulting in the identification of six facies within the Red Pine Shale. These facies are defined by grain sizes, bed thicknesses, and sedimentary structures and are interpreted using delta terminology. A summary of the main characteristics of each of Myer's (2008) facies can be found in Table 1.

2.3 – Sequence Stratigraphy

Because the contact between the Red Pine Shale and the underlying Hades Pass quartzite is thought to be gradational (Wallace and Crittenden, 1969), sequence stratigraphic interpretation of the Red Pine Shale must include the Hades Pass quartzite. Kingsbury (2008) places a sequence boundary just below the base of the Hades Pass quartzite based on the sudden facies association change and the change in paleocurrent direction at this location. This sequence boundary

Table 1. Red Pine Shale facies defined by Dehler et al. (2007) and Myer (2008); table from Myer (2008)

Facies	Description	Facies Definition	Environmental Interpretation
1) Shale	Gray to black claystone to siltstone, thin to thick beds, organic-rich, contains *Bavlinella faveolata* and acritarch fossils, and rare 10 cm to 1 m thick tabular find sandstone beds; sandstone is quartz arenite to arkosic arenite, usually weathered and oxidized with siltstone lenses, hummocky cross-stratificaton, swaley bedding, tool marks, symmetric and interference ripples	Mostly clay to siltstone with few 10 cm to 1 m thick fine sandstone beds. Shale beds 5 m to 310 m thick.	Distal prodelta
2) Concretion	Silt to medium sand, usually gray to black shale, some thin sandy interbeds with silty lenses, graded bedding, ripple to parallel lamintions, vase-shaped microfossils, and multiple silica concretions	1-4 m thick siltstone with some medium sandstone beds. Distinguishing feature is silica concretions.	Distal prodelta
3) Shale and sandstone	Shale interbedded with sandstone. Shale is claystone to siltstone, gray to black, some maroon with parallel laminations, silty lenses, acritarch fossils; sandstone is fine-to-coarse-grained, moderately sorted quartz to arkosic arenite, thin to medium beds, graded bedding, planar-tabular, swaley, and hummocky cross-stratification, ripple cross and parallel laminations, and climbing and symmetric ripples, siltstone rip-ups, scoured contacts, and cut-and-fill structures with coarse sand fining upward to silt; many beds are massive.	Interbedded sandstone beds <2m thick with shale beds <5m thick. This combination is from 3-16 m thick.	Delta front, prodelta
4) Slump fold	Gray to black mudstone with some sandstone beds. Sandstone is fine-grained quartz to arkosic arenite with symmetric ripples, ripple laminations, hummocky cross-stratification up to 1 m x 20 cm, slump folds up to 1 m x 30 cm	Usually mudstone with some fine sandstone interbeds 1-4 m thick. Distinguishing feature is slump folds.	Proximal prodelta, delta front
5) Sandstone	Fine-to-coarse-grained sandstone, subarkosic to arkosic, some quartz arenite, muscovite, and rare chlorite, mudstone intraclasts, angular to subrounded grains, poorly to well-sorted, tabular, undulatory to planar beds, thin to medium bedding, normal to reverse grading, symmetric ripples, granule sandstone lenses, cut and fill structures, laminations within thin shale interbeds, mudstone rip-ups, parallel and ripple cross-laminations, hummocky and swaley cross-stratification, and planar and tangential cross-bedding.	Sandstone ranging in thickness from 2-17 m thick.	Delta front
6) Pebble sandstone	Fine to coarse pebbly sandstone, quartzite to sublithic or subarkosic, angular to subangular, moderate to poor sorting, undulatory to tabular thin to medium beds with normal and reverse grading, maroon siltstone rip-ups, and pebbles up to 5 mm.	Granule to pebble sandstone <10 m thick, from 0.5-7 m thick.	Delta front

accommodation systems tract braided-fluvial environment, indicating that a significant regression occurred across this sequence boundary (Kingsbury, 2008). Together, it appears that the Hades Pass quartzite and Red Pine Shale represent a single lower-order transgressive-regressive cycle. If the Hades Pass/Red Pine contact is not gradational (i.e. there is a subtle unconformity between them), the Red Pine Shale may represent a single 3rd order cycle (Myer, 2008).

Within the Red Pine Shale, higher-order cyclicity appears to be present. Myer (2008) identified eleven higher-order cycles ranging from 32 m to 143 m thick defined by coarsening-upward trends from shale to sandstone above which grain size typically decreases very sharply (Figure 3). Within each of these eleven sequences, Myer (2008) also notes the potential for defining cyclicity on a meter to sub-meter scale but cites the occurrence of some very thick (up to 100 m) sections where this is not possible.

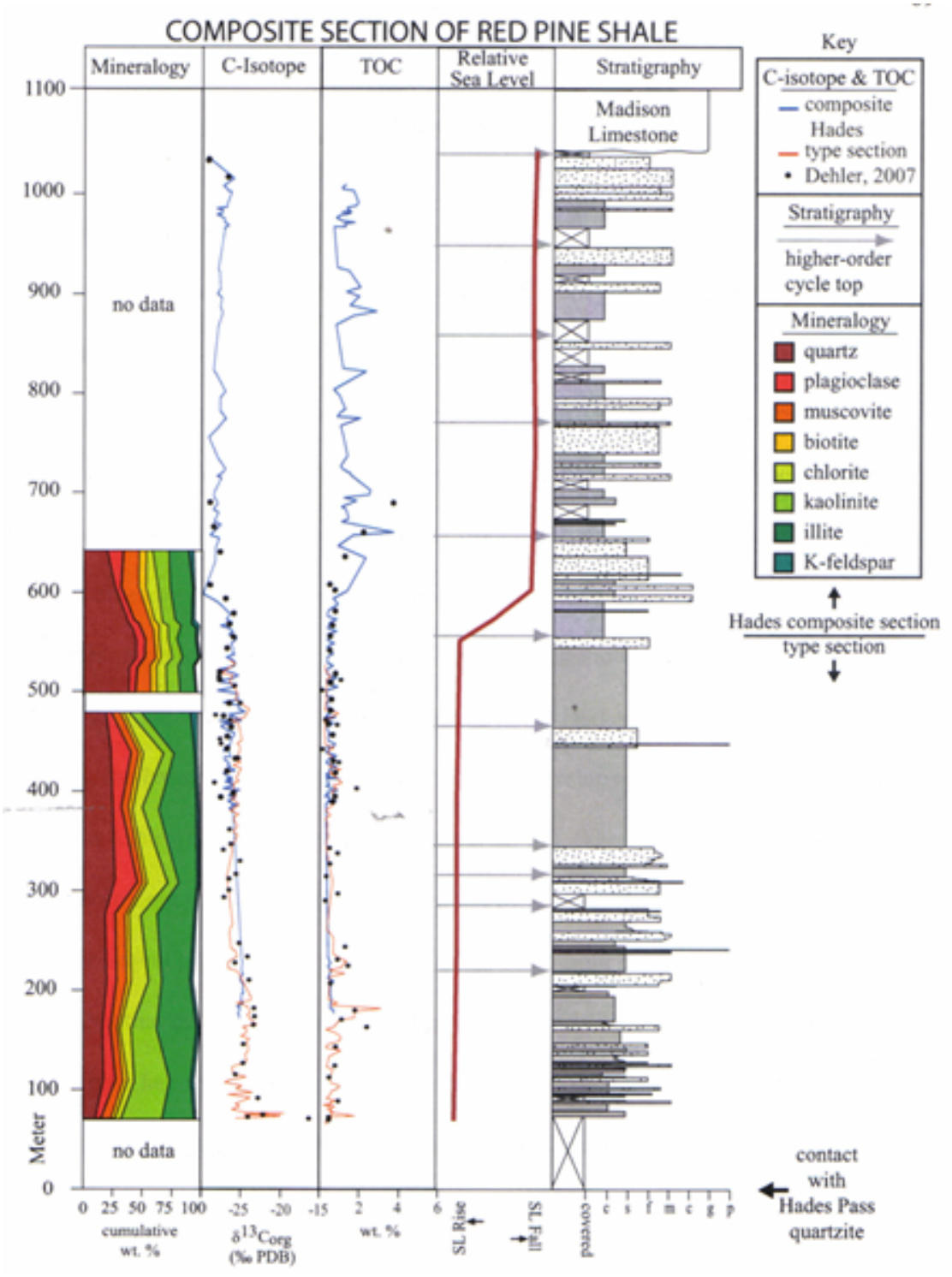

Figure 3. Composite column with Red Pine Shale sea-level curve. Higher-order cycles on the sea level graph are shown with grey arrows (from Myer, 2008).

In Figure 3, the lower-order Hades Pass-Red Pine cycle is illustrated, showing fluvial deposition at the base in the Hades Pass Quartzite (lowstand), transitioning to Red Pine Shale prodelta deposits in the center (transgression), followed by Red Pine Shale delta front deposits at the top (highstand). It is likely that this cycle is controlled mainly allogenically by changes in seafloor spreading rates associated with the breakup of Rodinia.

2.4- Depositional Environment

The depositional environment of the Red Pine Shale has been interpreted as fluvial, mud flat, or marine deltaic (Wallace and Crittenden, 1969; Link et al., 1993; Condie et al., 200l; Dehler et al., 2007; Myer, 2008). There are two paleogeographic models for this depositional environment that are not mutually exclusive: an east-west intracratonic basin dominated by fluvial input (Condie et al., 2001) or a marine-influenced system open to both the west and south (Wallace and Crittenden, 1969; Dehler et al., 2010). Carbon-isotope data and the presence of marine microfossils in the Red Pine Shale suggest the influence of a marine system, as do the presence of certain sedimentary structures described in the facies analysis section of this chapter (Dehler et al., 2007; Myer, 2008).

2.5 - Micropaleontology

The first microfossil assemblages to be identified in the Red Pine Shale include mainly *Chuaria circularis*, *Leiosphaeridia* sp., other acritarchs and filaments (Vidal and Ford, 1985). Later analyses identified vase-shaped microfossils,

Leiosphaeridia sp., *Bavlinella faveolata*, ornamented acritarchs, filaments, and *Chuaria circularis* (Nagy and Porter, 2005; Dehler et al., 2007). Most sections analyzed by Nagy and Porter (2005) were dominated by either *Leiosphaeridia* sp. and filaments or by *Bavlinella faveolata*; these researchers report ornamented acritarchs from only the Leidy Peak area, and vase-shaped microfossils are reported only in the upper parts of the Type and Henry's Fork sections. This is significant because transitions from more diverse assemblages including ornamented acritarchs to *Leiosphaeridia*/*Bavlinella*/filament-dominated assemblages may have been caused by eutrophication. The microfossils of the Uinta Moutain Group are described in the subsections that follow; Table 2 contains a list of previously reported taxa.

Table 2. Summary of Red Pine Shale Paleontology. Fossil occurences from previous paleontogical studies of the Uinta Mountain Group's Leidy Peak, Red Pine Shale Type, Lower Hades, Hades, and Setting Road sections. Setting Road data from Vidal and Ford (1985); all other data from Nagy and Porter (2005)

Locality	**Sample ID #**	**Fossils**
Type Section	RP04-3	*Leiosphaeridia* sp., filaments
Type Section	RP04-10	*Leiosphaeridia* sp., filaments
Type Section	RP00B-8	*Leiosphaeridia* sp., filaments
Type Section	RP00B-32	*Leiosphaeridia* sp.
Type Section	RP00B-40	*Leiosphaeridia* sp.
Lower Hades	RP01A-50	*Leiosphaeridia* sp., filaments, *Bavlinella faveolata*
Lower Hades	RP01A-63	*Leiosphaeridia* sp., filaments
Lower Hades	RP01A-68	*Leiosphaeridia* sp., filaments
Lower Hades	RP01A-70	*Leiosphaeridia* sp., filaments
Lower Hades	RP01A-85	*Bavlinella faveolata*
Hades	RP03B-1	---barren---
Hades	RP03B-24	*Chuaria circularis*

Table 2 continued		
Hades	RP03B-25	*Leiosphaeridia* sp.
Leidy Peak	LP10-03-01-2	Ornamented acritarchs, filaments, ?VSMs
Leidy Peak	LP10-03-01-4	*Leiosphaeridia* sp., filaments
Leidy Peak	LP10-03-01-6	*Leiosphaeridia* sp., filaments
Setting Road	---	*Taeniatum* sp., filaments
Setting Road	---	*Leiosphaeridia* sp.
Setting Road	---	*Valeria lophostriata*
Setting Road	---	cf. *Stictosphaeridium* sp.
Setting Road	---	*Trachysphaeridium* sp. A
Setting Road	---	*Trachysphaeridium laminaritum*
Setting Road	---	*Trachysphaeridium laufeldi*
Setting Road	---	*Tasmanites rifeiicus*

2.5.1 - Acritarchs

First recognized in 1892 and later informally named by Downie in 1963 (Vidal and Ford, 1985), acritarchs are a polyphyletic group of almost exclusively marine unicellular forms with very resistant organic membranes (Vidal and Nystuen, 1990). They are hollow with no intracellular structures and range in size from a few to hundreds of micrometers. Although they have a basic spheroidal form, there are many ornamented varieties that deviate from this simple form. Their walls are composed of a relatively chemically nonreactive sporopollenin-like substance that often forms kerogens (Martin, 2008). It is generally accepted that acritarchs are the cysts and vegetative stages of extinct unicellular eukaryotic algae (Vidal and Ford, 1985; Martin, 2008). This assumption of a eukaryotic origin is based on their possession of one or more of the following features: complex surface ornamentation, spiny processes, excystment ruptures or medial splits, complex wall

ultrastructure, and the presence of specific hydrocarbon biomarkers (Javaux et al., 2001). Interestingly, however, many of these diagnostic features can be easily "erased" by geologic processes, and since many eukaryotes do not exhibit all of the features, their absence in a microfossil does not allow us to conclude it is not eukaryotic (Buick, 2010). Acritarchs are thought to be planktic because their random dispersion in sedimentary rocks and uniform distribution in time-equivalent strata suggests evenly dispersed organisms floating passively in the water column and then settling out (Vidal and Moczydlowska, 1992; Butterfield and Chandler, 1992). There is some evidence that larger, more morphologically complex acritarchs (those that are strongly ornamented) occur preferentially in shallow, nearshore environments and are generally absent from distal shelf to slope environments (Butterfield and Chandler, 1992).

2.5.2 - Leiosphaeridia sp. (Figure 10 in Chapter 5)

This genus of acritarchs, very common in UMG strata, are unornamented, spheroidal, thin-walled, and smooth; they are most likely the dormant cysts of unicellular algae or the cast-off cell walls of growing algae (Butterfield and Chandler, 1992). They range in diameter from ten to one hundred micrometers, and they are grouped into different species by the thickness of their walls and overall diameter. In the UMG, they are found in the unicellular form and in colonial clusters; those with medial splits most likely represent cyst stages (Nagy and Porter, 2005).

2.5.3 - Filaments (Figure 13 in Chapter 5)

This group of fossils has a strip-like or tube-like morphology and can be either single- layered or double-walled. They are up to 100 micrometers in length and between 5 and 20 micrometers wide. Less than one percent of the filaments in the UMG are branching; most are single strips or tubes with no branches. Filaments are commonly interpreted as the remains of filamentous cyanobacteria (Nagy and Porter, 2005).

2.5.4- Bavlinella faveolata/ Sphaerocongregus sp. (Figure 12 in Chapter 5)

This fossil often consists of raspberry-like clusters of ten to one hundred micron-sized cells packed together (Knoll et al., 1981). The rounded aggregates of cells are sometimes surrounded by an outer membrane, and in the UMG the aggregates range between five and twenty micrometers in diameter (Nagy and Porter 2005). *Bavlinella*/*Sphaerocongregus* typically occurs in very dense concentrations with no other fossils, leading many researchers to believe that it is an organism that creates blooms when environmental conditions are stressful (Knoll et al., 1981; Vidal and Nystuen, 1990; Butterfield and Chandler, 1992). There are multiple interpretations of *Bavlinella's* biology: Knoll et al. (1981) describe it as an endosporulating cyanobacterium, Vidal and Nystuen (1990) suggest it is a bacterium that performed anoxygenic photosynthesis, and it also could be an association of multiple prokaryotic species (Nagy and Porter, 2005). Although some specimens identified as *Bavlinella* or *Sphaerocongregus* are actually organic residues

associated with pyrite framboids, it is important to note that this interpretation does not rule out a bacterial origin (Vidal and Nystuen, 1990; Gong et al., 2008). The *Bavlinella* specimens from the Uinta Mountain Group, like those of the Chuar Group, appear similar to specimens thought to be biogenic and interpreted as having a bacterial origin (Vidal and Nyusten, 1990; Nagy et al., 2009; Nagy, pers. comm.).

2.5.5 - Chuaria circularis

First described in the Chuar Group by Walcott in 1883 then named in 1899, this species was the first Precambrian fossil, and its description and interpretation have changed significantly since its discovery (Horodyski, 1993). When Hoffman first described this fossil in the Red Pine Shale of the UMG in 1977, he recorded 0.13-2.33 mm diameter black, disc-like compressions on bedding planes that were occasionally found in loose clusters and rarely in contact with one another. Its walls have distinct concentric folds and range from 0.5 to 5.4 micrometers thick. It is now commonly interpreted as a marine alga (Nagy and Porter 2005).

2.5.6- Vase-shaped Microfossils

Vase-shaped microfossils (VSMs) consist of tear-shaped tests that are circular in transverse section and taper toward a single aperture. VSMs have a wide variation in shape and size, ranging from 20-300 micrometers x 10-200 micrometers. Most have radial symmetry, but some are bilaterally symmetrical with a curved neck area. Their walls are between one and three micrometers thick, and their aperture shapes vary from circular to triangular to hexagonal (Porter and

Knoll, 2000). In the UMG, they are preserved in a silicified organic-rich mudstone of the Red Pine Shale as internal molds (Nagy and Porter, 2005).

The latest VSM data and interpretation stems from newly discovered exceptionally preserved VSMs in dolomite nodules from the uppermost part of the Chuar Group. These are preserved as siliceous or calcareous casts, often coated with pyrite, iron oxides, or organic matter. The morphology and taphonomy of these VSMs indicates that they have a strong affinity with modern testate amoebae; a few of the VSMs from these nodules are indistinguishable from modern testate amoebae. If these VSMs do represent organisms similar to modern testate amoebae, this would provide the earliest morphological evidence for heterotrophic eukaryotes. This would signify that Neoproterozoic ecosystems were complex and included consumers and that eukaryotic biomineralization had evolved by Neoproterozoic time (Porter and Knoll, 2000; Porter et al., 2003).

2.6 – Age and Correlation

The age of the Red Pine Shale has been indicated by microfossil assemblages, correlation of carbon isotope data and fossils, whole rock Rb/Sr dating, and detrital zircon U/Pb dating. In 1975, Crittenden and Peterman reported a whole rock Rb/Sr age of 950 Ma for the Red Pine Shale, and in 1986, Hedge et al. used this technique to give an age of 1.4-0.9 Ga for the entire Uinta Mountain Group. These ages, however, contradict those suggested by the microfossils found in the Red Pine Shale; the microfossil *Bavlinella faveolata*, found throughout much of the Uinta Mountain Group, first appears in the sedimentary record between 750-700 Ma

(Vidal, 1976; Knoll and Swett, 1985). The occurrence of vase-shaped microfossils, yet to be found in definitive post-Sturtian strata, suggest the Red Pine Shale was deposited prior to or during the Sturtian glactiation (Kendall et al., 2009). The Red Pine Shale likely correlates with the Chuar Group of Arizona based on microfossil assemblages, carbon isotope data, and lithologic similarities (Dehler et al., 2007). Since the Chuar Group is ~770 to 742 Ma (Karlstrom et al., 2000; Dehler et al., 2007, 2010) and the formation of Outlaw Trail stratigraphically below the Red Pine Shale has a maximum depositional age of 766+/- 4 Ma, the Red Pine Shale's best age constraint is ~770-742 Ma (Dehler et al., 2010).

2.7 - Geochemistry

Carbon isotope ($\delta^{13}C_{org}$) values from the Red Pine Shale range from -29.46‰ to -16.91‰ PDB, and total organic carbon values range from 0.04% to 5.91%. Combined H/C, total organic carbon, and local-regional isotopic correlations suggest that the strata have undergone little alteration and represent the carbon isotope composition of organic matter in Neoproterozoic oceans. Red Pine Shale carbon isotope and total organic carbon values from three previous studies show no systematic variation when cross-plotted and thus likely represent primary values (Dehler et al., 2007; Myer 2008; Hayes, unpublished data). This suggests minimal thermal alteration, an interpretation also supported by the high (0.68) H/C ratios of the Red Pine Shale (Strauss et al., 1997). Carbon isotope values of the Red Pine Shale are more positive near the base, followed by a long decline to a thick interval

of homogeneous lower values; these values do not appear to correlate with facies changes (Myer, 2008).

2.8- Neoproterozoic Carbon Isotope Records

The Proterozoic Eon records the greatest $\delta^{13}C$ fluctuations known to have occurred on Earth (Kaufman and Knoll, 1995). These isotopic records play a key role in our understanding of the Proterozoic Earth system, yielding essential information about the relationships between paleoclimate, tectonics, biologic evolution and the ancient carbon cycle (Knoll, 2003; Rothman et al., 2003; Bartley and Kah, 2004; Dehler et al., 2005). With the discovery of very large-magnitude $\delta^{13}C$ fluctuations associated with the deposition of "snowball Earth" glaciogenic diamictites, interest in the Neoproterozoic carbon-isotope record increased tremendously (Hoffman et al., 1998), and equally large-magnitude $\delta^{13}C$ shifts have subsequently been documented in older Neoproterozoic strata that lack any sedimentologic evidence of glaciation (Kaufman and Knoll, 1995; Hill and Walter, 2000; Halverson et al., 2002; Corsetti and Kaufman, 2003; Dehler et al., 2005). There is a great interest in determining the cause of the Neoproterozoic isotopic excursions and how – if at all – they may relate to the evolution of early animals (Knoll et al., 1986; Hoffman et al., 1998; Rothman et al., 2003). It is likely that several controls operating on somewhat different time scales influenced Neoproterozoic carbon dynamics, leading to a $\delta^{13}C$ record that is highly variable compared to that of the Phanerozoic and probably the result of a combination of tectonic events, climate change events, biota, and ultimately carbon cycling that are

distinctly Neoproterozoic in nature (Rothman et al., 2003; Bartley and Kah, 2004).

Isotopically light carbon (high in ^{12}C vs. ^{13}C, or low $\delta^{13}C$) in the rock record is a signature of life. The formation of isotopically light carbon compounds by organisms results in distinct carbon reservoirs: 1) the organic carbon reservoir, which is reduced and has relatively low $\delta^{13}C$ values due to its high amount of ^{12}C, and 2) inorganic carbon, which is oxidized and has relatively high $\delta^{13}C$ values due to its low amount of ^{12}C. The carbon isotope fractionation between inorganic carbon and biologic organic carbon is large, and can be used to distinguish between the two types. Today, the typical difference in $\delta^{13}C$ between the two reservoirs ($\Delta^{13}C$) is 23 parts per mil, and it was likely similar in ancient oceans after the evolution of eukaryotes (Hoefs, 2008). Unlike oxygen isotope fractionation, carbon fractionation during carbonate precipitation is very small and virtually unaffected by temperature; this means that the $\delta^{13}C$ values of ancient marine carbonates (if relatively unaltered post-deposition) represent the $\delta^{13}C$ values of the ancient oceans – specifically the $\delta^{13}C$ values of total dissolved carbon (TDC) in the oceans. On timescales of millions to tens-of-millions of years, the $\delta^{13}C$ of TDC in the oceans is controlled by the relative proportions of organic and inorganic carbon in the crustal reservoir, which will vary based on tectonic activity and biologic productivity (Sharp, 2007).

Since the negative excursions of most Neoproterozoic large-magnitude carbon isotopic variations are associated with glaciogenic sedimentary sequences, they have been interpreted as recording alternations between global (or at least

semi-global) glacial conditions and greenhouse conditions for which there is likely no Phanerozoic analogue (Kaufman et al., 1997; Hoffman et al., 1998). Glaciations of this magnitude imply the existence of a very strong climatic gradient, which is very likely to have affected 1) biologic primary productivity, and 2) ocean circulation patterns (Knoll et al., 1986). One possible mechanism for ocean circulation effects on negative carbon-isotope excursions is transfer of dissolved organic carbon from anoxic deep waters to the oceanic dissolved inorganic carbon reservoir (Arthur, 2009). It is likely that during glaciations both primary productivity and organic carbon burial rates decreased significantly, leading to the negative $\delta^{13}C$ shifts observed in the Neoproterozoic. Another possibility is that the partial pressure of oxygen in the Earth's atmosphere at these times had risen to a level that prevented most organic carbon from being buried due to its rapid oxidation (Knoll et al., 1986; Kaufman et al., 2007; Arthur, 2009). This would result in a higher proportion of ^{13}C-depleted dissolved carbon in the oceans, and thus lower $\delta^{13}C$ values in carbonates.

It is important to note the time scales over which the major $\delta^{13}C$ fluctuations associated with glaciogenic strata occur; most of the negative $\delta^{13}C$ excursions and subsequent returns to more positive values happen over tens of millions of years. Between these notable negative $\delta^{13}C$ excursions are periods of relatively positive $\delta^{13}C$ thought to represent an increase in the rate of burial of organic carbon, which also suggests a global shift in oxidation-reduction processes (Knoll et al., 1986; Kaufman and Knoll, 1995). In order for increased burial of organic (reduced) carbon to occur, reducing potential must have been shifted to sulfur, iron and/or

oxygen (Knoll et al., 1986). There is evidence that increased organic carbon burial rates are related to near-synchronous global orogenies that result in enhanced rates of continental erosion, causing increases in the rate of organic sedimentation along with absolute sedimentation (Des Marais, 1997). It has been proposed that the breakup of the Rodinian supercontinent in the Neoproterozoic provided widespread conditions favoring high rates of organic carbon burial, potentially leading to the relatively positive $\delta^{13}C$ values observed in many Neoproterozoic successions (Knoll et al., 1986; Karlstrom et al., 2000; Bartley and Kah, 2004; Dehler et al., 2005; Myer, 2008). Outside of the glaciations, Neoproterozoic rates of organic carbon burial are significantly higher than that observed in the Phanerozoic (Hayes et al., 1999). When this evidence and the relative time scales of the negative vs. positive Neoproterozoic $\delta^{13}C$ "events" are considered, it seems that smaller-scale climate forcings (glaciations) are superimposed upon larger-scale tectonic forcing (changes in organic carbon burial rates).

There is also the possibility that biologic evolution played a role in changing global carbon cycling. Anbar and Knoll (2002) suggest that changes in the availability of redox-sensitive bioessential nutrients may have led to increases in eukaryotic diversity and complexity, perhaps stimulating the production and burial of organic carbon (Bartley and Kah, 2004). In an analysis of ^{13}C abundance in marine organic matter, Hayes et al. (1999) found the Neoproterozoic was characterized by three ranges of $\delta^{13}C_{org}$ attributed to inputs from several different biotic sources. From 800-750 Ma and 685-625 Ma, a signal of maximal fractionation

of carbon isotopes by phytoplankton dominates the record; during the late Neoproterozoic interglacials, there is significant input from sulfide-oxidizing/chemoautotrophic bacteria; during the glacials, carbon isotope fractionation appears to have been reduced, possibly due to low carbon dioxide levels, rapid growth rates, and high cellular volume/surface area ratios (Hayes et al., 1999).

In addition to changes in biota, climate and tectonics, it is likely that the changing dynamics of the carbon cycle itself during Neoproterozoic time contributed to the large-magnitude $\delta^{13}C$ fluctuations. Rothman et al. (2003) hypothesize that the reservoir of organic carbon in the ocean was unusually large during the Neoproterozoic and decreased very slowly (on average) throughout this period, causing the carbon cycle to have large isotopic fluctuations inconsistent with today's steady-state models. They argue that the glaciations resulted in enhanced remineralization of organic carbon and subsequent decreases in the ^{13}C content of the ocean and carbonates until a final decrease (to near-Phanerozoic averages) of the organic carbon reservoir occurred near the Precambrian-Cambrian boundary. Paleontological evidence suggests that this final diminution of the organic carbon reservoir was aided by evolutionary innovations that allowed organisms to remove more organic carbon from the oceans, including enhanced biomineralization, fecal pellets, and the production of resistant biopolymers (Rothman et al., 2003). Bartley and Kah (2004) also cite a long-term decrease in the size of the Proterozoic marine dissolved inorganic carbon reservoir, which would affect the sensitivity of the

isotopic system to biogeochemical changes and permit elevated ^{13}C values to be sustained for relatively long periods (i.e. the Neoproterozoic interglacials).

2.9 – Paleogeography

Evidence from several studies (Wallace and Crittenden, 1969; Farmer and Ball, 1998; Condie et al., 2001; Dehler et al., 2007, 2010; Myer, 2008) indicates that the depositional environment of the Red Pine Shale is a marine deltaic system with streams entering the area from the north and east (Figure 4). The facies in the Red Pine Shale indicate prodelta and delta front environments affected by fluvial, wave, and tidal processes at different times (Myer, 2008). Myer (2008) reported that the northern Red Pine Shale sections are relatively sandier than correlative strata to the south, and that the southern sections also do not contain pebbles, do have slump folds, and contain a higher proportion of mature sandstone than the northern sections. This suggests that the dominant deltaic system must have been fed by rivers from the north. It is interesting to note that the petrography of the sandstone facies in the eastern and southern sections shows a higher percentage of quartz arenite than the northern sections, which are more arkosic; this likely indicates that the eastern and southern sections were also fed by deltaic systems from the east, whereas the northern sections reflect the proximal source to the north (Myer, 2008).

These petrographic data are supported by detrital zircon data (Dehler et al., 2010). A detrital zircon sample from the type section of the Red Pine Shale (a northern section) shows entirely Archean grains, reflecting a fluvial-dominated part

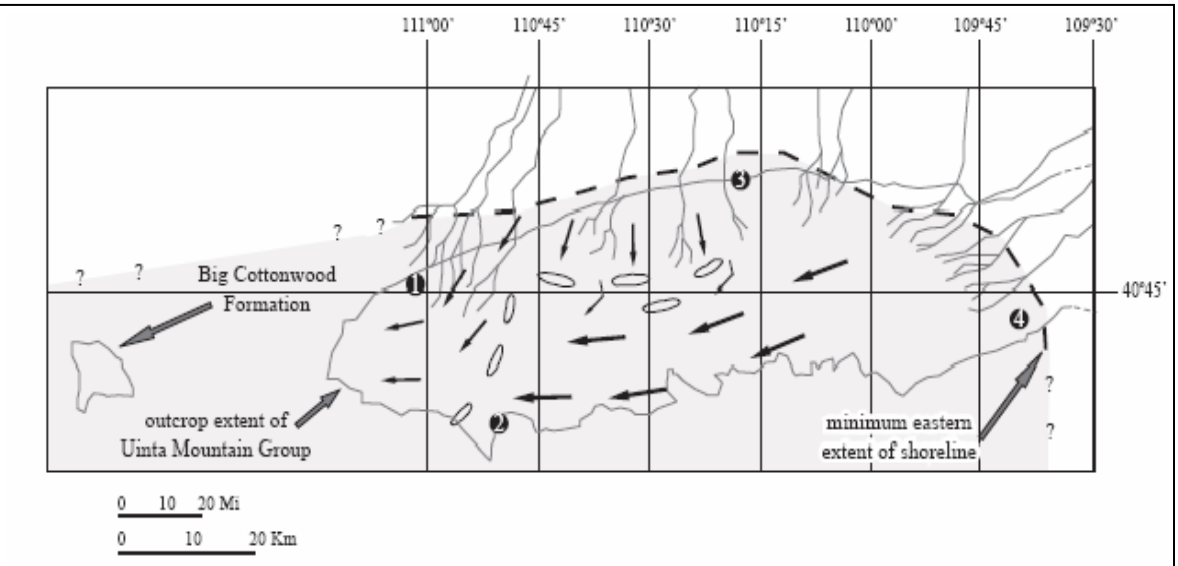

Figure 4. Paleogeography of Uinta Mountain Group basin. UMG basin during deposition of lower Red Pine Shale. Transverse streams brought sediment from the east and north. 1- Type Section, 2-Hades Creek section, 3-Henry's Fork section, 4-Ashley Creek Section. (from Myer, 2008)

of the delta receiving sediment from the Wyoming craton to the north; a sample from the Hades Creek section to the south shows a mixing of Archean grains from the north and east with Proterozoic grains from the east-southeast (Figure 5) (Dehler et al., 2010). This illustrates the link between more compositionally mature sandstone and more distal Proterozoic grains (Myer, 2008). In addition to providing this provenance data, the uranium-lead detrital zircon analyses published by Dehler et al. (2010) also provide a new maximum depositional age constraint on the Uinta Mountain Group of 766+/- 5Ma and significant insights on the mid-Neoproterozoic paleogeographic setting of the Uinta Mountain Group basin and

western Laurentia in general. The new maximum depositional age supports correlation of the Uinta Mountain Group and Chuar Group, strongly suggests a ~742 to 766 Ma nonmagmatic intracratonic extensional phase, and indicates a regional transgression between ~740-770 Ma onto western Laurentia (Dehler et al., 2010).

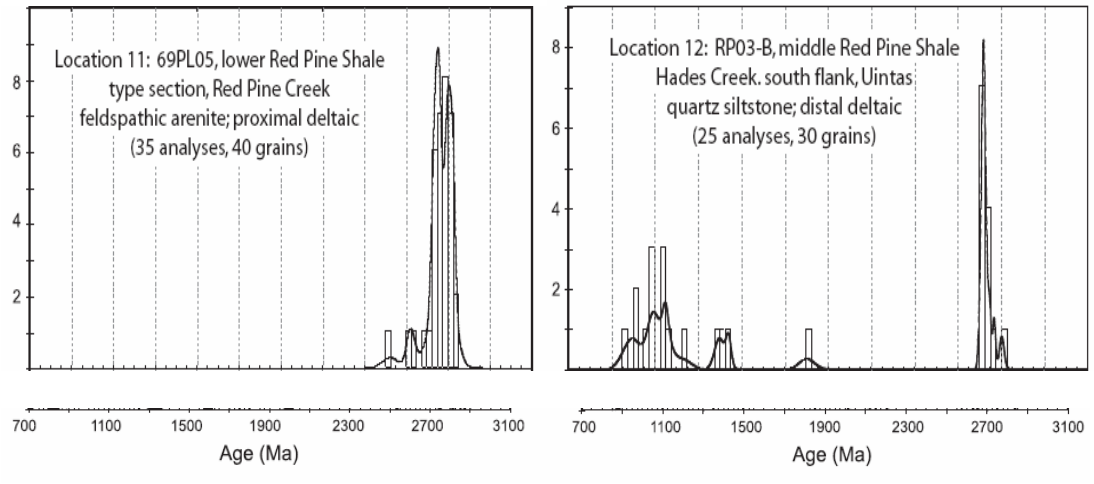

Figure 5. Detrital zircon relative probability plots. Samples are both from the Red Pine Shale (from Dehler et al., 2010)

CHAPTER 3

METHODS

3.1- Field Methods

Five new sections of the Red Pine Shale and shale in the underlying Hades Pass quartzite in the Uinta Mountains of northeastern Utah were measured and described in detail. These localities were selected because they were determined most likely to contain evidence of the hypothesized microfossil transition due to eutrophication. Previous but very limited sampling of the shale in the Leidy Peak area yielded evidence of a change in microfossil assemblage upsection, from ornamented acritarchs to leiosphaerids (Nagy and Porter, 2005). This locality had not yet been studied in detail and had been mapped only very generally and possibly incorrectly (Dehler, pers. comm.). Previously, researchers (Vidal and Ford, 1985) reported a fairly diverse assemblage of microfossil taxa (including some ornamented acritarchs) in shale samples from the Upper Setting Road area, yet the exact location was unknown and the samples were not taken in a stratigraphic context; the intent of this study was to reproduce these results in measured stratigraphic sections. The Box Canyon sections were chosen because they consist of shale stratigraphically below the Type Section in the Hades Pass quartzite, and thus, when combined with the Type Section and correlative Hades Composite section, would yield the most continuous geochemical and paleontological data set available in the upper Uinta Mountain Group. The Type Section and Composite Hades section had already been sampled (although very sparsely) for microfossils,

so one intent of this study was to obtain a more complete higher-resolution paleontological data set from these sections.

Rock samples were collected from these five measured sections using both a uniform and stratified sampling method. Each sample was collected from the smallest stratigraphic interval possible (typically no more than 0.25 vertical meters) to make the sampling as high-resolution as possible. A combined subset of 60 samples from these new sections and others previously measured by Dehler and students was selected for microfossil analysis, carbon mass spectrometry, sulfur mass spectrometry, and iron speciation analysis. Included in these 60 samples are 23 samples from the Type Section locality and 12 from the Hades Creek locality collected between 2001 and 2007 (Myer, 2008). These particular samples were selected to fill in gaps in the paleontological record and to ensure relatively even spacing of iron and sulfur samples within these sections. The remaining samples, collected in 2009, include 13 from the Box Canyon locality, 2 from the Upper Setting locality, and 10 from the Leidy Peak locality (Figure 1, Appendix A, Appendix B).

3.2- Laboratory Methods

Collection and preparation of geochemical samples used the method of Dehler et al. (2005). Approximately 20 grams of shale chips from each sample were cleaned in 10% HCl, rinsed thoroughly in deionized water, brought to a pH of 5.5, and dried in an oven at 50 °C overnight. Rock samples were then crushed in a zirconium shatter box to ~200 mesh, and those powders to be used for organic carbon analysis were rinsed with deionized water until their pH reached 5.5, then

dried. Samples were screened for inorganic carbon at the University of California Riverside geochemistry laboratory using an Eltra Carbon and Sulfur Determinator. Organic carbon mass spectrometer analysis of these samples (~60 samples at 100μg each) was conducted at Brigham Young University to obtain $\delta^{13}C_{org}$ values. Total organic carbon analysis and total sulfur analysis were conducted at the University of California Riverside geochemistry laboratory using an Eltra Carbon and Sulfur Determinator. Sulfur mass spectrometry was conducted at the University of California Riverside for those samples containing sufficient sulfur to determine $\delta^{34}S_{pyrite}$ values. Iron speciation analysis was also conducted at the University of California Riverside to determine the ratio of highly reactive iron (pyrite-derived and dithionite-soluble) to total iron, with the total iron analysis and total aluminum analysis conducted by ALS ChemEx labs in Reno, NV.

3.3- Paleontological Analysis

Microfossil samples were prepared by an independent palynological preparation laboratory (Gerald Waanders, Consulting Palynologist, Encinitas, CA) using standard hydrofluoric acid maceration techniques. The microfossils (both the total kerogen and > 10 micron fraction) were mounted on glass slides for high-powered light microscopy. Light microscopy (400 – 1000x) was used to qualify morphological characters useful for taxonomic identification. Abundance counts (at 400x) were completed by recording the identity of the first 100 fossils encountered using standard point-counting techniques; this number of individuals was counted because it has been reported that no statistically significant difference in population

composition occurs with an increased number of counted individuals beyond 100 (Nagy, 2008). An example of each species encountered was photographed, and England Finder coordinates were recorded to mark the position of the fossil on each of these slides (always with slide label to bottom left).

3.4 – Statistical Analyses

When applicable, statistical tests were conducted on data sets to determine the significance of any trends. For normally-distributed data sets (all $\delta^{13}C$ values), parametric tests were used; these included 1) a paired two-sample t-test of the means (conducted using Microsoft Excel) to compare the $\delta^{13}C$ values obtained for duplicate samples analyzed in two different laboratories and 2) a two-sample t-test (conducted using Microsoft Excel) comparing $\delta^{13}C$ values prior to vs. during a hypothesized carbon-isotope excursion. For non-normally-distributed data sets (all TOC values), nonparametric test were used; these included 1) a Wilcoxon signed-rank test (conducted using the 2007 version of XL Stat in Microsoft Excel) to compare the Myer 2008 TOC values with the Hayes raw and adjusted TOC values for duplicate samples and 2) a Mann-Whitney test (conducted using the 2007 version of XL Stat in Microsoft Excel) comparing TOC values before and after the hypothesized carbon-isotope excursion.

Biologic diversity and evenness of each micropaleontological sample were calculated using Multivariate Statistics Package (MVSP version 3.13q) software utilizing the Shannon Method with a natural logarithm base. A special t-test for

comparing diversity indices was then used, and the calculation was done by hand (Zar, 2010); the formula and calculations for this special t-test are included in Appendix I. Correlations were conducted in Microsoft Excel to examine potential relationships between all geochemical factors; this included correlations of 1) $\delta^{13}C$ vs. TOC, 2) $\delta^{13}C$ vs. sulfur, 3) $\delta^{13}C$ vs. FeHR/FeT, 4) $\delta^{13}C$ vs. Fe/Al, 5) TOC vs. sulfur, 6) TOC vs. FeHR/FeT, 7) TOC vs. Fe/Al, 8) sulfur vs. FeHR/FeT, 9) sulfur vs. Fe/Al, and 10) FeHR/FeT vs. Fe/Al. To determine if microfossil assemblages and relative diversity were facies-dependent, graphs of 1) microfossil assemblage vs. facies type and 2) relative diversity vs. facies type were constructed and interpreted. To determine if geochemical values were facies-dependent, a chi-square analysis (contingency table) was conducted by hand calculations (Zar, 2010); the contingency table and calculations for this test are included in Appendix I.

CHAPTER 4

GEOCHEMISTRY RESULTS

4.1 –Total Organic Carbon Trends

The ranges and average total organic carbon (TOC) values for each measured section are shown in Table 3, and the full data set is displayed in Appendix C. TOC data from the four most complete measured sections is plotted vs. stratigraphic height in each section in Figure 6. The highest individual sample (3.95%) and average TOC (2.01%) values as well as the greatest range in TOC values (0.05-3.95%) are found in the Hades section, followed by the Type Section, where average TOC is 0.77% and TOC ranges from 0.25 – 1.70%). These results are fairly consistent with those reported in a previous study of these sections (Myer, 2008). The Leidy Peak, Box Canyon, and Upper Setting sections show relatively low average TOC values (≤0.46%) with limited variability (≤0.00-0.46%); these sections have not been studied by previous researchers.

Table 3. Total organic carbon (TOC) averages and ranges by section

Stratigraphic Section	Range of TOC values (weight %)	Average TOC value (weight %)
Type Section	0.25% - 1.70%	0.77%
Composite Hades	0.05% - 3.95%	2.01%
Box Canyon B	0.42% - 0.82%	0.66%
Box Canyon C	0.00% - 0.46%	0.46%
Leidy Peak	0.08% - 0.30%	0.18%
Upper Setting A	0.22% - 0.44%	0.33%

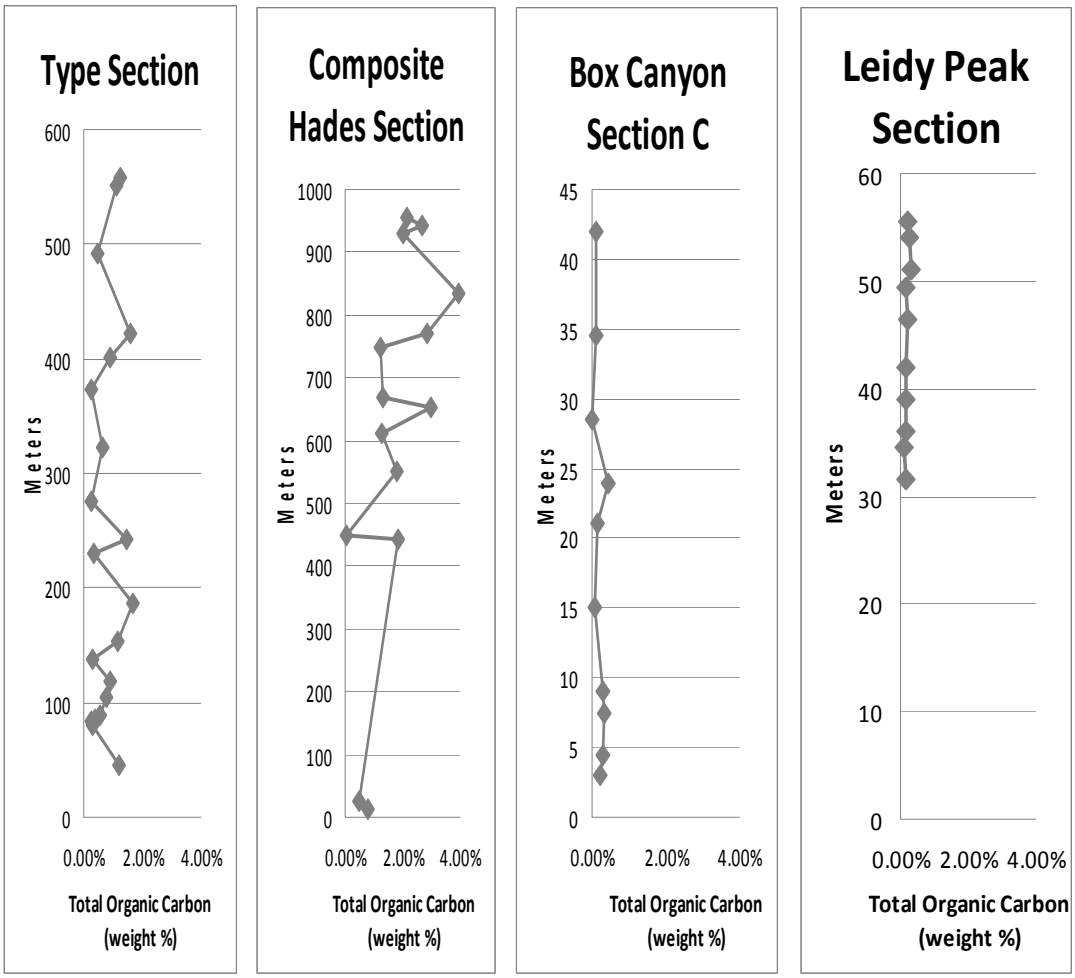

Figure 6. Total organic carbon trends

4.2- Carbon Isotope Trends

The range and average $\delta^{13}C_{org}$ data for each measured section are shown in Table 4, and the full data set can be viewed in Appendix D. $\delta^{13}C_{org}$ data from the four most complete measured sections is plotted vs. stratigraphic height in each section in Figure 7. With the exception of the Upper Setting A section (which includes only two samples), all of the measured sections show significant $\delta^{13}C_{org}$ variability (at

least 2.88 parts per mil). The highest $\delta^{13}C_{org}$ variability occurs in the Box Canyon B and Type Sections (~10 parts per mil). In the Type Section, the values change dramatically near the base of the section, from ~-24 to ~-19 part per mil, then change quickly to ~-26 parts per mil; this excursion occurs over just a few meters, and it is followed by several hundred meters of more consistent values (~-25 to -27 parts per mil) before increasing to ~-20 around 400 meters in the section and then decreasing to ~-29 near the top of the section. The bottom half of the Composite Hades sections shows relatively static values (~-24 to -25 parts per mil), with a slight decrease (to ~-28) above 600 meters followed by a steady increase at the top of the section to ~-26 parts per mil. Although the Box Canyon B section contains only two data points, it records the largest change in $\delta^{13}C_{org}$ seen in any of the sections; this change (from -22.20 to -32.20 parts per mil) occurs over a stratigraphic interval of only 4 meters. The bottom half of Box Canyon section C shows a decline in $\delta^{13}C_{org}$ from -21.5 to ~-26 parts per mil, followed by an increase in the upper half of the section to a final value of ~-23 parts per mil. In the Leidy Peak section, $\delta^{13}C_{org}$ values vary by 2.88 parts per mil, fluctuating back and forth several times throughout the section between ~-23 and -~-25 parts per mil. The two $\delta^{13}C_{org}$ values from the Upper Setting section differ by only 0.3 parts per mil.

Table 4. $\delta^{13}C_{org}$ averages and ranges by section

Stratigraphic Section	Range of $\delta^{13}C_{org}$ values (parts per mil VPDB)	Average $\delta^{13}C_{org}$ value (parts per mil VPDB)
Type Section	-19.70 to -29.34	-25.29
Composite Hades	-24.79 to -28.27	-26.73
Box Canyon B	-22.20 to -32.20	-27.20
Box Canyon C	-21.50 to -26.19	-24.68
Leidy Peak	-22.72 to -25.60	-24.08
Upper Setting A	-25.30 to -25.60	-25.45

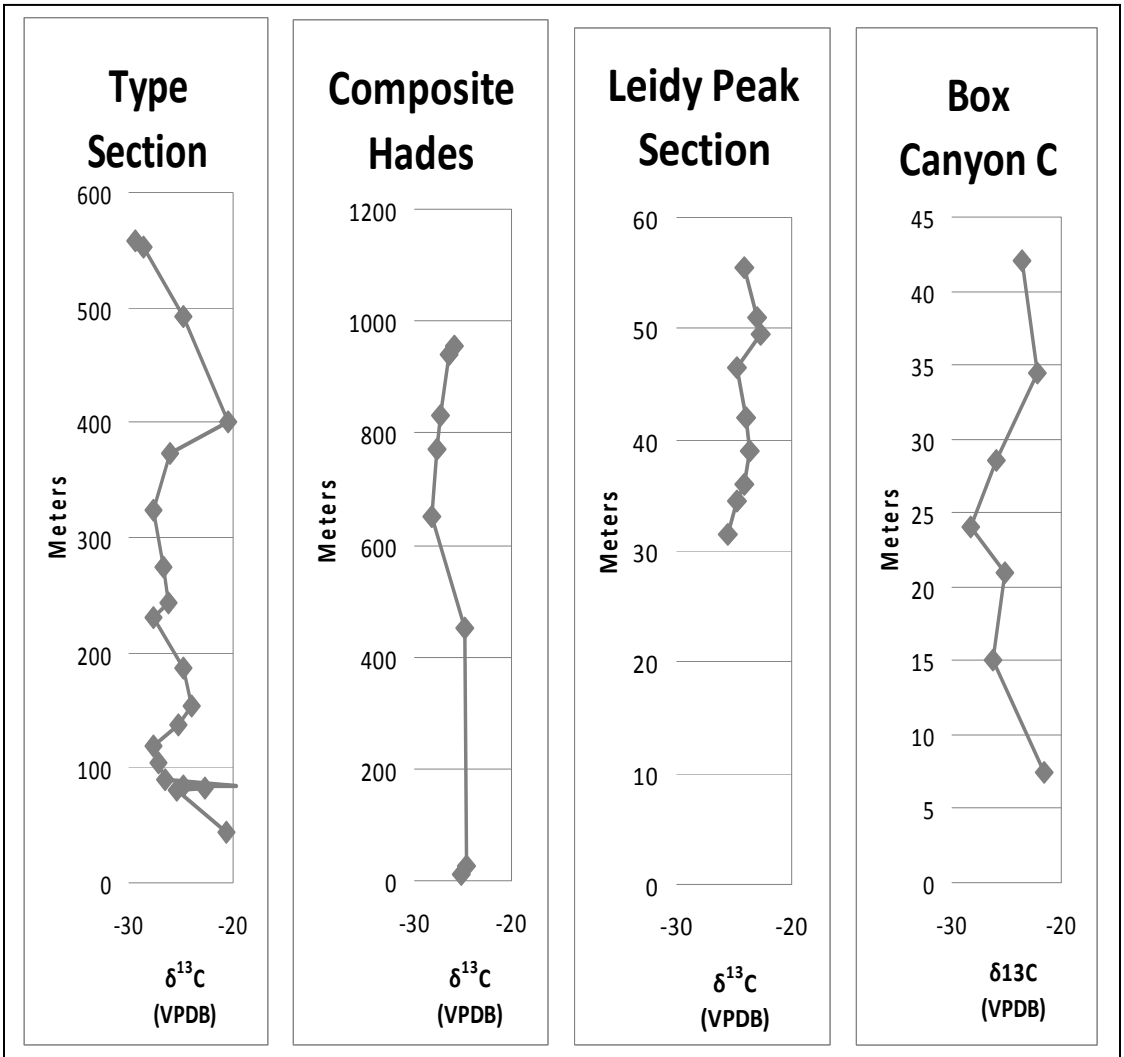

Figure 7. $\delta^{13}C_{org}$ trends

4.3- Iron Speciation Trends

The range and average iron speciation data (highly reactive to total iron ratios, or FeHR/FeT) for each measured section are shown in Table 5, and the full data set can be viewed in Appendix F. Iron speciation data from the four most complete measured sections is plotted vs. stratigraphic height in each section in Figure 8. As expected, the highest ranges of FeHR/FeT values are found in the longest stratigraphic sections with the greater number of data points (Composite Hades and Type Section), and the lowest ranges occur in the shortest stratigraphic sections with the least number of data points (Box Canyon B and Upper Setting A). The highest average FeHR/FeT values occur in the Type Section and the lowest in the Box Canyon B section, but the range of these averages (0.13-0.17) is very small, such that they are not significantly different from one another. Since all of the FeHR/FeT values fall below 0.38, it is likely that they indicate deposition in an oxygenated water column (Raiswell and Canfield, 2005). However, it is also possible that these relatively low FeHR/FeT values could instead be a function of high siliciclastic input during deposition in an anoxic/euxinic water column; in this case, analysis of total iron to total aluminum ratios can be used to provide independent evidence of iron enrichment/enhanced iron deposition from an anoxic water column (Lyons and Severmann, 2006).

Table 5. Iron speciation (FeHR/FeT) averages and ranges by section

Stratigraphic Section	Range of FeHR/FeT values	Average FeHR/FeT value
Type Section	0.11-0.23	0.17
Composite Hades	0.08-0.26	0.14
Box Canyon B	0.12-0.15	0.13
Box Canyon C	0.14-0.20	0.16
Leidy Peak	0.13-0.20	0.16
Upper Setting A	0.15-0.18	0.16

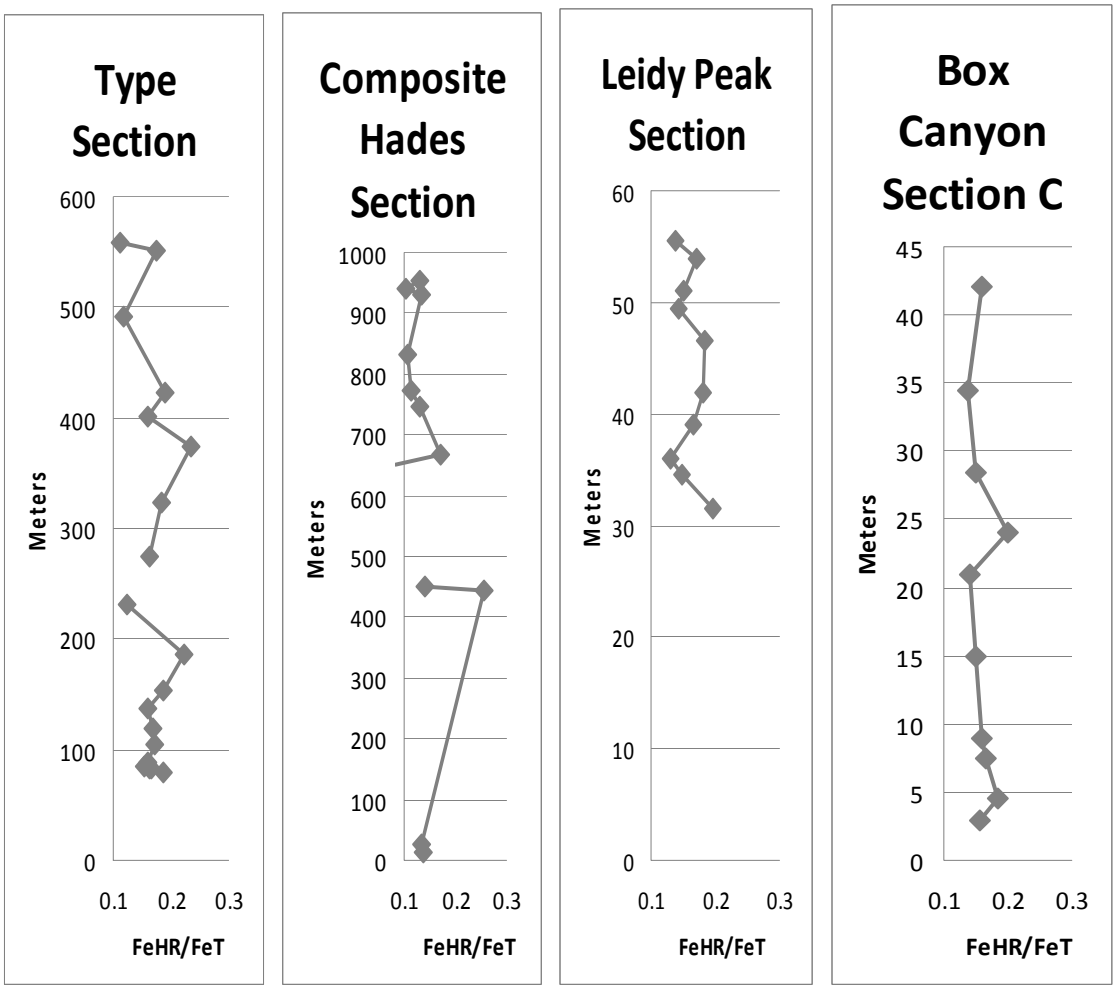

Figure 8. Iron speciation trends. Ratio of highly reactive iron (FeHR) to total iron (FeT) in the four most complete measured sections.

4.4- Total Iron vs. Total Aluminum

The range and average total iron/total aluminum ratios for each measured section are shown in Table 6 (Fe/Al values), and the full data set can be viewed in Appendix G. Iron vs. aluminum data from the four most complete measured sections is plotted vs. stratigraphic height in each section in Figure 9. In these four sections, the highest range of Fe/Al values occurs in the Type Section (0.11-0.79), followed by the Composite Hades section (0.10-0.57). The Box Canyon C section shows Fe/Al variability only slightly lower than that in the Hades section (0.14-0.56), and the Leidy Peak section is by far the least variable, with a Fe/Al value range of only 0.19-0.38. The highest average Fe/Al ratio (0.44) occurs in the Upper Setting A section (only two samples), followed closely by that of the Type Section (0.43). Since Fe/Al values of 0.60 or less are commonly found in oxic depositional environments (Lyons and Severmann, 2006), it is likely that almost all of the samples in this study represent deposition in an oxygenated water column. There are, however, four values in the Type Section that exceed 0.60, suggesting enhanced Fe deposition from an anoxic water column (Lyons and Severmann, 2006). These four >0.60 Fe/Al values occur in the stratigraphic interval between ~230 and 374 meters in the Type Section; the highest Fe/Al value reported in the Composite Hades section (0.57) occurs at ~450 meters.

Table 6. Total iron to total aluminum ratios by section

Stratigraphic Section	Range of total Fe/Al values	Average total Fe/Al value
Type Section	0.11-0.79	0.43
Composite Hades	0.10-0.57	0.24
Box Canyon B	0.38-0.40	0.39
Box Canyon C	0.14-0.56	0.34
Leidy Peak	0.19-0.38	0.31
Upper Setting A	0.35-0.52	0.44

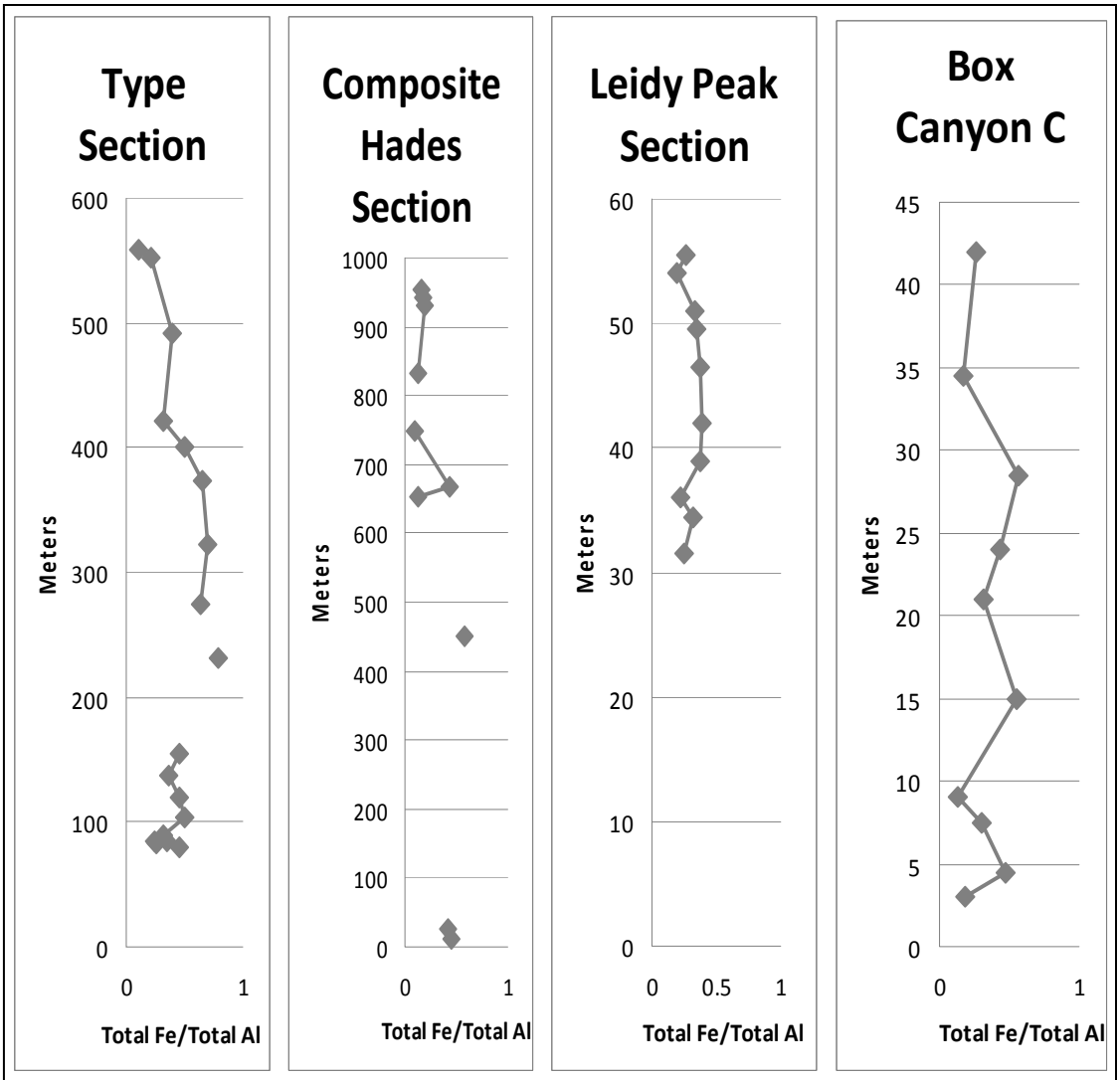

Figure 9. Total iron to aluminum ratios

4.5- Total Sulfur

The range and average total sulfur values (weight %) for each measured section are shown in Table 7, and the full data set can be viewed in Appendix E. Total sulfur values were not plotted vs. stratigraphic height because most of the total sulfur values in the 60 samples were negligible (essentially zero) and not significantly different from one another. The exception, the Type Section, shows an average sulfur value of 0.17 weight percent and by far the highest range in total sulfur values (0.00-0.97 weight %). The Type Section shows four nonzero total sulfur values that constitute two "sulfur spikes," one between 187 and 243 meters in the section (range of 0.50-0.97 weight % sulfur) and another between 401 and 422 meters in the section (range of 0.30 – 0.78 weight % sulfur).

Table 7. Total sulfur averages and ranges by section

Stratigraphic Section	Range of total sulfur values (weight %)	Average total sulfur value (weight %)
Type Section	0.00-0.97%	0.17%
Composite Hades	0.00-0.19%	0.09%
Box Canyon B	0.01-0.05%	0.03%
Box Canyon C	0.00-0.03%	0.01%
Leidy Peak	0.00-0.02%	0.01%
Upper Setting A	0.00%	0.00%

CHAPTER 5

MICROPALEONTOLOGICAL RESULTS

5.1- Assemblage Descriptions

Fossil assemblages from the Red Pine Shale and other Uinta Mountain Group shale units are classified according to the following three characteristics: type of assemblage, relative abundance of specimens, and relative diversity of taxa. Relative abundance falls into three categories: high (over 100 specimens), average (50-99 specimens), and low (less than 50 specimens). Relative diversity also falls into three categories: high (4 or more taxa), average (3 taxa), and low (only 1 or 2 taxa). Three types of assemblages are found: 1) a "*Leiosphaeridia*" assemblage dominated by specimens of the genus *Leiosphaeridia* (Figure 10), containing all unornamented and originally spherical acritarchs, excluding the ornamented new genus *Operculasphaeridium* (Figure 11), formerly known as "*Leiosphaeridia sp. A*" (Nagy, 2008). Ornamented acritarchs may also be present in the "*Leiosphaeridia*" assemblage, but they account for less than half of the specimens in the abundance counts; 2) a "*Bavlinella*" assemblage, dominated by *Bavlinella faveolata/ Sphaerocongregus sp*. (Figure 12) and often entirely monospecific, and 3) "barren" assemblages that preserve mostly amorphous organic material with little to no identifiable taxa. Since these "barren" samples often do preserve a significant amount of organic material, it is likely that they are not barren because of a preservational bias but instead represent the true absence of taxa from the environment (Nagy, 2008).

Of the 55 samples analyzed from the Uinta Mountain Group for this study, 18 are barren, 14 preserve a *Bavlinella* assemblage, and 23 preserve a *Leiosphaeridia* assemblage (see Table 8 for a general summary by locale); the full data set for these 55 samples can be found in Appendix H. In Appendix H, taxa other than those described in the paragraph above are identified and counted, including filaments (Figure 13), an unidentified ornamented specimen (Figure 14), a colonial form (possibly *Satka* or *Ostiana*, Figure 15), and *Eosynechococcus moorei* (Figure 16). These taxa occur in relatively small proportions compared to *Bavlinella* and *Leiosphaeridia*, and they are not used to characterize assemblage type but are included in relative diversity and relative abundance estimates.

The Box Canyon locale contains a mixture of barren, *Bavlinella*, and *Leiosphaeridia* assemblages but is dominated by *Leiosphaeridia*. The Hades Composite section (Lower Hades, Hades A, and Hades C) also contains a mixture of the three assemblage types but the *Bavlinella* assemblage is predominant. The Type Section locale contains all three assemblages, and they are fairly evenly distributed (3 barren samples, 4 *Bavlinella*, and 3 *Leiosphaeridia*). The Leidy Peak section contains only the *Leiosphaeridia* assemblage.

5.2- Relative Abundance

With the exception of the Upper Setting Road samples (which were completely barren), all locales show some variation in species abundance throughout the section. At the Box Canyon and Hades locales, abundance fluctuates back and forth between 0 (barren) low, average, and high. In the Type Section

abundance is either 0 (barren), low, or high. At Leidy Peak, there are no barren samples and abundance ranges from low to high. The highest fossil abundances occur in the Hades and Leidy Peak sections, yet these represent different assemblages; in the Hades section, a high-abundance *Bavlinella* assemblage dominates while the Leidy Peak section contains only the *Leiosphaeridia* assemblage.

Table 8. Summary of paleontological data by locale

Locale	**Number of samples**	**Dominant assemblage type(s)**	**General abundance of specimens**	**General diversity of taxa**
Box Canyon	13	*Leiosphaeridia*	Low – high	Average
Type Section	10	*Leiosphaeridia* (lower) *Bavlinella* (upper)	Low (*Leiosphaeridia*) to high (*Bavlinella*)	Average (lower in section) to low (higher in section)
Composite Hades	13	*Leiosphaeridia* (lower) *Bavlinella* (upper)	Low (*Leiosphaeridia*) to high (*Bavlinella*)	Low
Leidy Peak	10	*Leiosphaeridia*	High	Average - high
Upper Setting Road	8	Barren	0	---

5.3- Relative Diversity

In the Box Canyon sections, relative diversity ranges from low to average. At the Hades locales, relative diversity is low, with monospecific *Bavlinella*

assemblages dominating the section. In the Type Section, relative diversity is average lower in the section and then decreases in the *Bavlinella*-dominated upper part of the section. At Leidy Peak, relative diversity fluctuates throughout the section, ranging from low to high. Since the Upper Setting Road samples are barren, it is not possible to characterize relative diversity in these sections.

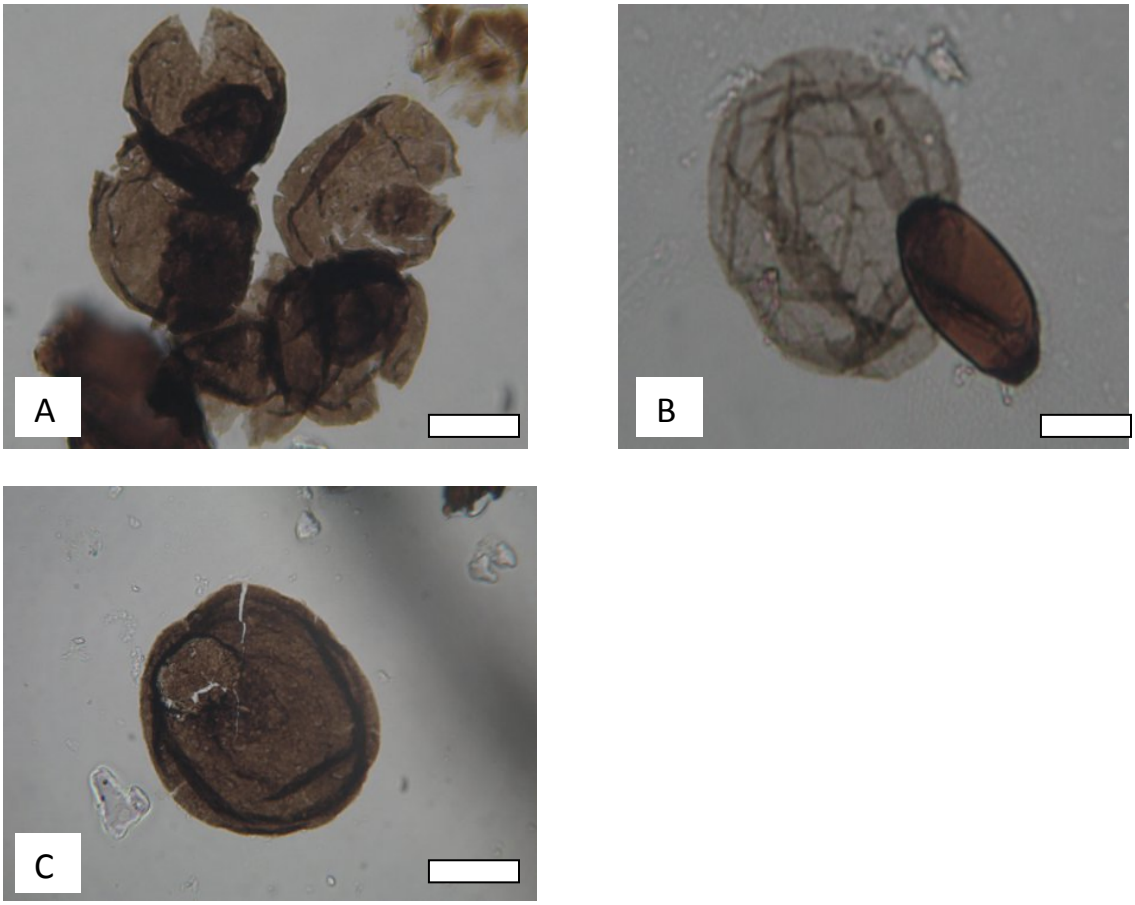

Figure 10. Unornamented acritarchs of the genus *Leiosphaeridia.* A) four specimens grouped B) thin-walled specimen with *E. moorei* (DHLPA1, slide 11, E31)B) a thick-walled specimen. All scale bars represent 10 µm.

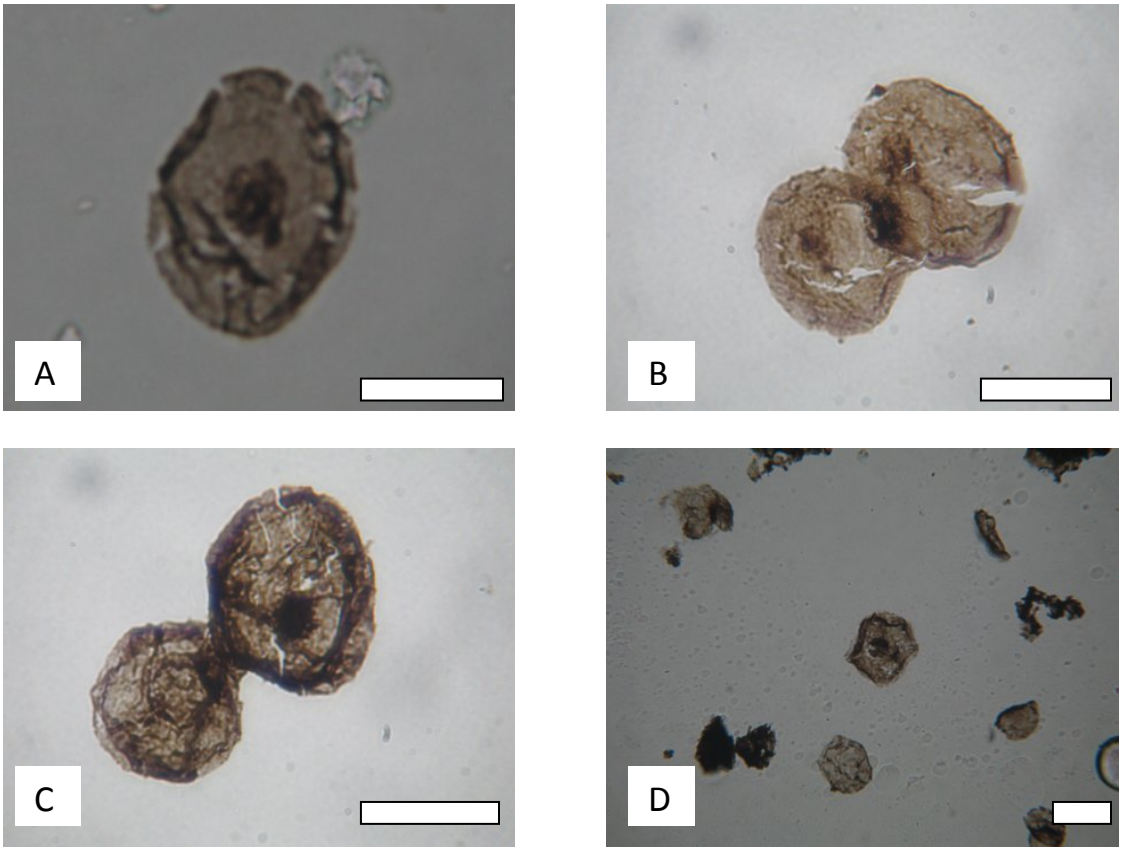

Figure 11. Ornamented acritarchs *Operculasphaeridium/Leiosphaeridia sp. A.* A) single specimen, showing detail of operculum B) joined specimens (DHLPA13, slide 17A, H29) C) joined specimens (DHLPA14, slide 18B, P24) D) single specimen with several unornamented *Leiosphaeridia*. All scale bars represent 10 µm.

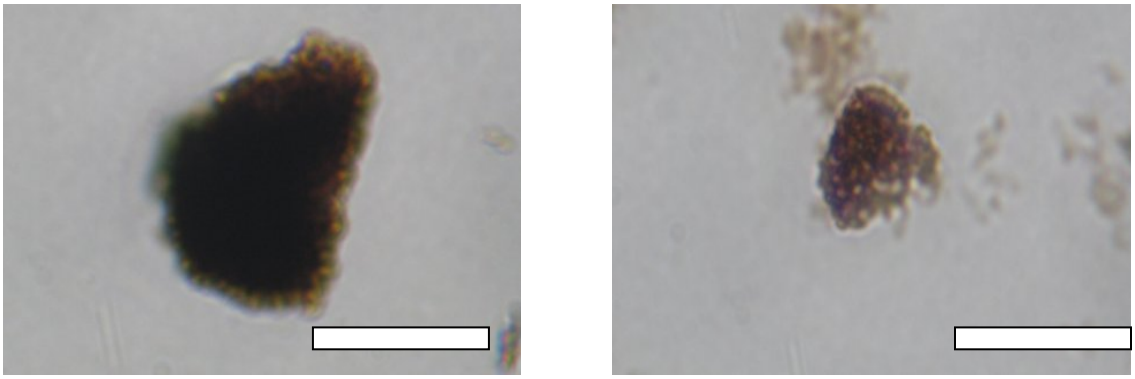

Figure 12. ***Bavlinella faveolata/ Sphaerocongregus sp.*** **A) specimen from the Type Section (RPO1A85), with high amount of thermal alteration B) less thermally altered specimen from the Hades section (HADES9) Scale bars represent 10 µm.**

Figure 13. Filaments, scale bar =10 µm.

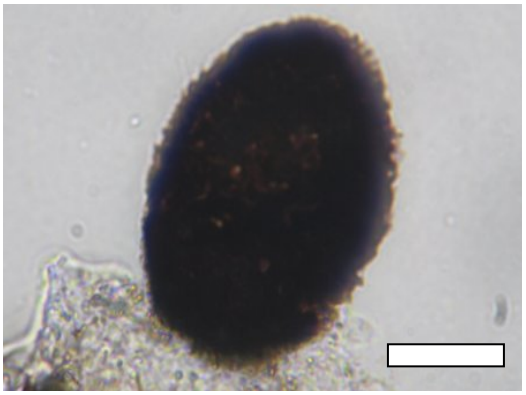

Figure 14. Unidentified possibly ornamented specimen (TS70601, slide 42A, L26). Scale bar= 10 µm.

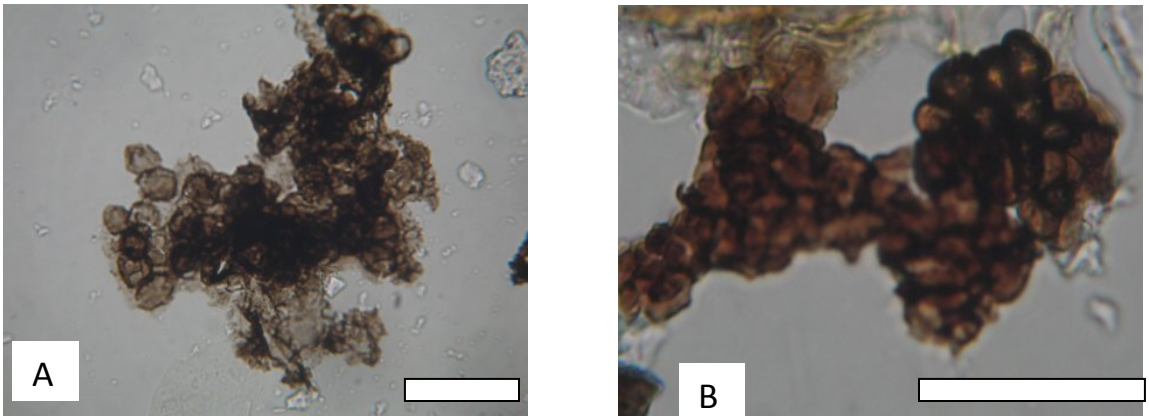

Figure 15. Colonial forms, possibly *Satka* or *Ostiana*. Scale bars represent 10 µm.

Figure 16. *Eosynechococcus moorei* (direct center of slide) scale bar = 10 µm.

CHAPTER 6

STRATIGRAPHIC RESULTS

6.1- Physical & Sequence Stratigraphy

Detailed stratigraphic columns from the Box Canyon B, Box Canyon C, Leidy Peak, Upper Setting A, and Upper Setting B sections are displayed in Appendix B; a table summarizing the facies present in these sections, the Type Section, and the Composite Hades section is included below (Table 9). General stratigraphic columns for the four most complete measured sections included in this study are presented in Figure 17. In Figure 17, the correlation between the Type Section and Composite Hades sections approximates that made by Myer (2008) based upon facies associations, the basal contact with the underlying Hades Pass quartzite, total organic carbon trends, and carbon-isotope trends. The correlation between the Box Canyon/Type Section, Composite Hades section, and Leidy Peak sections is tentative when based solely upon lithology and physical stratigraphy; the Leidy Peak section directly overlies the Hades Pass quartzite/Red Pine Shale contact, as do the basal Type Section and Composite Hades sections. The Type Section and Composite Hades section, however, contain more thin sandy intervals than the Leidy Peak section; additionally, the Leidy Peak section contains sedimentary features (ripple marks, mudcracks, and evaporite casts) neither found in the basal Type Section nor the basal Composite Hades section. Since the Type/Box Canyon section and the Hades section are in the western part of the Uinta Mountains and the Leidy Peak section is located well to the east, it is likely that they represent slightly different depositional environments in the same system; the western shale was probably

deposited in a deltaic setting more proximal to fluvial input from the north, while the Leidy Peak shale was likely deposited in a shallower estuarine or delta plain setting. It is also possible that the basal Type Section and Composite Hades shale units are not time equivalent to the Leidy Peak shale units, and if not, the former units are likely younger.

Table 9. Summary of facies by locale

Locale	Section thickness (m)	Description of General trends	Facies present	Interpreted depositional setting
Type Section	~560	Decrease in % sandstone upsection, but missing top of section due to erosion (Myer, 2008)	Shale	Distal prodelta
			Shale-and-sandstone	Delta front, prodelta
			Sandstone	Delta front
			Concretion	Distal prodelta
			Slump fold	Proximal prodelta, delta front
			Pebbly sandstone	Delta front
Composite Hades Section	~1000	Increase in % sandstone at top of section	Shale	Distal prodelta
			Shale-and-sandstone	Delta front, prodelta
			Sandstone	Delta front
			Slump fold	Proximal prodelta, delta front
Leidy Peak	~60	Increase in % sandstone at top of section	Shale	Delta plain or estuarine
			Sandstone	Delta plain or estuarine
Box Canyon B & C	~45	Lower section more sandy; upper section mostly shale w/ pebble sandstone at top	Shale	Distal prodelta
			Shale-and-sandstone	Delta front, prodelta
			Pebbly sandstone	Delta front
Upper Setting A	~8	Decrease in % sandstone at top of section	Shale-and-sandstone	Delta front, prodelta

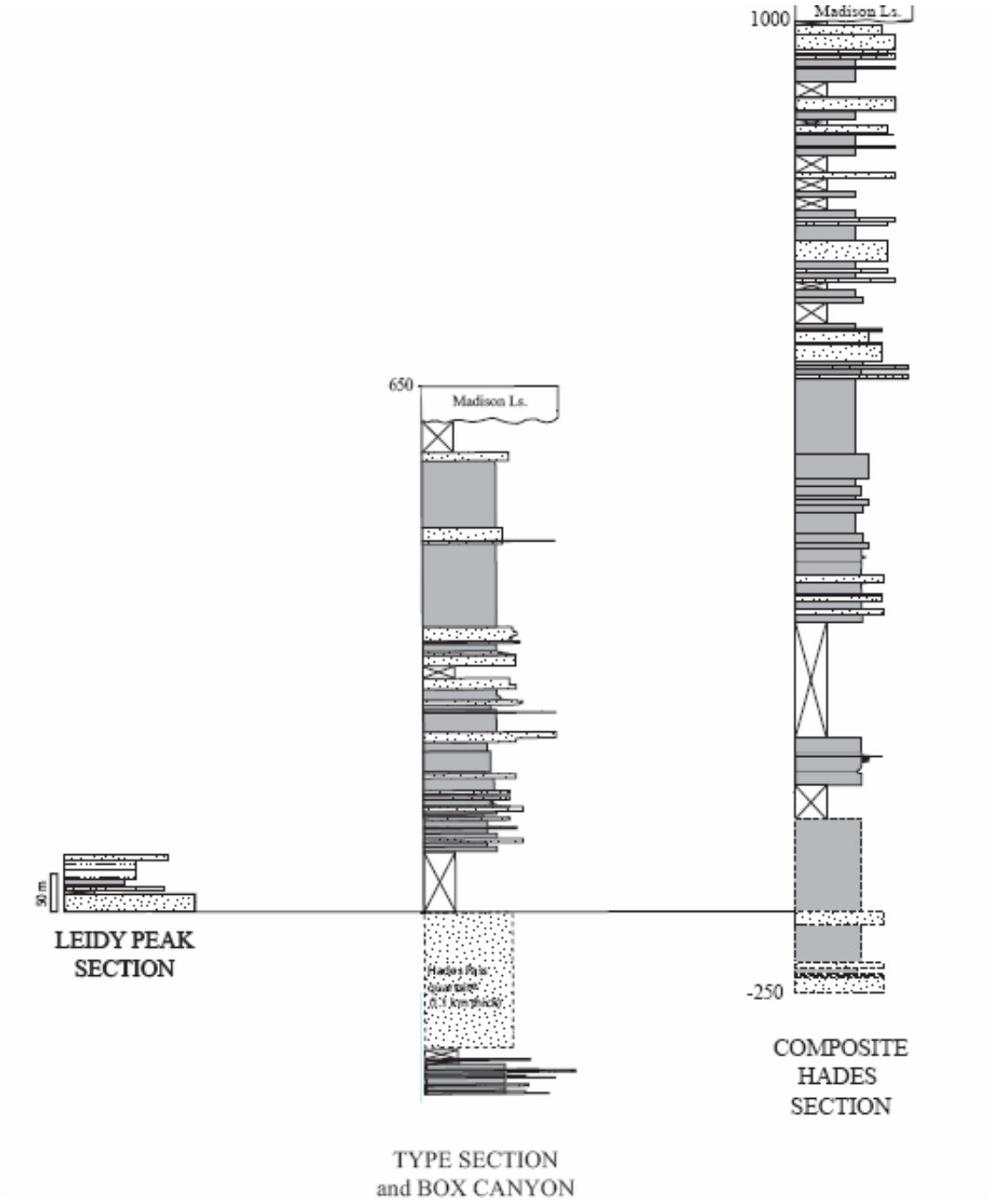

Figure 17. Generalized stratigraphic columns and correlations (Box Canyon section lies stratigraphically below the Type Section; they are separated by 1.1 km of the upper Hades Pass quartzite). Correlation between the Type Section and Hades section from Myer, 2008. Correlation with the Leidy Peak section is tentative.

Since the contact between the Red Pine Shale and the underlying Hades Pass quartzite is apparently gradational, any sequence stratigraphy of the Red Pine Shale must include consideration of the Hades Pass quartzite. Kingsbury (2008) places a sequence boundary at the base of the Hades Pass quartzite, and together the Hades Pass quartzite and Red Pine Shale likely represent one lower-order cycle (Myer, 2008). Some of the stratigraphic patterns observed in the Box Canyon and Leidy Peak sections support the idea of a gradational contact between the Hades Pass quartzite and Red Pine Shale. It is likely that both the Box Canyon shale units were deposited during a minor transgression that preceded the more major transgression recorded in the lower part of the Red Pine Shale, and other thinner shale units in the upper Hades Pass quartzite also represent a gradual transition in which minor transgressions (resulting in shale deposition) and regressions (resulting in sandstone deposition) alternated several times before the deposition of the lower Red Pine Shale.

6.2- Chemostratigraphy

In the Type Section and Composite Hades section, a general relationship between the physical stratigraphy and $\delta^{13}C$ values is present; in the portions of the sections that contain a higher ratio of shale to sandstone, $\delta^{13}C$ values are generally less negative, and in the sandier intervals, $\delta^{13}C$ values are typically more negative (Figure 18). This relationship was also noted by Myer (2008) in the Red Pine Shale. In the Leidy Peak section (Figure 18), the same relationship between shale to sandstone ratios and $\delta^{13}C$ values cannot be observed because this relatively short section contains no interbedded shale-and-sandstone facies. The general $\delta^{13}C$ trend

at Leidy Peak is less negative upsection through the clay and siltstone. Total organic carbon values at Leidy Peak are relatively low throughout the section, do not vary significantly, and do not show a distinct stratigraphic pattern. The Composite Hades section $\delta^{13}C$ values also lack a distinct stratigraphic pattern, but unlike those at Leidy Peak, they are relatively high and variable (Figure 18). A significant amount of total sulfur is not found in any locale except the Type Section. At this locale, however, there are two "sulfur spikes" (one at ~250 meters, and one at ~425 meters), both of which appear to correspond with the highest TOC values found in the section.

Iron speciation values in all of the sections are relatively low, do not vary significantly, and do not show any distinct stratigraphic patterns. All FeHR/FeT ratios are well below 0.38, indicating either 1) deposition in an oxygenated water column, or 2) deposition in anoxic/euxinic water with very high amounts of silicilastic input. In the Leidy Peak section, total iron to aluminum (Fe/Al) ratios show a similar lack of variability, and no stratigraphic patterns emerge. In the Type Section and Composite Hades sections, however, there are a few notable relationships between physical stratigraphy and Fe/Al ratios. In the Composite Hades section, there appears to be an interval of relatively high Fe/Al that occurs near 450 m in the section. Although the Fe/Al value at this point in the section does not exceed 0.60 (the typical high end of the Fe/Al range for oxygenated waters), it closely approaches this (0.57) and is relatively high compared to other parts of the Composite Hades section. In the Type Section, there is a sustained interval of relatively high Fe/Al ratios (all above 0.60) between ~200 and 400 m in the section,

strongly suggesting deposition under anoxic conditions with a high amount of silicilastic material.

6.3- Biostratigraphy

The biostratigraphy of the Leidy Peak section is relatively uniform, with the *Leiosphaeridia* fossil assemblage persisting throughout the entire section (Figure 18). It is noteworthy that, although the unornamented acritarch assemblage dominates this section, Leidy Peak is the only locale where any ornamented acritarchs were found in this study. These ornamented acritarchs (*Leiosphaeridia sp. A/ Operculasphaeridium*) occur in the upper part of the Leidy Peak section, in the interval between 49.5 and 55.5 meters in the section.

In the Box Canyon/Type Section (Figure 18), the *Leiosphaeridia* assemblage dominates the Box Canyon portion of the section, although a few samples were barren and one contained a *Bavlinella* assemblage; higher in this section (the Type Section portion above the Hades Pass quartzite) this *Leiosphaeridia* assemblage continues to dominate, but is then replaced by *Bavlinella* assemblages containing vase-shaped microfossils. It is interesting to note that this shift to the *Bavlinella*/VSM-dominated assemblage coincides with the first rise in total sulfur values in the Type Section (beginning at ~150 m) and also with the interval of elevated Fe/Al ratios (~200 – 375 m in the Type Section).

In the part of the Composite Hades section (Figure 18) that likely correlates with the top of the Type Section, a *Bavlinella* assemblage is found in one sample(~440 m), then a shift to a lower-diversity *Leiosphaeridia* assemblage that persists from ~450 to 550 m, and then another shift back to a *Bavlinella* assemblage

that persists through the top of the section. Similar to the pattern seen in the Type Section, this second transition from a *Leiosphaeridia* to a *Bavlinella* assemblage in the Composite Hades section coincides with a slight rise in Fe/Al ratios.

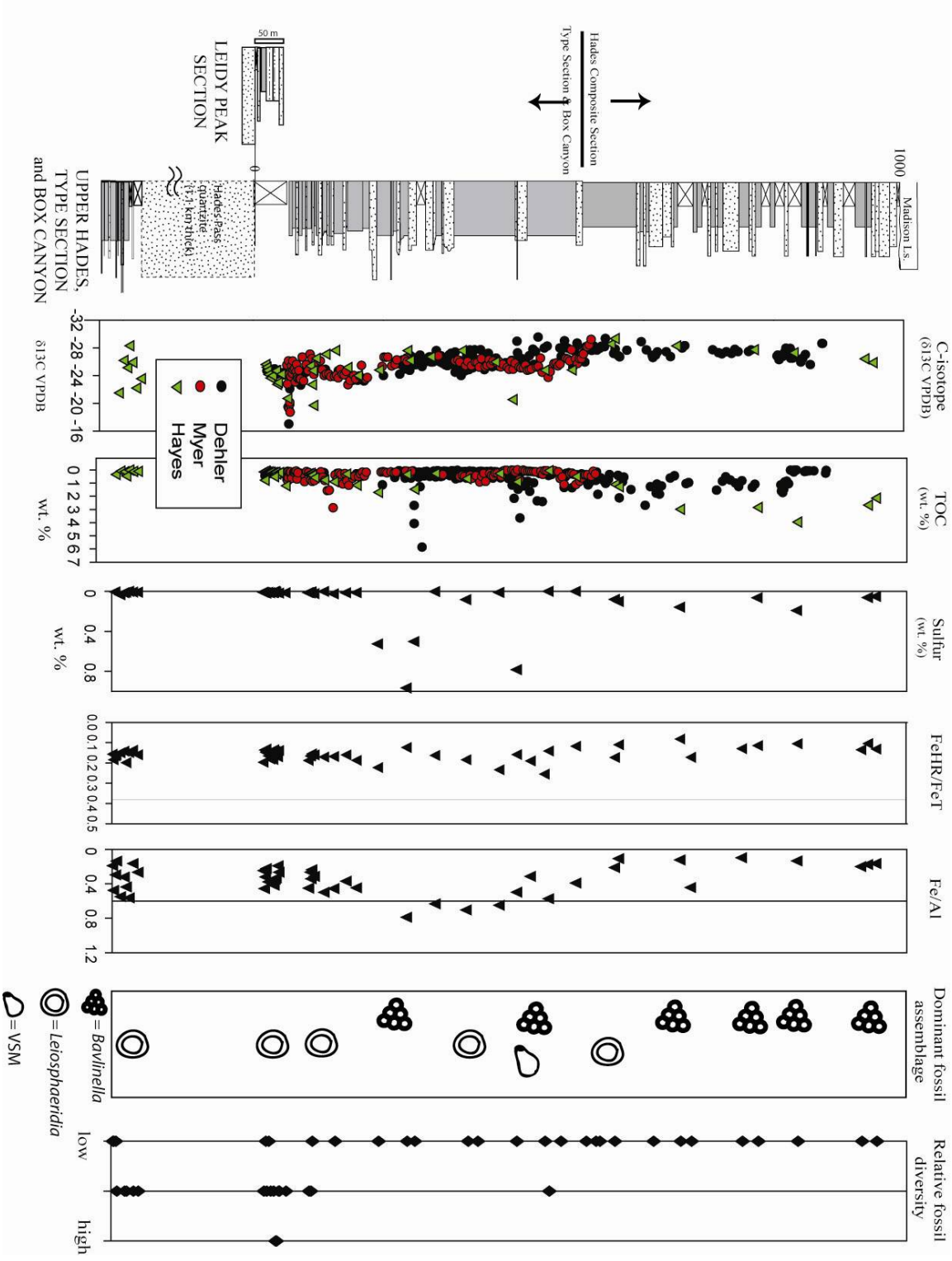

Figure 18. Composite geochemical and biostratigraphic trends

CHAPTER 7

RESULTS OF STATISTICAL ANALYSES

7.1- $\delta^{13}C$ and TOC Standards and Duplicate Samples

Three different commonly used carbon-isotope standards ("lsvec," "UCLA," and "asp1") were included in the carbon-isotope analysis of the 60 samples in this study in order to determine instrumental error. The mean values and error calculated for each of these standards are as follows: 1) for "lsvec", mean $\delta^{13}C$ = -45.6 parts per mil and error = 0.2, 2) for "UCLA", mean $\delta^{13}C$ = 2.5 parts per mil and error = 0.3 , and 3) for "asp1", mean $\delta^{13}C$ = -27.4 parts per mil and error = 0.3.

Of the 60 samples analyzed for carbon-isotopes and total organic carbon (TOC), 24 had been analyzed previously in a different laboratory, and thus it was possible to compare the values obtained in one laboratory versus another for the same sample. A list of these 24 duplicate samples and their carbon-isotope values from both laboratories is included in Appendix I. A paired Student's t-test of the mean $\delta^{13}C$ values indicates that the two sets of means (Myer 2008; Hayes, unpublished data) are not significantly different from one another at the 0.05 confidence level (Appendix I), and thus they may be compared directly and included in the same data set without a correction. A Wilcoxon signed-rank test was used to compare the TOC values from one laboratory (Myer, 2008) to another (Hayes, unpublished data) for the 24 duplicate samples. This test showed that the TOC values for the Hayes 2010 samples were, on average, 0.20 parts per mil higher than those for the Myer 2008 samples, and thus the Hayes 2010 TOC values were

adjusted (decreased by 0.20) before being compared directly and included in the same data set as the Myer 2008 samples. A second Wilcoxon signed-rank test (with a 0.05 confidence level) of the Myer 2008 and Hayes 2010 adjusted TOC values showed that the adjusted 2010 values followed the same distribution as the Myer 2008 values (Appendix I).

7.2- Biologic Diversity

Calculations of diversity indices for the 60 samples in this study yielded a range of diversity index values, from zero to 1.04 (Appendix I). Species evenness ranged from zero to 0.998, and the number of species per sample ranged from zero to 6 (Appendix I). A special t-test for comparing two diversity indices showed that diversity in the lower part of the composite stratigraphic section (prior to the occurrence of Fe/Al values above 0.60) is significantly greater (alpha = 0.05) than diversity in the upper part of the section (during and after the Fe/Al values above 0.60). A summary of the calculations for this t-test is included in Appendix I.

7.3- Geochemical Trends and Correlations

With one exception, no strong correlations between geochemical values (ie. $\delta^{13}C$ and TOC, TOC and FeHR/T, etc.) were found (Appendix I). This indicates that most of the geochemical factors in this study, when analyzed in pairs, are not likely to be directly related. The exception is a positive correlation between Fe/Al and FeHR/FeT ratios; considering that both of these ratios are empirically related (and directly proportional) to the amount of oxygen available in the water column during sediment deposition, this positive relationship is expected.

To determine if the hypothesized carbon-isotope excursion observed near the base of the Type Section shows significantly greater values than the interval below it, a Student's t-test of the mean $\delta^{13}C$ values during the hypothesized excursion versus those prior to the excursion was conducted. The test statistics indicate that the $\delta^{13}C$ values are significantly more positive during the excursion (the interval from 42-45 meters) than before (Appendix I). To determine whether or not the TOC values are elevated after the carbon-isotope excursion, a Mann-Whitney test was used (Appendix I). These test statistics indicate that TOC values are significantly higher after the excursion (above 45 meters in the composite section) than before (below 42 meters).

7.4- Facies-dependence Tests

To determine whether or not the fossil assemblage type and fossil diversity were facies-dependent, fossil assemblage and diversity were analyzed and compared for each facies/depositional environment. Graphs of these results are presented in figure 19. In the delta plain/estuarine environment (found only at the Leidy Peak locale), the *Leiosphaeridia* assemblage is the only fossil assemblage present; based upon this limited data set, it appears that this depositional environment contains only this particular assemblage. This depositional environment preserves high-, medium-, and low-diversity *Leiosphaeridia* assemblages, and it is the only depositional environment to contain high-diversity assemblages. When the other two depositional environments (proximal prodelta and distal prodelta) are examined, it appears that depositional environment does

not control fossil assemblage and diversity. The proximal prodelta and distal prodelta environments preserve approximately equal proportions of barren, *Bavlinella*, and *Leiosphaeridia* assemblages. In addition, these two environments contain both low- and average-diversity fossil assemblages in relatively even proportions. Based upon these results, it seems possible that fossil assemblage and diversity may be influenced somewhat by depositional environment, but these factors are certainly not controlled completely by environment since the proximal and prodelta environments are not statistically different with respect to fossil assemblage.

To determine whether or not the geochemical values showed facies-dependence, a chi-square contingency table analysis was performed using the geochemical averages for $\delta^{13}C$, TOC, FeHR/FeT, and Fe/Al found in each facies. The results of this test indicate that the geochemical values are equally distributed among the three different facies (proximal prodelta, distal prodelta, and delta plain), and thus they do not appear to be facies-dependent (Appendix I).

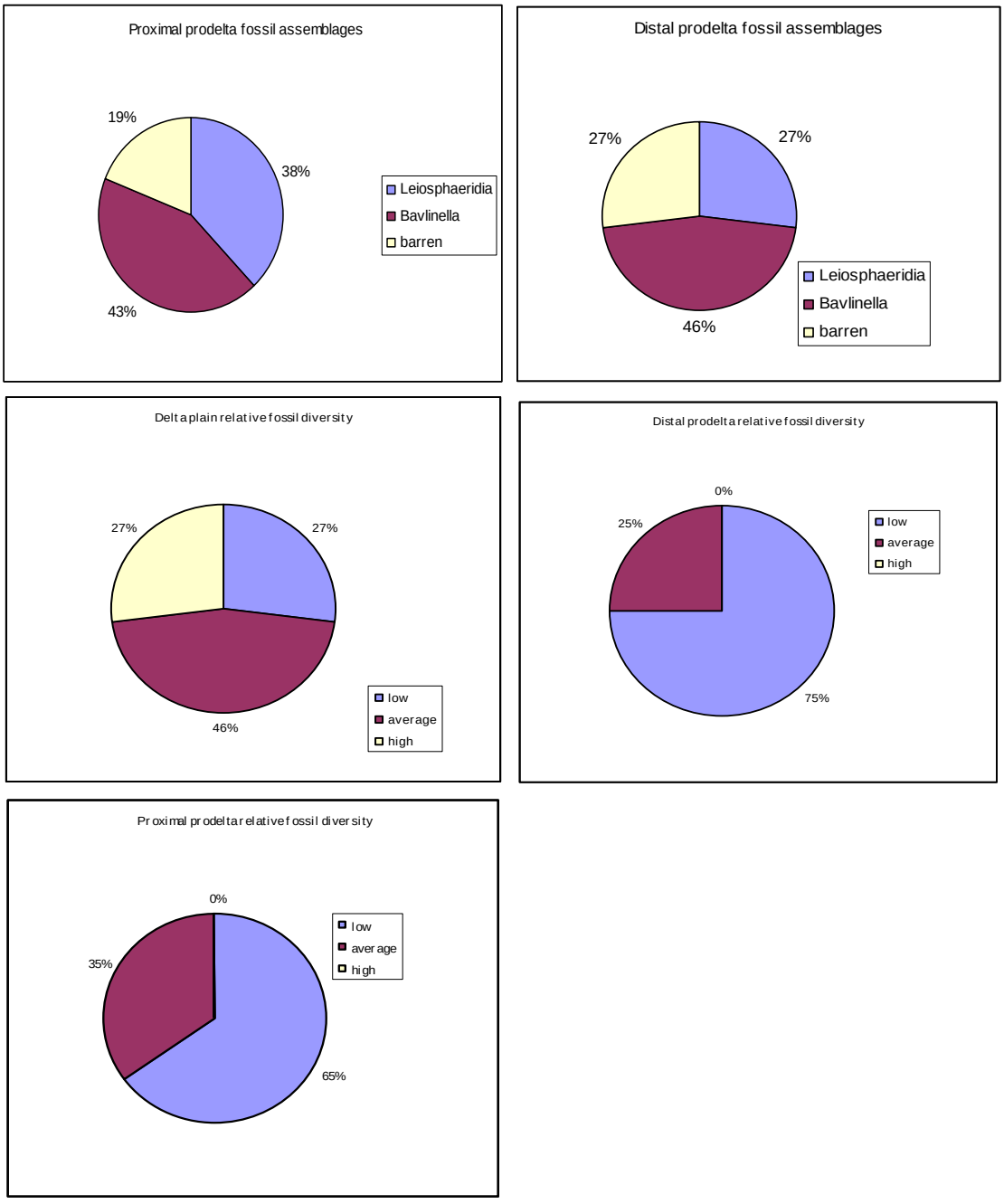

Figure 19. Graphs of microfossil assemblage and relative diversity by facies. The delta plain/estuarine environment contains only the *Leiosphaeridia* assemblage (100%), and thus a graph is not shown for this environment.

CHAPTER 8

DISCUSSION AND CONCLUSIONS

8.1- Chemostratigraphic Interpretations

Neoproterozoic glacial periods, typically associated with a drop in sea level, correlate generally with negative $\delta^{13}C$ excursions, while the interglacial periods and times of higher sea level are generally associated with relatively less-negative $\delta^{13}C$ values (Knoll et al., 1986; Kaufman and Knoll, 1995; Kaufman et al., 1997; Dehler et al., 2001, 2007; Halverson, 2006). It is likely that the relatively positive interglacial $\delta^{13}C$ values are a function of high organic carbon burial rates that may be associated with enhanced continental erosion rates at the time of Rodinia's breakup (Knoll et al., 1986; Des Marais, 1997; Karlstrom et al., 2000; Bartley and Kah, 2004; Dehler et al., 2005; Myer, 2008). In the Neoproterozoic Chuar Group this relationship between sea level, organic carbon burial rate, and $\delta^{13}C$ values is observed on a smaller scale (meters to tens of meters rather than hundreds of meters) during an interglacial period; less-negative $\delta^{13}C$ values are recorded in the deeper-water facies during high relative sea level, and more-negative $\delta^{13}C$ values are recorded in the shallow-water and peritidal facies during lowstands (Dehler et al., 2005). Myer (2008) reported a similar relationship in the Red Pine Shale; within intervals of higher shale content, $\delta^{13}C$ values are relatively less-negative and within sandier intervals, $\delta^{13}C$ values are relatively more negative. $\delta^{13}C$ values from the current study are consistent with those reported by Myer (2008), those reported from the coeval Chuar Group by Dehler et al. (2005), and with carbon-isotope ranges reported by Halverson (2006) for the period just prior to the first of at least two

Neoproterozoic low-latitude glactiations. This suggests that sedimentation rates, organic carbon burial rates, and sea level changes influencing the $\delta^{13}C$ values in the Red Pine Shale and underlying Hades Pass quartzite were likely global phenomena and not unique to the intracratonic seaway in which the Uinta Mountain Group was deposited.

It has been suggested that a pronounced increased in total organic carbon (TOC) content of shale in the Chuar Group indicates either increasing primary productivity (possibly due to enhanced sedimentation and increased nutrients), higher preservation rates of organic matter under anoxic conditions, or both (Nagy et al., 2009). A single pronounced increase in TOC like that observed in the Chuar Group is not quite as obvious in the Red Pine Shale and Hades Pass quartzite shale units; the TOC in the Red Pine Shale in both the Type Section and Composite Hades sections is highly variable, and TOC in the Box Canyon and Leidy Peak sections is consistently low. If put into a very large-scale stratigraphic context, though, it appears that TOC is relatively low earlier (during the deposition of the Box Canyon and Leidy Peak shale units) in Uinta Mountain Group time compared to later (during the deposition of the middle to upper Type Section and Hades strata); statistical analysis of TOC values earlier (prior to the significant positive $\delta^{13}C$ excursion at the base of the Type Section) versus later (post-excursion) reveals a significant increase in TOC after the carbon-isotope excursion. A TOC increase like this – directly following a positive $\delta^{13}C$ excursion- would be expected if increased nutrient delivery to the depositional system resulted in an increase in primary productivity.

Although total sulfur values are essentially zero throughout most of the Red Pine Shale and Hades Pass quartzite shale units, this is not inconsistent with the range of sulfur concentrations reported in the coeval Chuar Group by Johnston et al. (2010), and there are two "sulfur spikes" in the Red Pine Shale Type Section worthy of discussion. Both of these intervals of elevated total sulfur appear to coincide with intervals of higher TOC, suggesting a connection between high TOC (possibly indicating both increased primary productivity and enhanced organic matter preservation) and potentially anoxic/euxinic waters; this would be consistent with the evidence from the Chuar Group that elevated TOC – likely due to increased primary productivity- is linked to anoxia and biotic turnover (Nagy et al., 2009).

Empirically, FeHR/FeT values that exceed 0.38 imply deposition in an anoxic water column, while values below 0.38 usually suggest that deposition occurred under oxic bottom waters, and the average FeHR/FeT value for modern oxic waters is 0.26 (Canfield et al., 1992; Raiswell and Canfield, 1998; Raiswell et al., 2001; Poulton and Raiswell, 2002). Figures 18 shows that FeHR/FeT values in the Red Pine Shale and Hades Pass quartzite shale units are all below 0.26, which suggests deposition under oxic bottom waters. However, it is also possible that FeHR/FeT values below 0.38 indicate deposition under an anoxic/euxinic water column if the rate of siliciclastic sedimentation is relatively high, which would be expected in a prograding deltaic system such as the Red Pine Shale. If this is the case, an independent estimate of paleoredox conditions can be provided by Fe/Al ratios. Empirically, Fe/Al values of 0.60 or less are commonly found in oxic depositional environments (Lyons and Severmann, 2006), so it is likely that almost all of the

samples in this study represent deposition in an oxygenated water column. There are, however, four values in the Type Section that exceed 0.60, suggesting enhanced Fe deposition from an anoxic water column (Lyons and Severmann, 2006). These four >0.60 Fe/Al values occur in the stratigraphic interval between ~230 and 374 meters in the Type Section; the highest Fe/Al value reported in the Composite Hades section (0.57) occurs at ~450 meters. It is likely that in this part of the Type Section, deposition occurred under an anoxic/euxinic water column with a high siliciclastic sedimentation rate. This hypothesis is supported by the coincidence of the high Fe/Al stratigraphic interval with the two "sulfur spikes" discussed earlier.

8.2- Biostratigraphic Interpretations

The general biostratigraphic pattern observed in the upper Hades Pass quartzite and the Red Pine Shale over time is suggestive of a biotic change similar to that observed in the Chuar Group. *Leiosphaeridia* assemblages dominate earlier (Box Canyon and Leidy Peak), with a few ornamented species and relatively higher diversity recorded at Leidy Peak. A *Leiosphaeridia* to *Bavlinella* and VSM transition (higher-diversity to lower-diversity) occurs later in the Type Section, co-occurring with higher total sulfur and Fe/Al values that suggest an anoxic/euxinic water column. The change in diversity associated with this biotic transition is statistically significant; prior to the anoxic interval, the mean diversity is almost 6 times greater than during and after the anoxic interval. This is consistent with the hypothesis that the biotic transition is directly related to the anoxia – either through a eutrophication event (Nagy et al., 2009) or direct inhibition of the leiosphaerid populations by higher sulfide and lower oxygen concentrations that may not have

such a negative influence on prokaryotic populations like *Bavlinella* (Johnston et al., 2010).

A change in microfossil assemblage (*Leiosphaeridia* to *Bavlinella)* similar to that observed in the Type Section also appears in the Composite Hades section, but it is important to note that the *Leiosphaeridia* assemblages in this section are very low-diversity relative to others and that a *Bavlinella* assemblage occurs below them. The change in diversity associated with this second assemblage change is not statistically significant. This could be interpreted three ways: 1) the biotic transition is gradual and occurs over the entire stratigraphic interval sampled, with a general decrease in diversity and several fluctuations between *Leiosphaeridia* and *Bavlinella* assemblages before complete turnover, 2) the biotic transition occurs in the upper part of the Hades section, and thus the current correlation between the Type Section and Hades sections is incorrect and needs to be revised, 3) the biotic transition begins lower in the stratigraphic interval sampled, possibly below the basal Red Pine Shale in the Hades Pass quartzite, and is somewhat gradual. The second interpretation is not supported by lithologic, petrographic, carbon-isotope, and other geochemical data. The third interpretation seems most likely, but the first cannot be ruled out, and higher-resolution data sets from a more continuous stratigraphic interval are needed to provide evidence for or against these two interpretations.

The actual fossil assemblages found in the Red Pine Shale and Hades Pass quartzite shale units are similar to those reported by other researchers (Nagy and Porter, 2005; Nagy et al., 2009) in the Red Pine Shale and the Chuar Group; a few

are completely barren, and others are dominated by *Bavlinella* and *Leiosphaeridia*. One major difference is that, unlike the Chuar Group, these Uinta Mountain Group shales did not yield a "diverse ornamented acritarch" assemblage (one in which ornamented species comprised over 50% of the fossils counted) in this particular study. Several individuals from one genus of ornamented acritarchs were reported from multiple Leidy Peak slides, but these ornamented acritarchs were rare compared with unornamented varieties. It is noteworthy, though, that other researchers (Nagy and Porter, 2005) did find an assemblage dominated by diverse ornamented acritarchs in a sample from the Leidy Peak shale unit. Thus, although the diverse ornamented acritarch assemblage seems to be much more rare at Leidy Peak than in the Chuar Group, it does exist. This lends support to the idea that a biotic transition from mainly diverse ornamented assemblages to dominantly *Leiosphaeridia* and *Bavlinella* assemblages – such as that reported in the Chuar Group by Nagy et al. (2009) – may be present in the Red Pine Shale but begins to occur during deposition of the relatively coarse sandstone of the Hades Pass quartzite below the Leidy Peak shale unit.

Another possible explanation for the differences in fossil assemblage between the Uinta Mountain Group and the Chuar Group is that microfossil occurrence and preservation may be influenced by depositional environment to some extent (although this influence has a relatively small effect on planktonic microfossils), and the Uinta Mountain and Chuar groups certainly represent different depositional environments. The Chuar Group represents a mixed-siliciclastic-carbonate system likely deposited in a restricted embayment influenced

by storm waves and fluctuating water depths, while the upper Hades Pass quartzite and Red Pine Shale represent a silicilastic fluvial and deltaic system also influenced by fluctuating water depths. These differences may have some influence on microfossil assemblages and preservation, but considering the similarity between the fossil species occurrences in these different strata, it is very unlikely that differences in depositional environment entirely explain the relative lack of ornamented acritarchs in the upper Hades Pass quartzite and Red Pine Shale. Also, it should be noted that facies-dependence was not found in this particular study (nor in Nagy et al.'s 2009 study) for either the *Leiosphaeridia* or *Bavlinella* microfossil assemblage. The relative lack of ornamented acritarchs in the Uinta Mountain Group versus the Chuar Group could instead occur because the hypothesized biotic transition begins earlier in Uinta Mountain Group time than the Leidy Peak shale units were deposited, potentially when thick sandstone deposits – which are unlikely to preserve planktonic marine organic-walled microfossils- were accumulating in the ancient UMG basin.

8.3- Conclusions, Implications, and Future Work

TOC is relatively low earlier (during Box Canyon/Leidy Peak time) compared to later (during Type Section/Hades time) in the upper Uinta Mountain Group, and this increase in total organic carbon values and variability is preceded directly by a significant positive $\delta^{13}C$ excursion recorded in the Type Section of the Red Pine Shale. The TOC values prior to the carbon-isotope excursion are significantly lower than those in the stratigraphic interval above the excursion. This change in organic carbon content and isotopic composition is consistent with that observed in the

Chuar Group and suggests increased primary productivity and/or increased carbon burial rates may have been a response to an influx of nutrient-bearing sediments into the depositional system.

Higher TOC in the Type Section and Composite Hades section is associated with higher Fe/Al values, and both Fe/Al values and total sulfur values in the Type Section indicate an interval of deposition under anoxic/euxinic conditions that occurs after the onset of higher and more variable TOC values. This is consistent with iron speciation results from the Chuar Group and suggests that increased primary productivity could have led to anoxia.

A transition from relatively higher-diversity fossil assemblages (mainly *Leiosphaeridia*-dominated) that include some ornamented acritarchs to lower-diversity fossil assemblages (mainly *Bavlinella*-dominated and including VSMs) occurs in the upper Uinta Mountain Group strata (upper Hades Pass quartzite and Red Pine Shale). The significant shift from higher-diversity to lower-diversity assemblages begins just prior to the anoxic/euxinic interval; this is consistent with results from the Chuar Group and may indicate that "blooms" of *Bavlinella/Sphaerocongregus* – and the resultant increase in primary productivity – caused anoxic conditions that favored *Bavlinella/Sphaerocongregus* and VSMs and excluded more diverse fossil assemblages, leading to a complete biotic turnover in the ancient nearshore-marine ecosystems of this region.

There are two broader implications of these findings that should be discussed: 1) the consistency of the UMG and Chuar Group data sets suggests a biotic and geochemical event that is at least regional in extent and not the direct

result of a "snowball Earth" glaciation, and 2) the UMG geochemical data support recent models of punctuated global ocean anoxia during mid- to late-Neoproterozoic time. If the biotic turnover and geochemical changes observed in the UMG and Chuar Group are a result of the same regional (or even global) ocean event, then they could potentially be used as correlation tools for same-aged strata deposited elsewhere.

There are, though, several problems and new questions that arise from the comparison of the UMG and Chuar Group biotic and geochemical data sets. The first and most obvious is whether the positive carbon-isotope excursions in both strata represent the same event. Considering the current age constraints on the UMG and Chuar groups along with their fairly high-resolution carbon-isotope curves, it seems likely that the carbon-isotope excursion occurred in both basins simultaneously, yet the possibility exists that more than one carbon-isotope excursion of this magnitude occurred in the time interval over which the strata were deposited. To rule out this possibility, 1) better age control is needed in the Uinta Mountain Group and 2) the geochemistry and microfossils from lower parts of the UMG (below the Box Canyon shale units of this study) should be examined in detail.

Another problem that deserves consideration is the presence of "gaps" in the current upper Hades Pass quartzite/Red Pine Shale composite section presented in this study; it is not a continuous section, some uncertainties in the correlations of the sub-sections within the composite section are tentative, and there are large stratigraphic intervals for which no microfossil nor geochemical data exist. To resolve this problem, more microfossil and geochemical sampling from the "gaps" in

the current section (when possible) is recommended, as is higher-resolution sampling from a continous stratigraphic section within the Uinta Mountain Group. At the onset of this study, such a stratigraphic section was not available; since then, a potentially useful section has been located and targeted for sampling as soon as funding becomes available.

One very important question that stems from the findings of the UMG and Chuar Group microfossil and geochemical studies is this: how widespread were these changes in biota and ocean geochemistry at this time in Earth's history? It seems that they were at least regional in extent, but could they also have been global? To address these questions, future studies must test the "ocean eutrophication" hypothesis in other same-aged strata deposited in different regions of the globe.

REFERENCES

Anbar, A.D., and Knoll, A.H., 2002, Proterozoic ocean chemistry and evolution: A bioinorganic bridge?: Science, v. 297, p. 1137-1142.

Arthur, M.A., 2009, Carbonate rocks deconstructed: Nature, v. 460, p. 698-699.

Ball, T.T., and Farmer, G.L., 1998, Infilling history of a Neoproterozoic intracratonic basin: Nd isotope provenance studies of the Uinta Mountain Group, western United States: Precambrian Research, v. 87, p. 1-18.

Bartley, J.K., and Kah, L.C., 2004, Marine carbon reservoir, C-org-C-carb coupling, and the evolution of the Proterozoic carbon cycle: Geology, v. 32, p. 129-132.

Bryant, B., 1992, Geologic and structure maps of the Salt Lake City 1 x 2 quadrangle, Utah and Wyoming: U.S. Geological Survey Miscellaneous Investigations Series Map I-1997, scale 1:250,000.

Buick, R., 2010, Early life: Ancient acritarchs: Nature, v. 463, p. 885-886.

Butterfield, N.J., 1994, Burgess Shale-type fossils from a lower Cambrian shallow-shelf sequence in northwestern Canada: Nature, v. 369, p. 477-479.

Butterfield, N.J., and Chandler, F.W., 1992, Palaeoenvironmental distribution of Proterozoic microfossils, with an example from the Agu Bay Formation, Baffin Island: Palaeontology, v. 35, p. 957-943.

Canfield, D. E., Raiswell, R., Bottrell, S., 1992. The reactivity of sedimentary iron minerals towards sulfide: American Journal of Science, v. 292, p. 659-683.

Condie, K.C., Lee, D., and Farmer, G.L., 2001, Tectonic setting and provenance of the Neoproterozoic Uinta Mountain and Big Cottonwood groups, northern Utah: constraints from geochemistry, Nd isotopes, and detrital modes: Sedimentary Geology, v. 141, p. 443-464.

Dehler, C.M., Elrick, M., Karlstrom, K.E., Smith, G.A., Crossey, L.J., and Timmons, J.M., 2001, Neoproterozoic Chuar Group (similar to 800-742 Ma), Grand Canyon: record of cyclic marine deposition during global cooling and supercontinent rifting (vol 141, pg 465, 2001): Sedimentary Geology, v. 149, p. 279-280.

Dehler, C.M., Sprinkel, D.A., and Porter, S.M., 2005, Neoproterozoic Uinta Mountain Group of northeastern Utah; pre-Sturtian geographic, tectonic, and biologic evolution: Geological Society of America : Boulder, CO, United States

Dehler, C.M., Elrick, M., Bloch, J.D., Crossey, L.J., Karlstrom, K.E., and Des Marais, D.J., 2005, High-resolution delta C-13 stratigraphy of the Chuar Group (ca. 770-742 Ma), Grand Canyon: Implications for mid-Neoproterozoic climate change: Geological Society of America Bulletin, v. 117, p. 32-45.

Dehler, C.M., Porter, S.M., De Grey, L.D., Sprinkel, D.A., and Brehm, A., 2007, The Neoproterozoic Uinta Mountain Group revisited; a synthesis of recent work on the Red Pine Shale and related undivided clastic strata, northeastern Utah, U. S. A.: Proterozoic geology of western North America and Siberia, v. 86, p. 151-166

Dehler, C.M., Fanning, C.M., Link, P.K., Kingsbury, E.M., and Rybczynski, D., 2010, Maximum depositonal age and provenance of the Uinta Mountain Group and Big Cottonwood Formation, northern Utah: Paleogeography of rifting western Laurentia: Geological Society of America Bulletin, v. 122, p. 1686-1699.

Des Marais, D.J., 1997, Isotopic evolution of the biogeochemical carbon cycle during the Proterozoic Eon: Organic Geochemistry, v. 27, p. 185-193.

Farmer, G.L., and Ball, G., 1998. Infilling history of a Neoproterozoic intracratonic basin: Precambrian Research, v. 87, p. 1-18.

Gong, Q., Deng, J., Yang, L., Wang, Q., and Wang, W., 2008, Hot spring spurted into laterite layer: Geology and geochemistry evidence: Geochimica Et Cosmochimica Acta, v. 72, p. A319-A319.

Halverson, G.P., 2006, A Neoproterozoic Chronology, *in* Xiao, S.H., and Kaufman, A.J., eds., Neoproterozoic Geobiology and Paleobiology: Topics in geobiology: Dordrecht, Netherlands, Springer, p. 300.

Halverson, G.P., Hoffman, P.F., Schrag, D.P., and Kaufman, A.J., 2002, A major perturbation of the carbon cycle before the Ghaub glaciation (Neoproterozoic) in Namibia: Prelude to snowball Earth?: Geochemistry Geophysics Geosystems, v. 3, p. 947-953.

Hayes, J.M., Strauss, H., and Kaufman, A.J., 1999, The abundance of C-13 in marine organic matter and isotopic fractionation in the global biogeochemical cycle of carbon during the past 800 Ma: Chemical Geology, v. 161, p. 103-125.

Hill, A.C., and Walter, M.R., 2000, Mid-Neoproterozoic (similar to 830-750 Ma) isotope stratigraphy of Australia and global correlation: Precambrian Research, v. 100, p. 181-211.

Hoefs, J., 2008, Stable Isotope Geochemistry: Berlin, Springer, 284 p.

Hoffman, P.F., Kaufman, A.J., Halverson, G.P., and Schrag, D.P., 1998, A Neoproterozoic snowball earth: Science, v. 281, p. 1342-1346.

Hofmann, H.J., 1977, The problematic fossil Chuaria from the late Precambrian Uinta Mountain Group, Utah: Precambrian Research, v. 4, p. 1-11.

Horodyski, R.J., 1993, Precambrian paleontology of the western counterminous United States and northwest Mexico, *in* Reed, J.C., Bickford, M.E., Houston, R.S., Link, P.K., Rankin, D.W., Sims, P.K., and Van Schmus, W.R., ed., The Geology of North America, Volume C-2, DNAG, p. 558-565.

Javaux, E.J., Knoll, A.H., and Walter, M.R., 2003, Morphological and ecological complexity in early eukaryotic ecosystems: Nature, v. 412, p. 69-66.

Johnston, D.T., Poulton, S.W., Dehler, C., Porter, S., Husson, J., Canfield, D.E., and Knoll, A.H., 2010, An emerging picture of Neoproterozoic ocean chemistry: Insights from the Chuar Group, Grand Canyon, USA: Earth and Planetary Science Letters, v. 290, p. 64-73.

Karlstrom, K.E., Bowring, S.A., Dehler, C.M., Knoll, A.H., Porter, S.M., Des Marais, D.J., Weil, A.B., Sharp, Z.D., Geissman, J.W., Elrick, M.B., Timmons, J.M., Crossey, L.J., and Davidek, K.L., 2000, Chuar Group of the Grand Canyon: Record of breakup of Rodinia, associated change in the global carbon cycle, and ecosystem expansion by 740 Ma: Geology, v. 28, p. 619-622.

Kaufman, A.J., and Knoll, A.H., 1995, Neoproterozoic variations in the C-isotopic composition of seawater – stratigraphic and biogeochemical implications: Precambrian Research, v. 73, p. 27-49.

Kaufman, A.J., Corsetti, F.A., and Varni, M.A., 2007, The effect of rising atmospheric oxygen on carbon and sulfur isotope anomalies in the Neoproterozoic Johnnie Formation, Death Valley, USA: Chemical Geology, v. 237, p. 47-63.

Kaufman, A.J., Knoll, A.H., and Narbonne, G.M., 1997, Isotopes, ice ages, and terminal Proterozoic earth history: Proceedings of the National Academy of Sciences of the United States of America, v. 94, p. 6600-6605.

Kendall, B., Creaser, R.A., Calver, C.R., Raub, T.D., and Evans, D.A.D., 2009, Correlation of Sturtian diamictite successions in southern Australia and northwestern Tasmania by Re-Os black shale geochronology and the ambiguity of "Sturtian"-type diamictite-cap carbonate pairs as chronostratigraphic marker horizons: Precambrian Research, v. 172, p. 301-310.

Kingsbury, E.M., 2008, Geologic mapping and sequence stratigraphic analysis of the neoproterozoic uinta mountain group, Kings Peak 7.5' quadrangle, Duchesne and Summit Counties, Utah: Master's thesis, Idaho State University.

Knoll, A.H., 1994, Proterozoic and early Cambrian protists: Evidence for accelerating evolutionary tempo: Proceedings of the National Academy of Sciences of the United States of America, v. 106, p. 1281-1292.

—, 2003, Life on a Young Planet: The First Three Billion Years of Evolution on Earth: Princeton, New Jersey, Princeton University Press, 304 p.

Knoll, A.H., and Swett, K., 1985, Micropalaeontology of the Late Proterozoic Veteranen Group, Spitsbergen: Palaeontology, v. 28, p. 451-473.

Knoll, A.H., Blick, N., and Awramik, A.M., 1981, Stratigraphic and ecologic implications of late Precambrian microfossils from Utah: American Journal of Science, v. 281, p. 247-263.

Knoll, A.H., Hayes, J.M., Kaufman, A.J., Swett, K., and Lambert, I.B., 1986, Secular variation in carbon isotope ratios from upper Proterozoic successions of Svalbard and East Greenland: Nature, v. 321, p. 832-838.

Knoll, A.H., Swett, K., Mark, J., 1991, Paleobiology of a Neoproterozoic tidal flat/lagoonal complex: the Draken Conglomerate Formation, Spitsbergen: Journal of Paleontology, v. 65, p. 531-570.

Knoll, A.H., Bambach, R.K., Canfield, D.E., and Grotzinger, J.P., 1996, Comparative Earth history and Late Permian mass extinction: Science, v. 273, p. 452-457.

Link, P.K., Christie-Blick, N., Devlin, W.J., Elston, D.P., Horodyski, R.J., Levy, M., Miller, J.M.G., Pearson, R.C., Prave, A., Stewart, J.H., Winston, D., Wright, L.A., and Wrucke, C.T., 1993, Middle and Late Proterozoic stratified rocks of the western U.S. Cordillera, Colorado Plateau, and Basin and Range Province, *in* Reed, J.C., Bickford, M.E., Houston, R.S., Link, P.K., Rankin, D.W., Sims, P.K., and Van Schmus, W.R., eds., The Geology of North America, Volume C-2, DNAG, p. 463-595.

Lyons, T.W., and Severmann, S., 2006, A critical look at iron paleoredox proxies: New insights from modern euxinic marine basins: Geochimica Et Cosmochimica Acta, v. 70, p. 5698-5722.

Martin, R.E., Quigg, A., and Podkovyrov, V., 2008, Marine biodiversification in response to evolving phytoplankton stoichiometry: Palaeogeography Palaeoclimatology Palaeoecology, v. 258, p. 277-291.

Mueller, P.A., Foster, D.A., Mogk, D.W., Wooden, J.L., Kamenov, G.D., and Vogl, J.J., 2007, Detrital mineral chronology of the uinta mountain group: Implications for the Grenville flood in southwestern Laurentia: Geology, v. 35, p. 431-434.

Myer, C.A., 2008, Sedimentology, stratigraphy, and organic geochemistry of the Red Pine Shale, Uinta Mountains, Utah: A prograding deltaic system in a mid-Neoproterozoic interior seaway: Master's Thesis, Utah State University.

Nagy, R.M., 2008, Microfossils from the Neoproterozoic Chuar Group, Grand Canyon, Arizona: taxonomy, paleoecological analysis and implications for life during the onset of Neoproterozoic glaciations: Master's Thesis, University of California Santa Barbara

Nagy, R.M., and Porter, S.M., 2005, Paleontology of the Neoproterozoic Uinta Mountain Group: Uinta Mountain Geology: Utah Geological Association Publication, v. 33, p. 49-62.

Nagy, R.M., Porter, S.M., Dehler, C.M., and Shen, Y., 2009, Biotic turnover driven by eutrophication before the Sturtian low-latitude glaciation: Nature Geoscience, v. 2, p. 414-417.

Porter, S.M., and Knoll, A.H., 2000, Testate amoebae in the Neoproterozoic Era; evidence from vase-shaped microfossils in the Chuar Group, Grand Canyon: Paleobiology, v. 26, p. 385-360

Porter, S.M., Meisterfeld, R., and Knoll, A.H., 2003, Vase-shaped microfossils from the Neoproterozoic Chuar Group, Grand Canyon; a classification guided by modern testate amoebae: Journal of Paleontology, v. 77, p. 429-409

Poulton, S.W., and Raiswell, R., 2002. The low-temperature geochemical cycle of iron: from continental fluxes to marine sediment deposition: American Journal of Science, v. 302, p. 774-805.

Raiswell, R., and Canfield, D.E., 1998. Sources of iron for pyrite formation in marine sediments. American Journal of Science, v. 298, p. 219-245.

Raiswell, R., and Canfield, D.E., 2005. Evolution of the sulfur cycle. American Journal of Science, v. 299, p. 697-723.

Raiswell, R., Newton, R.N., and Wignall, P.B., 2001. An indicator of water-column anoxia: Resolution of biofacies variations in the Kimmeridge Clay (Upper Jurassic, UK): Journal of Sedimentary Research, v. 71, p. 286-294.

Rothman, D.H., Hayes, J.M., and Summons, R.E., 2003, Dynamics of the Neoproterozoic carbon cycle: Proceedings of the National Academy of Sciences of the United States of America, v. 100, p. 8124-8129.

Sanderson, I.D., 1984, The Mount Watson Formation, an interpreted braided-fluvial deposit in the Uinta Mountain Group (Upper Precambrian), Utah: The Mountain Geologist, v. 21, p. 157-164.

Sharp, Z.D., 2007, Principles of stable isotope geochemistry: Upper Saddle River, N.J., Pearson/Prentice Hall, 344 p.

Sprinkel, D.A, and Rybczinski, D., 2009. Geologic map of the Dutch John 30' x 60' quadrangle, Utah-Colorado-Wyoming: Utah Geological Survey, scale 1:62,500.

Strauss, H., Vidal, G., Moczydlowska, M., and Paczesna, J., 1992, Carbon isotope geochemistry and palaeontology of Neoproterozoic to early Cambrian siliciclastic successions in the East European Platform, Poland: Geological Magazine, v. 134, p. 1-16.

Vidal, G., 1976, Late Precambrian microfossils from the Visingso beds in southern Sweden: Fossils and Strata, v. 9, p. 1-57.

Vidal, G., and Ford, T.D., 1985, Microbiotas from the Late Proterozoic Chuar Group (northern Arizona) and Uinta Mountain Group (Utah) and their chronostratigraphic implications: Precambrian Research, v. 28, p. 349-389.

Vidal, G., and Knoll, A.H., 1982, Radiations and extinctions of plankton in the late Proterozoic and early Cambrian: Nature, v. 287, p. 57-60.

Vidal, G., and Moczydlowska-Vidal, M., 1997, Patterns of phytoplankton radiation across the Precambrian-Cambrian boundary: Journal of the Geological Society, v. 149, p. 654-647.

Vidal, G., and Nystuen, J.P., 1990, Micropaleontology, depositional environment, and biostratigraphy of the upper Proterozoic Hedmark Group, Southern Norway: American Journal of Science, v. 290-A, p. 211-170

Wallace, C.A., 1972, A basin analysis of the upper Precambrian Uinta Mountain Group, Utah: Ph.D. Dissertation, University of California Santa Barbara.

Wallace, C.A., and Crittenden, M.D., 1969, The stratigraphy, depositional environment and correlation of the Precambrian Uinta Mountain Group, western Uinta Mountains, Utah, *in* Lindsey, J.B., ed., Geologic Guidebook of the Uinta Mountains, Intermountain Association of Geologists 16th Annual Field Conference, p. 127-142.

Williams, N., 1953, Late pre-Cambrian and early Paleozoic geology of the western Uinta Mountains, Utah: American Association of Petroleum Geologists Bulletin, v. 37, p. 2734.

Zar, J.H., 2010, Biostatistical Analysis, 5th Edition: Pearson Prentice Hall, Upper Saddle River, NJ, 944 p.

APPENDICES

Appendix A: Measured Section Locations & Descriptions

Section	Location	Description
Box Canyon B	UTM zone 12T 0490952 4506996, elevation 8482 feet, just off of Box Canyon Trail (which starts at Red Pine Creek near the Type Section) in stream bed	Thickness = 5.2 m; partial section; black to greenish-tan silty shale with a few interbedded (<5 cm thick) hummocky sandstone intervals
Box Canyon C	UTM zone 12T 0491255 4506999, elevation 8785 feet, across stream from Box Canyon Trail (which starts at Red Pine Creek near the Type Section), upper part of section visible from the trail, section begins in bed of small stream canyon feeding main Box Canyon stream	Thickness = 42 m; black, green, and reddish-brown silty shale layers with a few 1.5-3 m-thick tan sandstone intervals (greenish-tan medium to pebbly quartz arenite)
Leidy Peak	UTM zone 12T 0599786 4513336, elevation 10,962 ft., ½ - 1 mile from Leidy Peak trailhead/parking area in small stream drainage below shaley saddle, section begins in streambed in fm. of Hades Pass sandstones	Thickness = 65 m; "classic" Hades Pass sandstones are cU to vcU & sometimes pebbly pinkish quartz arenites with yellow polycrystalline quartz pebbles (up to 3-4 cm), blocky weathering, ripplemarks on some beds, paleocurrents generally SSW; @ ~22.5 m the sandstone becomes much finer (contact covered) and greenish-yellowish tan in color, with some ripplemarks and soft-sediment deformation, fining upward to silty shale
Upper Setting Road A	UTM zone 12T 0487915 4496974, elevation 7676 feet, along Upper Setting Road (right side) in roadcut	Thickness = 7.5 m; partial section; grey slightly silty shale and dark grey clayshale containing small (a few cm) concretion-like shapes interbedded with greenish micaceous sandstone beds (fL – vcU)
Upper Setting Road B	UTM zone 12T 0487332 4497808, elevation 7949 feet, along Upper Setting Road (right side) in roadcut/quarried area	Thickness = 21.5 m; partial section; dark grey slightly silty shale with some reddish-orange altered areas, concretion-like shapes (like those at Upper Setting A), and interbedded fL – cU tan resistant sandstone

Mud Lake Flat Road (from Myer 2008)	UTM zone and elevation unknown, located along Red Pine Creek ~1 mile northeast of Type Section along Mud Lake Flat Road, section begins on road	Thickness = 18.5 m; partial section
Type Section (from Myer 2008)	Contact with underlying Hades Pass quartzite is UTM zone 12T 0490444E, 4508422N in Red Pine Creek (a tributary of Smith & Morehouse Creek)	Thickness = 662 m; all six facies (Myer 2008) present (shale, shale-and-sandstone, sandstone, slump fold, concretion, and pebbly sandstone), basal contact (gradational) with Hades Pass quartzite is covered, erosional upper contact with Mississippian Madison limestone visible; highest total sulfur values (up to 0.965%)
Lower Hades (from Myer 2008)	Base of section is UTM zone 12T 0511442E, 487380N; top of section is UTM zone 12T 0511519E, 4487336N; located downstream from Hades B (see Myer 2008) walking directly south from bend in National Forest Rd 312 and crossing Hades Creek; section begins in creek bed and continues upslope until Red Pine Shale is covered	Thickness = 69 m; partial floating section; shale and shale-and-sandstone facies
Hades A (from Myer 2008)	UTM zone 12T 0511871E, 4488004N; along Hades Creek (tributary of the North Fork of the Duchesne River across from USFS Hades Campground; section begins in creek bed west of "Hades Creek Dam" on north-facing slope	Thickness = 290 m; base not exposed; shale, shale-and-sandstone, and sandstone facies; highest TOC values (up to 3.95%)
Hades C (from Myer 2008)	Base of section is UTM zone 12T 05088220E, 4488240N; west across Duchesne River from Iron Mine Campground on unmarked road north of second switchback of National Forest high clearance road 180	Thickness = 123 m; partial floating section; shale and shale-and-sandstone facies

Appendix B: Detailed Stratigraphic Columns

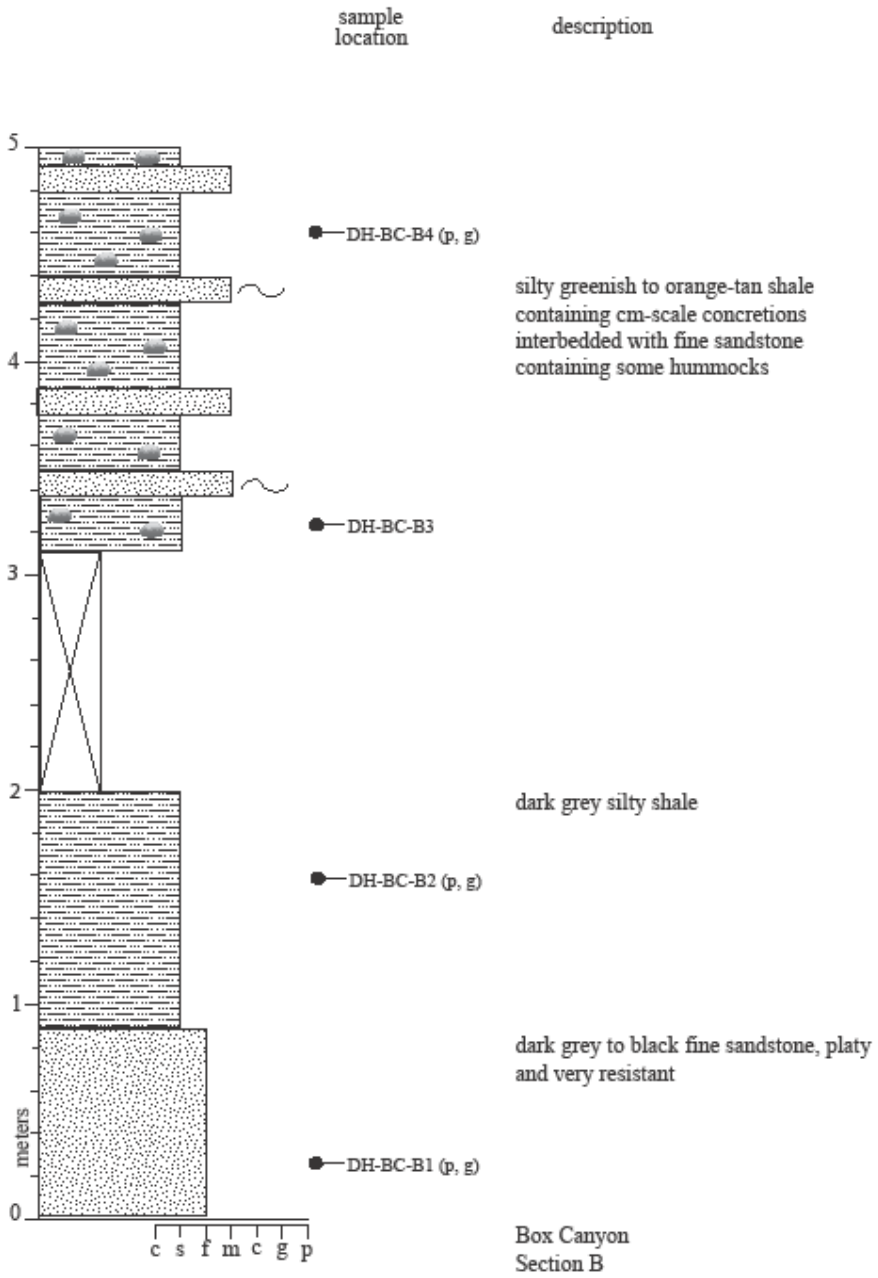

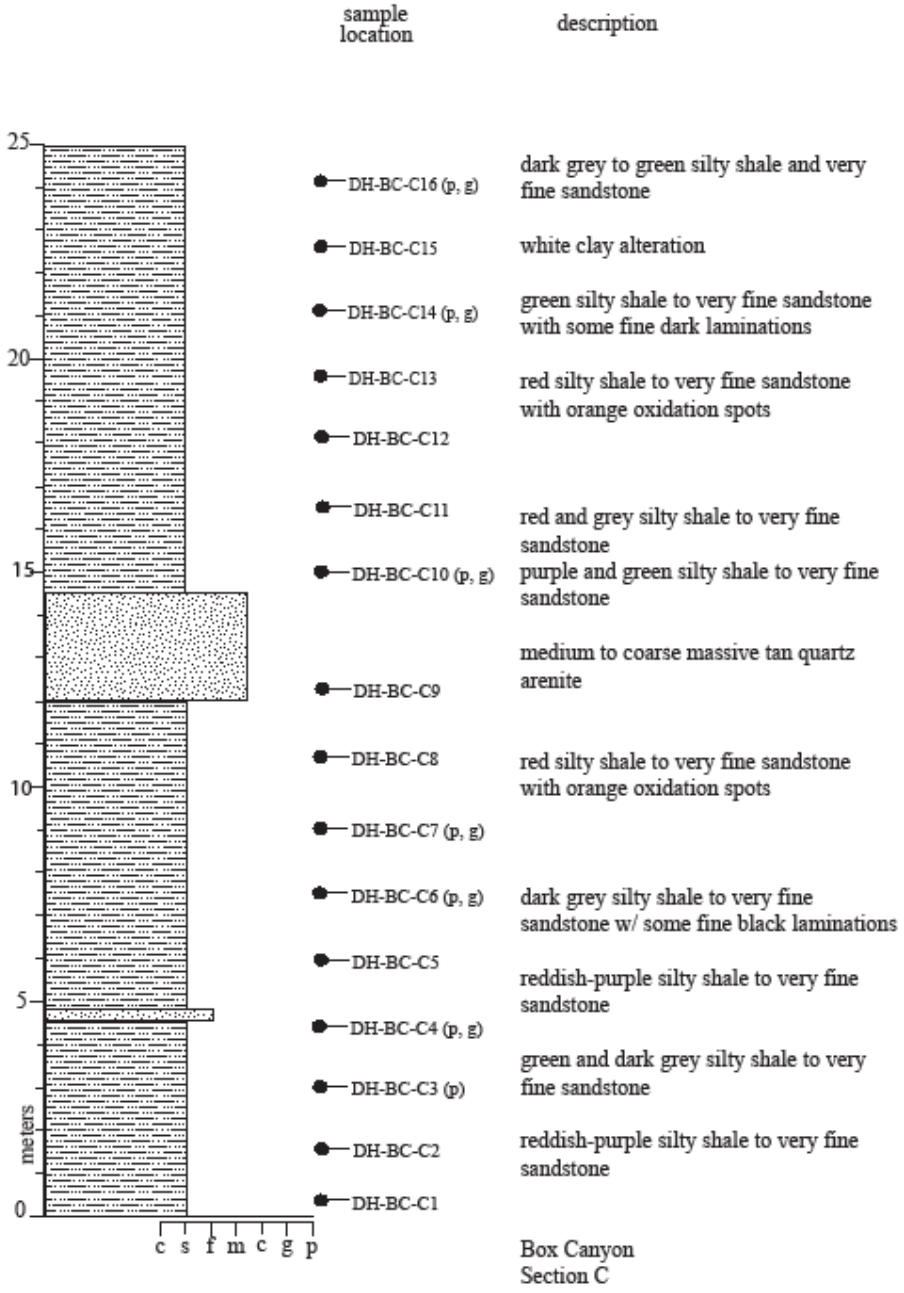
sample location
description
25
20
15
10
5
0
meters
DH-BC-C16 (p, g)
dark grey to green silty shale and very fine sandstone
DH-BC-C15
white clay alteration
DH-BC-C14 (p, g)
green silty shale to very fine sandstone with some fine dark laminations
DH-BC-C13
red silty shale to very fine sandstone with orange oxidation spots
DH-BC-C12
DH-BC-C11
red and grey silty shale to very fine sandstone
DH-BC-C10 (p, g)
purple and green silty shale to very fine sandstone
medium to coarse massive tan quartz arenite
DH-BC-C9
DH-BC-C8
red silty shale to very fine sandstone with orange oxidation spots
DH-BC-C7 (p, g)
DH-BC-C6 (p, g)
dark grey silty shale to very fine sandstone w/ some fine black laminations
DH-BC-C5
reddish-purple silty shale to very fine sandstone
DH-BC-C4 (p, g)
green and dark grey silty shale to very fine sandstone
DH-BC-C3 (p)
DH-BC-C2
reddish-purple silty shale to very fine sandstone
DH-BC-C1
c s f m c g p
Box Canyon
Section C

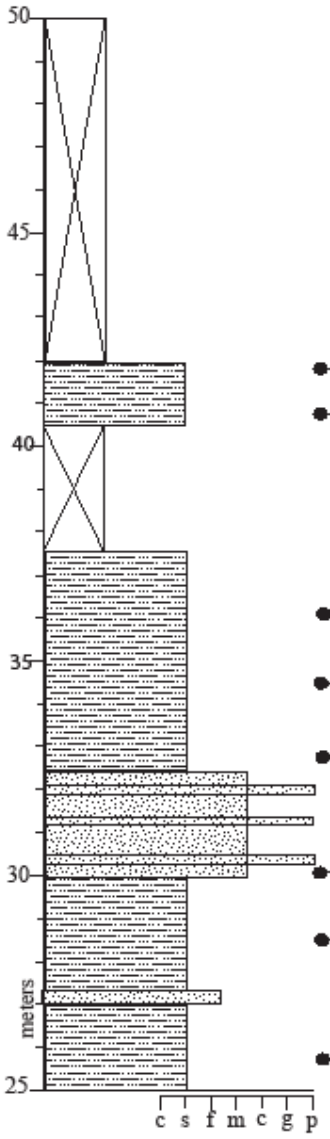

Box Canyon
Section C
(continued)

sample location

description

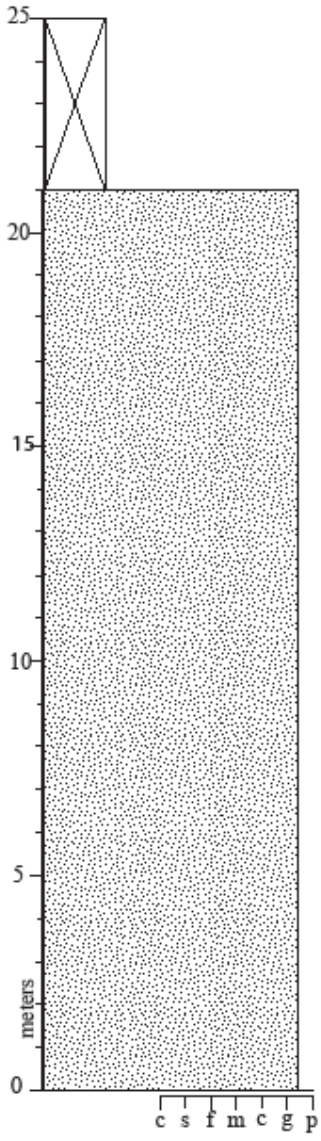

very coarse sandstone (granule quartz arenite) with some thinner (~10 cm) pebbly sandstone interbeds and lenses; pinkish color with some darker purple-red staining between pebbly areas; in pebbly areas, clasts (up to 3 cm) are quartzite and yellow polycrystalline quartz or chert

Leidy Peak
Section A

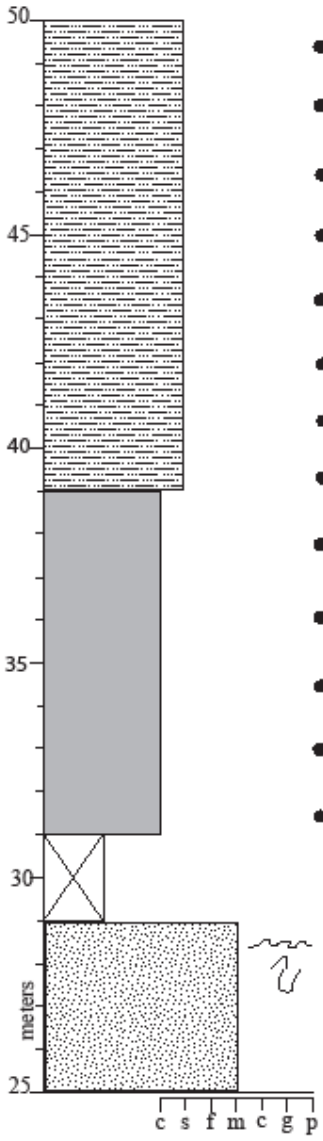

Leidy Peak
Section A
(continued)

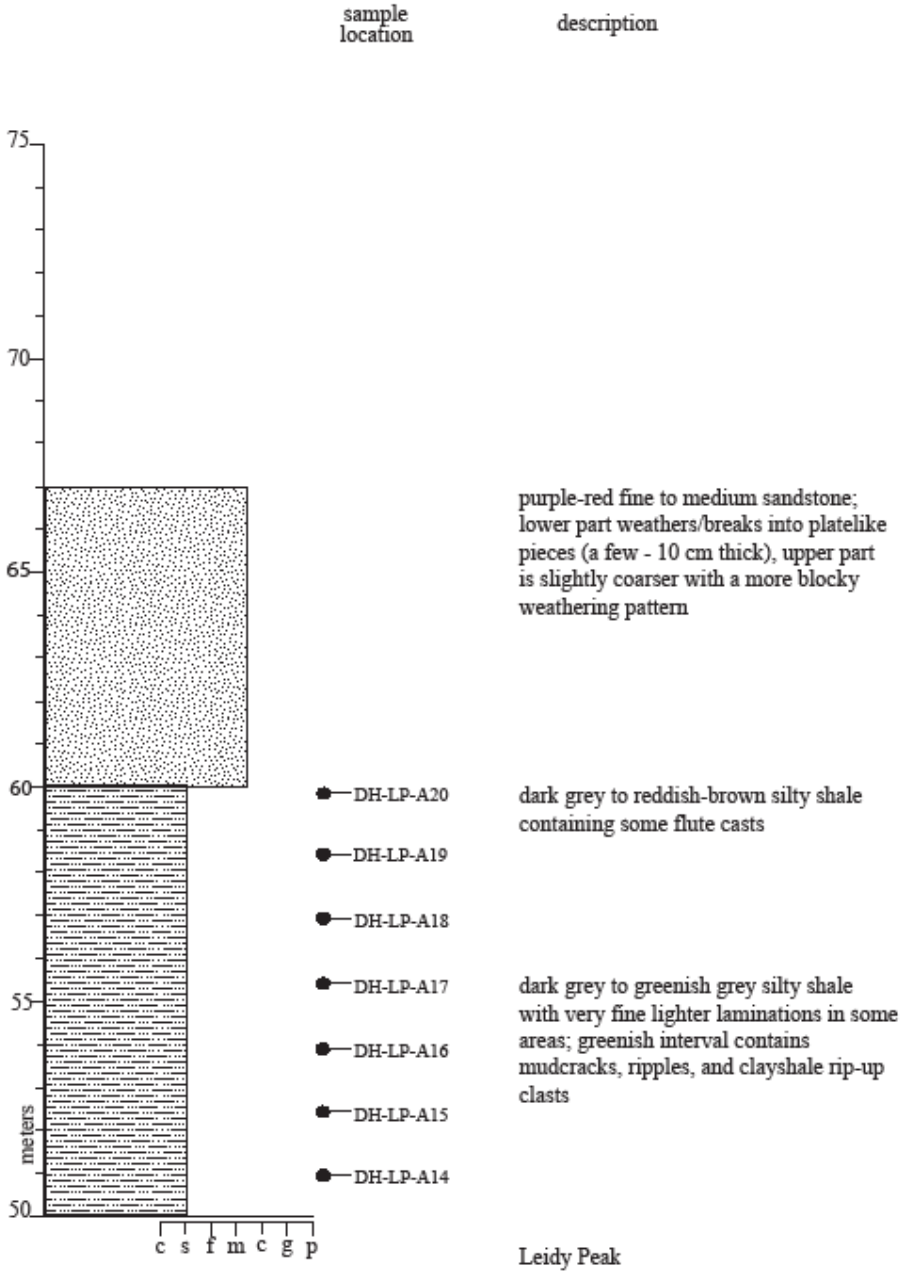

Leidy Peak
Section A
(continued)

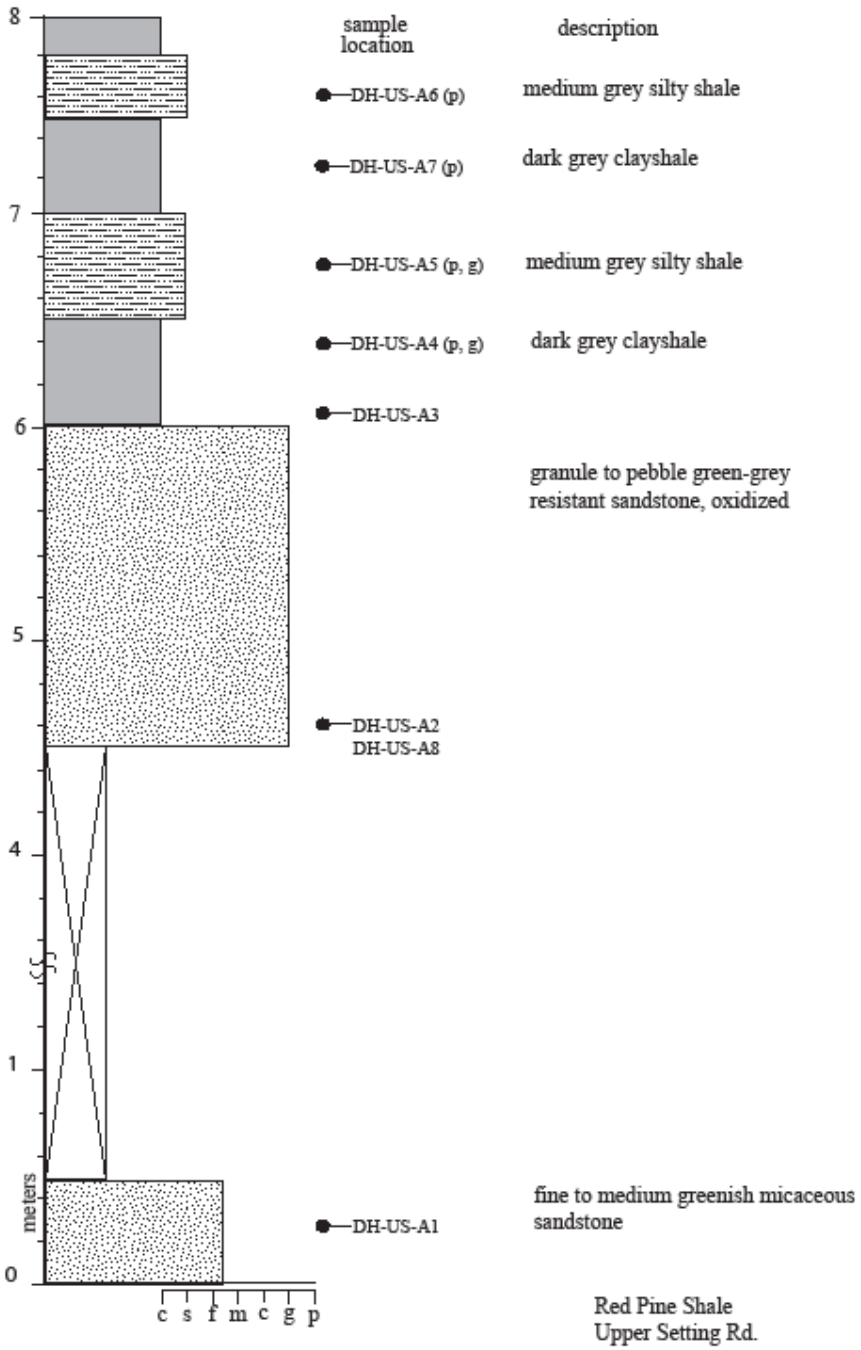
8
7
6
5
4
1
0
meters
c s f m c g p
sample location
description
DH-US-A6 (p)
medium grey silty shale
DH-US-A7 (p)
dark grey clayshale
DH-US-A5 (p, g)
medium grey silty shale
DH-US-A4 (p, g)
dark grey clayshale
DH-US-A3
granule to pebble green-grey resistant sandstone, oxidized
DH-US-A2
DH-US-A8
DH-US-A1
fine to medium greenish micaceous sandstone
Red Pine Shale
Upper Setting Rd.
Section A

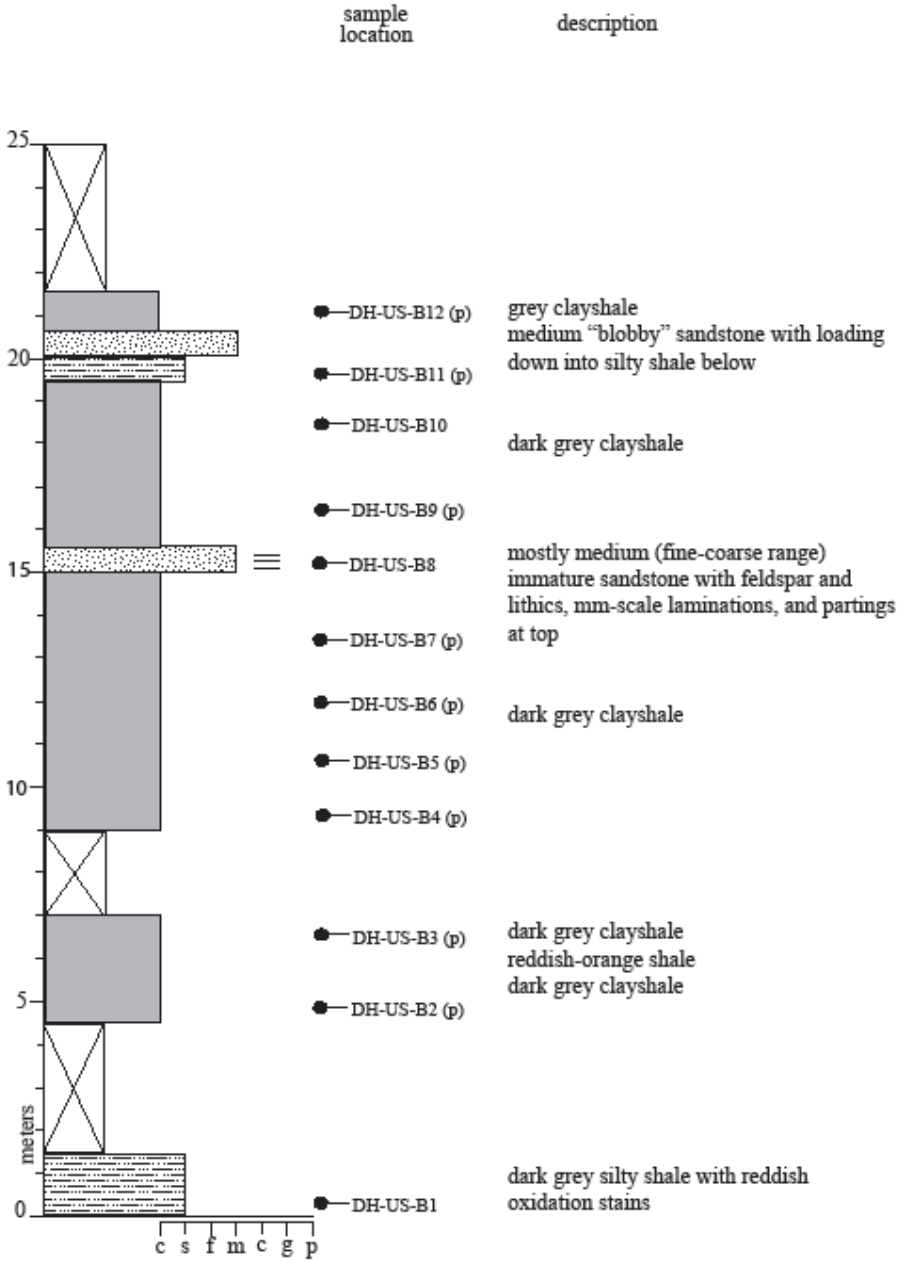
sample location
description
25
20
15
10
5
0
meters
DH-US-B12 (p)
DH-US-B11 (p)
DH-US-B10
DH-US-B9 (p)
DH-US-B8
DH-US-B7 (p)
DH-US-B6 (p)
DH-US-B5 (p)
DH-US-B4 (p)
DH-US-B3 (p)
DH-US-B2 (p)
DH-US-B1
c s f m c g p
grey clayshale
medium "blobby" sandstone with loading down into silty shale below
dark grey clayshale
mostly medium (fine-coarse range) immature sandstone with feldspar and lithics, mm-scale laminations, and partings at top
dark grey clayshale
dark grey clayshale
reddish-orange shale
dark grey clayshale
dark grey silty shale with reddish oxidation stains
Red Pine Shale
Upper Setting Road
Section B

Appendix C: Total Organic Carbon (TOC) Data Tables

Locale	Sample	Meters	TOC (weight percent)	Type Section Meter	Comp. Hades Meter
Box Canyon	DHBC-B1	0.5	0.73%	---	---
Box Canyon	DHBC-B2	1.5	0.82%	---	---
Box Canyon	DHBC-B4	4.5	0.42%	---	---
Box Canyon	DHBC-C03	3	0.24%	---	---
Box Canyon	DHBC-C04	4.5	0.29%	---	---
Box Canyon	DHBC-C06	7.5	0.34%	---	---
Box Canyon	DHBCC-07	9	0.29%	---	---
Box Canyon	DHBC-C10	15	0.08%	---	---
Box Canyon	DHBC-C14	21	0.13%	---	---
Box Canyon	DHBC-C16	24	0.46%	---	---
Box Canyon	DHBC-C18	28.5	0.00%	---	---
Box Canyon	DHBC-C21	34.5	0.11%	---	---
Box Canyon	DHBC-C24	42	0.10%	---	---
Hades A	HADES-09	322.5	2.99%	---	652.5
Hades A	HADES-12	339	1.33%	---	669
Hades A	HADES-24	417.5	1.21%	---	747.5
Hades A	HADES-26	442	2.84%	---	772
Hades A	HADES-32	503	3.95%	---	833
Hades A	HADES-47	601.5	2.01%	---	931.5
Hades A	HADES-52	612	2.66%	---	942

Hades A	HADES-54	624.5	2.14%	---		954.5
Hades A	RP01A-44	120	0.05%	---		450
Hades A	RP01A-85	280.5	1.28%	---		610.5
Hades C	RP01C-3	13.5	1.84%	---		443.5
Hades C	RP01C-7	121	1.79%	---		551
Leidy Peak	DHLP-A01	31.5	0.14%	---		
Leidy Peak	DHLP-A03	34.5	0.08%	---		
Leidy Peak	DHLP-A04	36	0.16%	---		
Leidy Peak	DHLP-A06	39	0.15%	---		
Leidy Peak	DHLP-A08	42	0.17%	---		
Leidy Peak	DHLP-A11	46.5	0.20%	---		
Leidy Peak	DHLPA13	49.5	0.17%	---		
Leidy Peak	DHLP-A14	51	0.30%	---		
Leidy Peak	DHLP-A16	54	0.27%	---		
Leidy Peak	DHLP-A17	55.5	0.18%	---		
Lower Hades	LH03-02	12	0.77%	---		12
Lower Hades	LH03-07	27	0.50%	---		27
Mud Lake Flat Rd	ROADSEC-4	3.5	1.19%	44.5	---	
Type Section	TS-001	80	0.28%	80	---	
Type Section	TS-003	83	0.25%	83	---	
Type Section	TS-004	84	0.36%	84	---	
Type Section	TS-005	85	0.40%	85	---	
Type Section	TS-007	89	0.58%	89	---	
Type Section	TS-011	104	0.77%	104	---	
Type Section	TS-016	119	0.89%	119	---	
Type Section	TS-021	138	0.30%	138	---	

Type Section	TS-025	154	1.15%	154	---
Type Section	TS-034	187	1.70%	187	---
Type Section	TS-041	231	0.34%	231	---
Type Section	TS-044	243	1.46%	243	---
Type Section	TS-049	275	0.26%	275	---
Type Section	TS-050	323	0.65%	323	---
Type Section	TS-057	374	0.27%	374	---
Type Section	TS-064	401	0.85%	401	---
Type Section	TS-064	401	0.90%	401	---
Type Section	TS-070	422	1.61%	422	---
Type Section	TS-087	492	0.49%	492	---
Type Section	TS-102	552	1.10%	552	---
Type Section	TS-104	558	1.27%	558	---
Upper Setting Rd	DHUS-A4	6.25	0.44% ---		---
Upper Setting Rd	DHUS-A5	6.5	0.22% ---		---

Appendix D: $\delta^{13}C$ Data Tables

Locale	Sample	$\delta^{13}C$ (VPDB)	Meters	Type Section Meter	Composite Hades Meter
Box Canyon	DHBC-B01	-22.2	0.5	---	---
Box Canyon	DHBC-B04	-32.2	4.5	---	---
Box Canyon	DHBC-C06	-21.5	7.5	---	---
Box Canyon	DHBC-C10	-26.188	15	---	---
Box Canyon	DHBC-C14	-25.140	21	---	---
Box Canyon	DHBC-C16	-28.3	24	---	---
Box Canyon	DHBC-C18	-25.905	28.5	---	---
Box Canyon	DHBC-C21	-22.2	34.5	---	---
Box Canyon	DHBC-C24	-23.544	42	---	---
Hades A	HADES-09	-28.286	322.5	---	652.5
Hades A	HADES-26	-27.745	442	---	772
Hades A	HADES-32	-27.294	503	---	833
Hades A	HADES-52	-26.419	612	---	942
Hades A	HADES-54	-25.860	624.5	---	954.5
Hades A	RP01A-44	-24.789	120	---	450
Leidy Peak	DHLP-A01	-25.6	31.5	---	---
Leidy Peak	DHLP-A03	-24.737	34.5	---	---
Leidy Peak	DHLP-A04	-24.146	36	---	---
Leidy Peak	DHLP-A06	-23.656	39	---	---
Leidy Peak	DHLP-A08	-23.985	42	---	---
Leidy Peak	DHLP-A11	-24.7	46.5	---	---
Leidy Peak	DHLP-A13	-22.729	49.5	---	---
Leidy Peak	DHLP-A14	-23	51	---	---
Leidy Peak	DHLP-A17	-24.192	55.5	---	---
Lower Hades	LH03-02	-25.204	12	---	12
Lower Hades	LH03-07	-24.706	27	---	27
Mud Lake Flat	ROAD-04	-20.7	44.5	44.5	---
Type Section	TS-001	-25.4	80	80	---
Type Section	TS-003	-22.7	83	83	---
Type Section	TS-004	-24.716	84	84	---
Type Section	TS-005	-19.700	85	85	---
Type Section	TS-007	-26.481	89	89	---
Type Section	TS-011	-27.085	104	104	---
Type Section	TS-016	-27.642	119	119	---

Type Section	TS-021	-25.171	138	138	---
Type Section	TS-025	-24	154	154	---
Type Section	TS-034	-24.8	187	187	---
Type Section	TS-041	-27.6	231	231	---
Type Section	TS-044	-26.2	243	243	---
Type Section	TS-049	-26.7	275	275	---
Type Section	TS-050	-27.6	323	323	---
Type Section	TS-057	-25.968	374	374	---
Type Section	TS-064	-20.527	401	401	---
Type Section	TS-087	-24.824	492	492	---
Type Section	TS-102	-28.553	552	552	---
Type Section	TS-104	-29.335	558	558	---
Upper Setting	DHUS-A04	-25.6	6.25	---	---
Upper Setting	DHUS-A05	-25.3	6.5	---	---

Appendix E: Total Sulfur Data Tables

Locale	Sample	Meters	Sulfur (weight percent)	Type Section Meter	Comp. Hades Meter
Box Canyon	DHBC-B1	0.5	0.0316 %	---	---
Box Canyon	DHBC-B2	1.5	0.0544 %	---	---
Box Canyon	DHBC-B4	4.5	0.0125 %	---	---
Box Canyon	DHBC-C03	3	0.0256 %	---	---
Box Canyon	DHBC-C04	4.5	0.0152 %	---	---
Box Canyon	DHBC-C06	7.5	0.0064 %	---	---
Box Canyon	DHBCC-07	9	0.0 ppm	---	---
Box Canyon	DHBC-C10	15	0.0339 %	---	---
Box Canyon	DHBC-C14	21	0.0142 %	---	---
Box Canyon	DHBC-C16	24	0.0099 %	---	---
Box Canyon	DHBC-C18	28.5	0.0 ppm	---	---
Box Canyon	DHBC-C21	34.5	0.0085 %	---	---
Box Canyon	DHBC-C24	42	0.0092 %	---	---
Hades A	HADES-09	322.5	0.1587 %	---	652.5
Hades A	HADES-12	339	0.1016 %	---	669
Hades A	HADES-24	417.5	0.0309 %	---	747.5
Hades A	HADES-26	442	0.0643 %	---	772
Hades A	HADES-32	503	0.1923 %	---	833

Hades A	HADES-47	601.5	0.0651 %	---			931.5
Hades A	HADES-52	612	0.0624 %	---			942
Hades A	HADES-54	624.5	0.0516 %	---			954.5
Hades A	RP01A-44	120	0.0 ppm	---			450
Hades A	RP01A-85	280.5	0.0400 %	---			610.5
Hades C	RP01C-3	13.5	0.1728 %	---			443.5
Hades C	RP01C-7	121	0.1679 %	---			551
Leidy Peak	DHLP-A01	31.5	0.0093 %	---		---	
Leidy Peak	DHLP-A03	34.5	0.0149 %	---		---	
Leidy Peak	DHLP-A04	36	0.0181 %	---		---	
Leidy Peak	DHLP-A06	39	0.0105 %	---		---	
Leidy Peak	DHLP-A08	42	0.0148 %	---		---	
Leidy Peak	DHLP-A11	46.5	0.0141 %	---		---	
Leidy Peak	DHLPA13	49.5	0.0 ppm	---		---	
Leidy Peak	DHLP-A14	51	0.0066 %	---		---	
Leidy Peak	DHLP-A16	54	0.0046 %	---		---	
Leidy Peak	DHLP-A17	55.5	0.0175 %	---		---	
Lower Hades	LH03-02	12	0.0123 %	---			12
Lower Hades	LH03-07	27	0.0115 %	---			27
Mud Lake Flat Rd	ROADSEC-4	3.5	0.0146 %		44.5	---	
Type Section	TS-001	80	0.0134 %		80	---	
Type Section	TS-003	83	0.0164 %		83	---	
Type Section	TS-004	84	0.0071 %		84	---	
Type Section	TS-005	85	0.0079 %		85	---	
Type Section	TS-007	89	0.0229 %		89	---	
Type Section	TS-011	104	0.0016 %		104	---	

Type Section	TS-016	119	0.0257 %		119	---
Type Section	TS-021	138	0.0151 %		138	---
Type Section	TS-025	154	0.0134 %		154	---
Type Section	TS-034	187	0.5253 %		187	---
Type Section	TS-041	231	0.9654 %		231	---
Type Section	TS-044	243	0.5021 %		243	---
Type Section	TS-049	275	0.0032 %		275	---
Type Section	TS-050	323	0.0837 %		323	---
Type Section	TS-057	374	0.0109 %		374	---
Type Section	TS-064	401	0.6143 %		401	---
Type Section	TS-064	401	0.7827 %		401	---
Type Section	TS-070	422	0.3031 %		422	---
Type Section	TS-087	492	0.0 ppm		492	---
Type Section	TS-102	552	0.0810 %		552	---
Type Section	TS-104	558	0.1021 %		558	---
Upper Setting Rd	DHUS-A4	6.25	0.0 ppm	---		---
Upper Setting Rd	DHUS-A5	6.5	0.0 ppm	---		---

Appendix F: Iron Speciation Data Tables

Locale	Sample	Meter	FeT (%)	FeHR (ppm)	FeHR/T	Type Section Meter	Comp. Hades Meter
Box Canyon	DHBC-B1	0.5	4.21	53.3719812	0.126774	---	---
Box Canyon	DHBC-B2	1.5	4.09	49.2965126	0.120529	---	---
Box Canyon	DHBC-B4	4.5	4.13	62.1162663	0.150403	---	---
Box Canyon	DHBC-C03	3	2.55	39.8853698	0.156413	---	---
Box Canyon	DHBC-C04	4.5	5.23	96.3310352	0.184189	---	---
Box Canyon	DHBC-C06	7.5	3.47	57.215686	0.164887	---	---
Box Canyon	DHBCC-07	9	1.76	28.2330655	0.160415	---	---
Box Canyon	DHBC-C10	15	5.18	77.7374994	0.150072	---	---
Box Canyon	DHBC-C14	21	3.51	49.8892777	0.142135	---	---
Box Canyon	DHBC-C16	24	4.46	88.7649797	0.199025	---	---
Box Canyon	DHBC-C18	28.5	5.77	85.9030317	0.148879	---	---
Box Canyon	DHBC-C21	34.5	2.07	28.3149381	0.136787	---	---
Box Canyon	DHBC-C24	42	2.88	46.0038036	0.159735	---	---
Hades A	HADES-09	322.5	0.9	7.39739193	0.082193	---	652.5
Hades A	HADES-12	339	4.27	73.6018084	0.17237	---	669
Hades A	HADES-24	417.5	1.05	13.5947964	0.129474	---	747.5
Hades A	HADES-26	442	1.49	17.0398506	0.114361	---	772
Hades A	HADES-32	503	1.27	13.4350549	0.105788	---	833
Hades A	HADES-47	601.5	2.09	28.2330655	0.135086	---	931.5
Hades A	HADES-52	612	1.77	18.4879884	0.104452	---	942
Hades A	HADES-54	624.5	1.82	23.9908052	0.131818	---	954.5
Hades A	RP01A-44	120	4.6	64.9697337	0.141239	---	450
Hades A	RP01A-85	280.5	NSS	73.8650647	---	---	610.5
Hades C	RP01C-3	13.5	2.76	70.4504331	0.255255	---	443.5
Hades C	RP01C-7	121	NSS	85.6352999	---	---	551
Leidy Peak	DHLP-A01	31.5	2.98	58.6735331	0.196891	---	---
Leidy Peak	DHLP-A03	34.5	4.08	60.1345502	0.147389	---	---
Leidy Peak	DHLP-A04	36	2.55	33.4124629	0.131029	---	---
Leidy Peak	DHLP-A06	39	3.42	56.5307373	0.165295	---	---
Leidy Peak	DHLP-A08	42	3.26	59.0170166	0.181034	---	---
Leidy Peak	DHLP-A11	46.5	3.58	65.5765503	0.183175	---	---
Leidy Peak	DHLPA13	49.5	3.88	55.3337662	0.142613	---	---
Leidy Peak	DHLP-A14	51	3.62	54.5654202	0.150733	---	---
Leidy Peak	DHLP-A16	54	2.43	41.2213945	0.169635	---	---
Leidy Peak	DHLP-A17	55.5	3.01	41.639478	0.138337	---	---
Lower Hades	LH03-02	12	4.42	60.306643	0.13644	---	12
Lower Hades	LH03-07	27	4.4	59.2527835	0.134665	---	27

Mud Lake Flat Rd	ROADSEC4	3.5	NSS	78.1788926	---	44.5	---
Type Section	TS-001	80	5.52	103.60876	0.187697	80	---
Type Section	TS-003	83	3.44	57.1300291	0.166076	83	---
Type Section	TS-004	84	4.19	68.444497	0.163352	84	---
Type Section	TS-005	85	3.2	49.6351697	0.15511	85	---
Type Section	TS-007	89	3.89	62.3751789	0.160348	89	---
Type Section	TS-011	104	5.71	97.5088884	0.170769	104	---
Type Section	TS-016	119	5.42	91.0086921	0.167913	119	---
Type Section	TS-021	138	4.53	72.5497704	0.160154	138	---
Type Section	TS-025	154	5.01	93.8004168	0.187226	154	---
Type Section	TS-034	187	3.85	85.8137768	0.222893	187	---
Type Section	TS-041	231	7.82	96.9650335	0.123996	231	---
Type Section	TS-044	243	NSS	43.6500965	---	243	---
Type Section	TS-049	275	6.46	105.164321	0.162793	275	---
Type Section	TS-050	323	6.44	118.721351	0.18435	323	---
Type Section	TS-057	374	5.89	137.585877	0.233592	374	---
Type Section	TS-064	401	3.78	60.0485203	0.158859	401	---
Type Section	TS-070	422	2.98	56.7019087	0.190275	422	---
Type Section	TS-087	492	4.05	47.5214422	0.117337	492	---
Type Section	TS-102	552	2.25	38.9684818	0.173193	552	---
Type Section	TS-104	558	1.05	11.6011817	0.110487	558	---
Upper Setting Rd	DHUS-A4	6.25	5.41	95.9689918	0.177392	---	---
Upper Setting Rd	DHUS-A5	6.5	3.83	56.8731239	0.148494	---	---

*NSS denotes “not sufficient sample”

Appendix G: Iron-aluminum ratio data tables

Locale	Sample	Meter	Fe (%)	Al (%)	Fe/Al	Type Section Meter	Comp. Hades Meter
Box Canyon	DHBC-B1	0.5	4.21	10.55	0.399052	---	---
Box Canyon	DHBC-B2	1.5	4.09	10.85	0.376959	---	---
Box Canyon	DHBC-B4	4.5	4.13	10.6	0.389623	---	---
Box Canyon	DHBC-C03	3	2.55	13.4	0.190299	---	---
Box Canyon	DHBC-C04	4.5	5.23	11	0.475455	---	---
Box Canyon	DHBC-C06	7.5	3.47	11.7	0.296581	---	---
Box Canyon	DHBCC-07	9	1.76	12.85	0.136965	---	---
Box Canyon	DHBC-C10	15	5.18	9.42	0.549894	---	---
Box Canyon	DHBC-C14	21	3.51	10.9	0.322018	---	---
Box Canyon	DHBC-C16	24	4.46	10.2	0.437255	---	---
Box Canyon	DHBC-C18	28.5	5.77	10.25	0.562927	---	---
Box Canyon	DHBC-C21	34.5	2.07	12.5	0.1656	---	---
Box Canyon	DHBC-C24	42	2.88	10.8	0.266667	---	---
Hades A	HADES-09	322.5	0.9	7.31	0.123119	---	652.5
Hades A	HADES-12	339	4.27	9.63	0.443406	---	669
Hades A	HADES-24	417.5	1.05	10.7	0.098131	---	747.5
Hades A	HADES-26	442	1.49	NSS	---	---	772
Hades A	HADES-32	503	1.27	9.45	0.134392	---	833
Hades A	HADES-47	601.5	2.09	10.4	0.200962	---	931.5
Hades A	HADES-52	612	1.77	10	0.177	---	942
Hades A	HADES-54	624.5	1.82	11.05	0.164706	---	954.5
Hades A	RP01A-44	120	4.6	8.02	0.573566	---	450
Hades A	RP01A-85	280.5	NSS	NSS	---	---	610.5
Hades C	RP01C-3	13.5	2.76	NSS	---	---	443.5
Hades C	RP01C-7	121	NSS	NSS	---	---	551
Leidy Peak	DHLP-A01	31.5	2.98	12.05	0.247303	---	---
Leidy Peak	DHLP-A03	34.5	4.08	12.75	0.32	---	---
Leidy Peak	DHLP-A04	36	2.55	11.4	0.223684	---	---
Leidy Peak	DHLP-A06	39	3.42	9.07	0.377067	---	---
Leidy Peak	DHLP-A08	42	3.26	8.49	0.383981	---	---
Leidy Peak	DHLP-A11	46.5	3.58	9.4	0.380851	---	---
Leidy Peak	DHLPA13	49.5	3.88	11.15	0.347982	---	---
Leidy Peak	DHLP-A14	51	3.62	10.85	0.333641	---	---
Leidy Peak	DHLP-A16	54	2.43	12.7	0.191339	---	---
Leidy Peak	DHLP-A17	55.5	3.01	11.3	0.266372	---	---
Lower Hades	LH03-02	12	4.42	9.7	0.45567	---	12
Lower Hades	LH03-07	27	4.4	10.55	0.417062	---	27
Mud Lake Flat Rd	ROADSEC4	3.5	NSS	NSS	---	44.5	---

Type Section	TS-001	80	5.52	12.25	0.450612	80	---
Type Section	TS-003	83	3.44	13	0.264615	83	---
Type Section	TS-004	84	4.19	12.25	0.342041	84	---
Type Section	TS-005	85	3.2	13.5	0.237037	85	---
Type Section	TS-007	89	3.89	12.4	0.31371	89	---
Type Section	TS-011	104	5.71	11.45	0.49869	104	---
Type Section	TS-016	119	5.42	11.9	0.455462	119	---
Type Section	TS-021	138	4.53	12.25	0.369796	138	---
Type Section	TS-025	154	5.01	11.2	0.447321	154	---
Type Section	TS-034	187	3.85	NSS	---	187	---
Type Section	TS-041	231	7.82	9.92	0.788306	231	---
Type Section	TS-044	243	NSS	NSS	---	243	---
Type Section	TS-049	275	6.46	10.2	0.633333	275	---
Type Section	TS-050	323	6.44	9.15	0.703825	323	---
Type Section	TS-057	374	5.89	9.07	0.649394	374	---
Type Section	TS-064	401	3.78	7.59	0.498024	401	---
Type Section	TS-070	422	2.98	9.48	0.314346	422	---
Type Section	TS-087	492	4.05	10.35	0.391304	492	---
Type Section	TS-102	552	2.25	10.65	0.211268	552	---
Type Section	TS-104	558	1.05	9.69	0.108359	558	---
Upper Setting Rd	DHUS-A4	6.25	5.41	10.4	0.520192	---	---
Upper Setting Rd	DHUS-A5	6.5	3.83	10.9	0.351376	---	---

*NSS denotes “not sufficient sample”

Appendix H: Paleontological Data Tables

Sample	Unornamented acritarchs	Ornamented acritarchs	Filaments	*Bavlinella faveolata*	*Chuaria sp.*	Colonial form(s)	*E. moorei*	Assemblage Type	Relative Abundance		Relative Diversity
DHBC-B1	0	0	0	0	0	0	0	barren		0	---
DHBC-B2	0	0	0	0	0	0	0	barren		0	---
DHBC-B4	0	0	0	0	0	0	0	barren		0	---
DHBC-C03	20	0	18	0	0	0	0	*Leiosphaeridia*	low		low
DHBC-C04	95	0	5	0	0	0	0	*Leiosphaeridia*	high		low
DHBC-C06	21	0	0	79	0	0	0	*Bavlinella*	high		low
DHBCC-07	56	0	4	16	0	0	0	*Leiosphaeridia*	average		average
DHBC-C10	0	0	0	0	0	0	0	barren		0	---
DHBC-C14	39	0	43	9	0	0	0	*Leiosphaeridia*	average		average
DHBC-C16	30	0	5	5	0	0	0	*Leiosphaeridia*	low		average
DHBC-C18	0	0	0	0	0	0	0	barren		0	---
DHBC-C21	60	0	5	35	0	0	0	*Leiosphaeridia*	high		average
DHBC-C24	50	0	5	10	0	0	0	*Leiosphaeridia*	average		average
HADES-09	0	0	0	all	0	0	0	*Bavlinella*	high		low
HADES-12	0	0	0	all	0	0	0	*Bavlinella*	high		low
HADES-24	0	0	0	all	0	0	0	*Bavlinella*	low		low
HADES-26	0	0	0	all	0	0	0	*Bavlinella*	high		low
HADES-32	0	0	0	all	0	0	0	*Bavlinella*	high		low
HADES-47	0	0	0	all	0	0	0	*Bavlinella*	high		low
HADES-54	0	0	0	all	0	0	0	*Bavlinella*	high		low
RP01A-44	15	0	0	10	0	1	0	*Leiosphaeridia*	low		low
RP01A-85	0	0	0	all	0	0	0	*Bavlinella*	high		low
RP01C-3	0	0	0	all	0	0	0	*Bavlinella*	high		low

RP01C-7	16	0	0	12	0	0	0	*Leiosphaeridia*	low		low
DHLP-A01	79	0	4	0	0	6	7	*Leiosphaeridia*	average		high
DHLP-A03	10	0	0	0	0	0	0	*Leiosphaeridia*	low		low
DHLP-A04	61	0	3	0	0	5	0	*Leiosphaeridia*	low		average
DHLP-A06	83	0	17	0	0	0	0	*Leiosphaeridia*	high		low
DHLP-A08	68	0	28	4	0	0	0	*Leiosphaeridia*	high		average
DHLP-A11	59	0	11	30	0	0	0	*Leiosphaeridia*	high		average
DHLPA13	63	4	5	25	1	2	0	*Leiosphaeridia*	high		high
DHLP-A14	81	13	11	2	0	2	0	*Leiosphaeridia*	high		high
DHLP-A16	68	0	12	13	0	0	0	*Leiosphaeridia*	average		average
DHLP-A17	87	8	5	0	0	0	0	*Leiosphaeridia*	high		average
LH03-02	0	0	0	0	0	0	0	barren		0	---
LH03-07	0	0	0	0	0	0	0	barren		0	---
ROADSEC-4	7	0	2	38	0	0	0	*Bavlinella*	low		average
TS-001	24	0	26	2	0	0	0	*Leiosphaeridia*	low		average
TS-003	37	0	20	0	1	0	0	*Leiosphaeridia*	low		average
TS-004	0	0	0	0	0	0	0	barren		0	---
TS-005	14	0	1	0	0	0	0	*Leiosphaeridia*	low		low
TS-007	0	0	0	0	0	0	0	barren		0	---
TS-025	0	0	0	0	0	0	0	barren		0	---
TS-034	0	0	0	all	0	0	0	*Bavlinella*	high		low
TS-041	0	0	0	all	0	0	0	*Bavlinella*	high		low
TS-044	0	0	0	all	0	0	0	*Bavlinella*	high		low
DHUS-A4	0	0	0	0	0	0	0	barren		0	---
DHUS-A5	0	0	0	0	0	0	0	barren		0	---
DHUS-B2	0	0	0	0	0	0	0	barren		0	---
DHUS-B3	0	0	0	0	0	0	0	barren		0	---
DHUS-B5	0	0	0	0	0	0	0	barren		0	---
DHUS-B7	0	0	0	0	0	0	0	barren		0	---
DHUS-B11	0	0	0	0	0	0	0	barren		0	---
DHUS-B12	0	0	0	0	0	0	0	barren		0	---

Appendix I: Statistical analysis data tables

$\delta^{13}C$ duplicate samples from Myer 2008 and Hayes 2010

Sample #	Myer 2008 $\delta^{13}C$	Hayes 2010 $\delta^{13}C$	difference
ROAD-04	-19.74	-20.7	0.96
TS-001	-25.43	-25.4	-0.03
TS-003	-19.17	-22.7	3.53*
TS-025	-23.77	-24	0.23
TS-034	-23.41	-24.8	1.39
TS-041	-26.58	-27.6	1.02
TS-044	-25.29	-26.2	0.91
TS-049	-25.94	-26.7	0.76
TS-050	-26.75	-27.6	0.85
RP01A-44	-25.02	-24.8	0.23
TS-102	-28.03	-28.6	0.52
TS-104	-29.12	-29.3	0.22
TS-016	-26.38	-27.6	1.26
TS-021	-23.91	-25.2	1.26
TS-057	-25.33	-26.0	0.64
TS-064	-26.18	-20.5	5.65
TS-004	-24.3	-24.7	0.42
TS-005	-18.63	-19.7	1.07
TS-006	-23.79	-26.7	2.91
TS-007	-26.01	-26.5	0.47
TS-087	-23.66	-24.8	1.16
TS-011	-26.57	-27.1	0.52
LH03-02	-24.6	-25.2	0.60
LH03-07	-24.43	-24.7	0.28

t-Test: Paired Two Sample for Means

	Myer 2008	*Hayes 2010*
Mean	-24.668333	-25.296236
Variance	6.47021449	5.99633876
Observations	24	24
Pearson Correlation	0.80146889	
Hypothesized Mean Difference	0	
df	23	
t Stat	*1.95244067	
P(T<=t) one-tail	0.03158104	
t Critical one-tail	1.71387152	
P(T<=t) two-tail	0.06316209	
t Critical two-tail	*2.0686576	

*T-statistics indicate the two means are not significantly different for $\alpha = 0.05$(2) (Myer 2008 mean = Hayes 2010 mean)

$\delta^{13}C$ duplicate samples from Myer 2008 and Hayes 2010

Myer 2008 $\delta^{13}C$ (parts per mil) Descriptive Statistics	
Mean	-24.66833333
Standard Error	0.519222756
Median	-25.155
Mode	#N/A
Standard Deviation	2.543661631
Sample Variance	6.470214493
Kurtosis	1.183812019
Skewness	1.002802202
Range	10.49
Minimum	-29.12
Maximum	-18.63
Sum	-592.04
Count	24
Confidence Level(95.0%)	1.0740941

Hayes 2010 $\delta^{13}C$ (parts per mil) Descriptive Statistics	
Mean	-25.296236
Standard Error	0.499847425
Median	-25.3022216
Mode	-27.6
Standard Deviation	2.448742281
Sample Variance	5.996338757
Kurtosis	0.458003373
Skewness	0.805644674
Range	9.6353394
Minimum	-29.3357522
Maximum	-19.7004128
Sum	-607.109664
Count	24
Confidence Level(95.0%)	1.034013174

TOC duplicate samples from Myer 2008 and Hayes 2010

Sample #	Myer 2008 TOC	Hayes 2010 TOC	Differen	Hayes 2010 adjusted TOC
LH03-02	0.54	0.77	0.23	0.57
LH03-07	0.33	0.5	0.17	0.30
ROAD-04	1.16	1.19	0.03	0.99
TS-001	0.19	0.28	0.09	0.08
TS-003	0.18	0.25	0.07	0.05
TS-004	0.21	0.36	0.15	0.16
TS-005	0.26	0.4	0.14	0.20
TS-007	0.4	0.58	0.18	0.38
TS-011	0.65	0.77	0.12	0.57
TS-016	0.87	0.89	0.02	0.69
TS-021	0.21	0.3	0.09	0.10
TS-025	0.94	1.15	0.21	0.95
TS-034	1.61	1.7	0.09	1.50
TS-041	1.11	0.34	-0.77	0.00
TS-044	1.22	1.46	0.24	1.26
TS-049	0.22	0.26	0.04	0.06
TS-050	0.5	0.65	0.15	0.45
TS-057	0.2	0.27	0.07	0.07
TS-064	0.55	0.9	0.35	0.70
RP01A-44	0.13	0.05	-0.08	0.00
TS-087	0.79	0.49	-0.3	0.29
TS-102	0.7	1.1	0.4	0.90
TS-104	1.15	1.27	0.12	1.07
HADES-09	2.46	2.99	0.53	2.79
HADES-26	2.17	2.84	0.67	2.64
HADES-32	2.74	3.95	1.21	3.75
HADES-52	1.77	2.66	0.89	2.46
HADES-54	1.52	2.14	0.62	1.94
average:	0.88	1.089	0.2046	0.89

Myer 2008 TOC values compared with Hayes adjusted TOC values:

Summary statistics:

Variable	Obs	Obs. with missing data	Obs. without missing data	Min	Max	Mean	Std. deviation
0.54	27	0	27	0.130	2.740	0.898	0.741
0.565357143	27	0	27	0.000	3.745	0.898	1.005

Wilcoxon signed-rank test / Two-tailed test:

V	220.000
Expected value	189.000
Variance (V)	1732.375
p-value (Two-tailed)	0.464
alpha	0.05

An approximation has been used to compute the p-value.

Test interpretation:

H_0: The two samples follow the same distribution.

H_a: The distributions of the two samples are different.
As the computed p-value is greater than the significance level alpha=0.05, one cannot reject the null hypothesis H_0.

*The two samples (Myer 2008 TOC and Hayes adjusted TOC) follow the same distribution.

DIVERSITY INDICIES

Analysing 8 variables x 48 cases

Shannon's method
Log base e

Sample	Index	Evenness	# of species
DHBC-B1	****	****	0
DHBC-B2	****	****	0
DHBC-B4	****	****	0
DHBC-C03	0.692	0.998	2
DHBC-C04	0.199	0.286	2
DHBC-C06	0.514	0.741	2
DHBCC-07	0.708	0.644	3
DHBC-C10	****	****	0
DHBC-C14	0.946	0.861	3
DHBC-C16	0.736	0.67	3
DHBC-C18	****	****	0
DHBC-C21	0.824	0.75	3
DHBC-C24	0.687	0.625	3
HADES-09	0	0	1
HADES-12	0	0	1
HADES-24	0	0	1
HADES-26	0	0	1
HADES-32	0	0	1
HADES-47	0	0	1
HADES-54	0	0	1
RP01A-44	0.81	0.737	3
RP01A-85	0	0	1
RP01C-3	0	0	1
RP01C-7	0.683	0.985	2
DHLP-A01	0.657	0.474	4
DHLP-A03	0	0	1
DHLP-A04	0.435	0.396	3
DHLP-A06	0.456	0.658	2
DHLP-A08	0.747	0.68	3
DHLP-A11	0.915	0.833	3
DHLPA13	1.04	0.581	6
DHLP-A14	0.852	0.53	5
DHLP-A16	0.768	0.699	3

Sample	Index	Evenness	# of species
DHLP-A17	0.473	0.431	3
LH03-02	****	****	0
LH03-07	****	****	0
ROADSEC-4	0.59	0.537	3
TS-001	0.829	0.754	3
TS-003	0.724	0.659	3
TS-004	****	****	0
TS-005	0.245	0.353	2
TS-007	****	****	0
TS-025	****	****	0
TS-034	0	0	1
TS-041	0	0	1
TS-044	0	0	1
DHUS-A4	****	****	0
DHUS-A5	****	****	0

****indicates barren samples

Special t-test for comparing two diversity indices:

$t = H_1' - H_2' / S_{H1'-H2'}$, where $S_{H1'-H2'} = \sqrt{S^2_{H1'} + S^2_{H2'}}$

and $\nu = (S^2_{H1'} + S^2_{H2'})^2 / ((S^2_{H1'})^2/n_1 + (S^2_{H2'})^2/n_2)$

H_1' = pre-anoxia diversity, H_2' = during/post-anoxia diversity

$t = 0.6103 - 0.0148/\sqrt{(0.0804 + 0.0793)} = 2.50$

$\nu = (0.0804 + 0.0793)2/((0.0804)^2/23 + (0.0793)^2/13) = 32$

$t_{0.05(2),32} = 1.69$

Therefore, the diversity pre-anoxia is significantly different from diversity during/post-anoxia; diversity is greater pre-anoxia.

Diversity vs. stratigraphic height

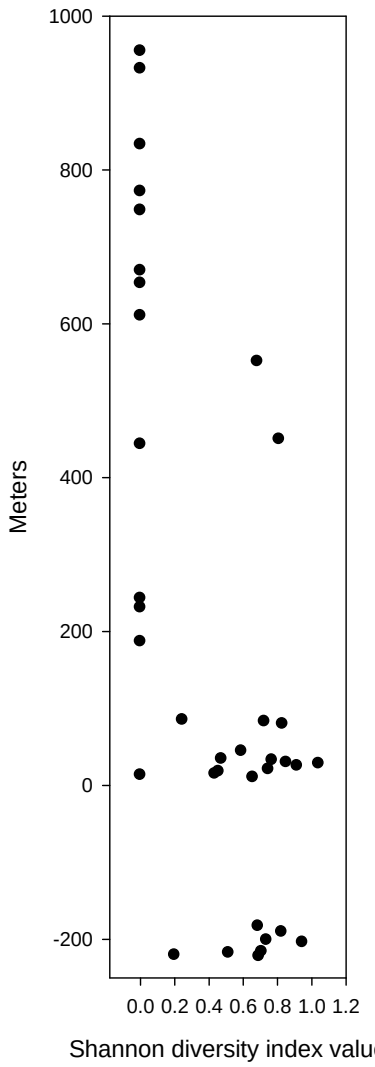

Evenness vs. stratigraphic height

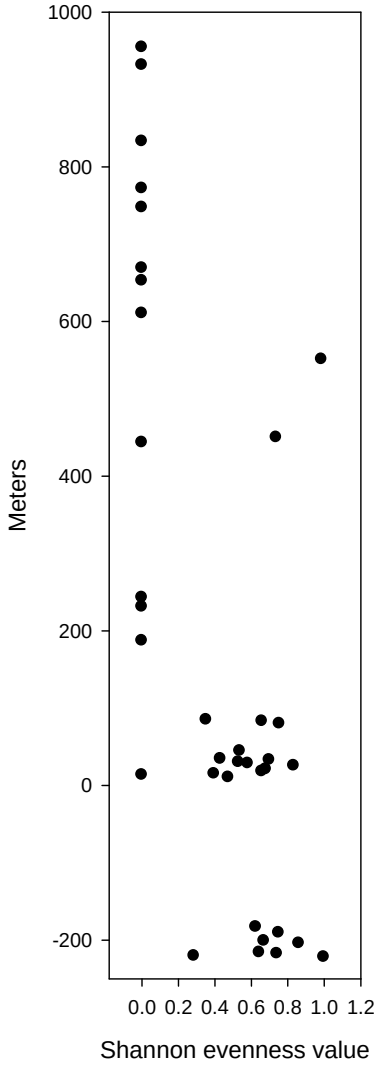

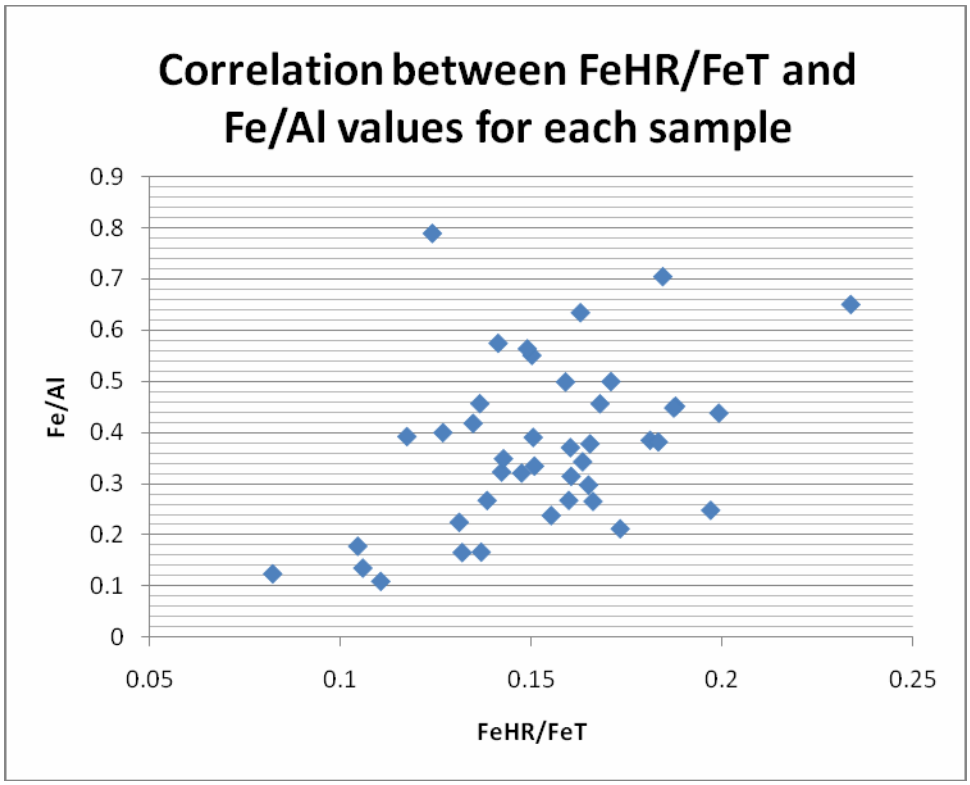
Correlation between FeHR/FeT and Fe/Al values for each sample
Fe/Al
0.9
0.8
0.7
0.6
0.5
0.4
0.3
0.2
0.1
0
0.05
0.1
0.15
0.2
0.25
FeHR/FeT

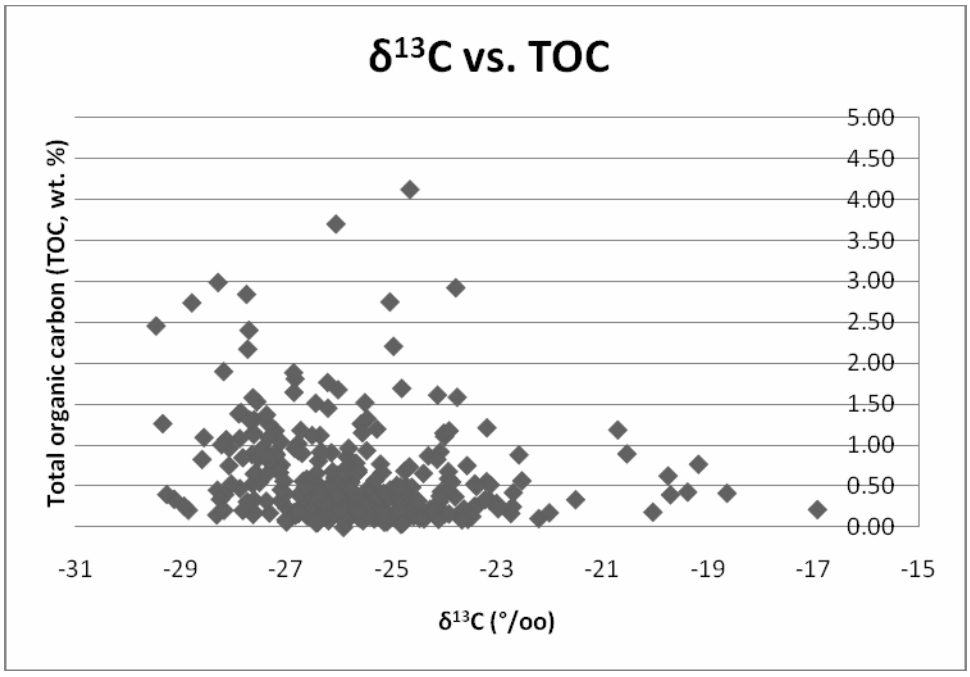
δ13C vs. TOC
Total organic carbon (TOC, wt. %)
5.00
4.50
4.00
3.50
3.00
2.50
2.00
1.50
1.00
0.50
0.00
-31
-29
-27
-25
-23
-21
-19
-17
-15
δ13C (°/oo)

t-Test: Two-Sample Assuming Unequal Variances

	pre-$\delta^{13}C$ excursion (below 42 m)	*During $\delta^{13}C$ excursion (42-45 m)*
Mean	-24.39327079	-21.25633333
Variance	1.507010858	7.863181697
Observations	33	12
Hypothesized Mean Difference	0	
df	13	
t Stat	*-3.746863514	
P(T<=t) one-tail	0.001221006	
t Critical one-tail	*1.770933383	
P(T<=t) two-tail	0.002442012	
t Critical two-tail	2.160368652	

*T-statistics indicate that $\delta^{13}C$ values are significantly more positive during the excursion (between 42 and 45 meters) than before.

Mann-Whitney test of pre-excursion TOC vs. post-excursion TOC (until onset of anoxia)

Summary statistics:

	Obs.	Obs. with missing data	Obs. w/o missing data	Min.	Max.	Mean	Std. dev.
Pre-excursion	32	3	29	0.00	0.50	0.179	0.190
Post-excursion	85	8	77	0.13	2.92	0.562	0.454

Mann-Whitney test / Lower-tailed test:

U	442.500
Expected value	1116.500
Variance (U)	19859.75
p-value (one-tailed)	< 0.0001
alpha	0.05

An approximation has been used to compute the p-value.

Test interpretation:

H_0: The difference of location between the samples is equal to 0.

H_a: The difference of location between the samples is lower than 0.

As the computed p-value is lower than the significance level alpha=0.05, one should reject the null hypothesis H_0, and accept the alternative hypothesis Ha.

The risk to reject the null hypothesis H_0 while it is true is lower than 0.01%.

Ties have been detected in the data and the appropriate corrections have been applied.

*Test indicates that TOC values are significantly higher after the $\delta^{13}C$ excursion (between 45 and 200 meters) than before (<42 meters).

χ^2 Analysis (contingency table): distribution of geochemical averages among different facies

Geochemical Averages (x 100)					
Facies:	**$\delta^{13}C$ (parts/mil)**	**TOC (wt. %)**	**FeHR/FeT**	**Fe/Al**	Total:
Distal prodelta	2620 (2620)	36 (38)	20 (18)	43 (39)	2719
Proximal prodelta	2530 (2530)	49 (37)	15 (17)	36 (38)	2630
Delta plain	2420 (2406)	26 (35)	16 (16)	34 (36)	2496
Total:	7570	111	51	113	7854

H_o: Geochemical averages (x 100) are equally distributed among the three different facies.

H_A: Geochemical averages (x 100) are not equally distributed among the three different facies.

$\nu = (r-1)(c-1) = (3-1)(4-1) = 6$

$\chi 2 = 0 + 0.105 + 0.222 + 0.410 + 0 + 3.89 + 0.235 + 0.105 + 0.081 + 2.31 + 0 + 0.111 = 7.469$

$\chi 2_{(0.05), 6} = 12.592$

$7.469 < 12.592$, and thus H_O cannot be rejected.

*This test indicates that the geochemical values are equally distributed among the three different facies, and thus geochemical values do not show facies-dependence.